# OPTOELECTRONICALLY ACTIVE METAL-INORGANIC FRAMEWORKS AND SUPRAMOLECULAR EXTENDED SOLIDS

Joshua F. Ivy, B.S.

Dissertation Prepared for the Degree of

DOCTOR OF PHILOSOPHY

UNIVERSITY OF NORTH TEXAS

August 2018

APPROVED:

Mohammad A. Omary, Major Professor
Francis D'Souza, Committee Member
Deborah Hunka, Committee Member
Legrande Slaughter, Committee Member
Hong Wang, Committee Member
Michael Richmond, Chair of the Department of Chemistry
Su Gao, Dean of the College of Science
Victor Prybutok, Dean of the Toulouse Graduate School

Ivy, Joshua F. *Optoelectronically Active Metal-Inorganic Frameworks and Supramolecular Extended Solids*. Doctor of Philosophy (Chemistry), August 2018, 115 pp., 8 tables, 71 figures, 124 numbered references.

Metal-organic frameworks (MOFs) have been intensely researched over the past 20 years. In this dissertation, metal-inorganic frameworks (MIFs), a new class of porous and nonporous materials using inorganic complexes as linkers, in lieu of traditional organic linkers in MOFs is reported. Besides novel MIF regimes, the previously described fluorous MOF "FMOF-1", is re-categorized herein as "F-MIF1". F-MIF-1 is comprised of $[Ag_4Tz_6]^{2-}$ (Tz = 3,5-bis-trifluoromethyl-1,2,4-triazolate) inorganic clusters connected by 3-coordinate $Ag^+$ metal centers. Chapter 2 describes isosteric heat of adsorption studies of F-MIF1 for $CO_2$ at near ambient temperatures, suggesting promise for carbon capture and storage. We then successfully exchanged some of these Ag(I) centers with Au(I) to form an isostructural Au/F-MIF1. Other, nonporous MIFs have been synthesized using $Ag_2Tz_2$ clusters with bridging diamine linkers 4,4'-bipyridine, pyrazine, and a Pt(II) complex containing two oppositely-situated non-coordinating pyridines. This strategy attained luminescent products better-positioned for photonic devices than porous materials due to greater exciton density.

Chapter 3 overviews work using an entirely inorganic luminescent complex, $[Pt_2(P_2O_5)_4]^{4-}$ (a.k.a. "PtPOP") to form new carbon-free MIFs. PtPOP is highly luminescent in solution, but as a solid shows poor quantum yield (QY ~0.02) and poor stability under ambient conditions. By complexing PtPOP to various metals, we have shown a dramatic enhancement in its solid-state luminescence (by an order of magnitude) and stability (from day to year scale). One embodiment (MIF-1) demonstrates microporous character.

Chapter 4 overviews the design and application of new MIF linkers. Pt complexes based upon (pyridyl)azolates, functionalized with carboxylic acid groups, have been synthesized. These complexes, and their esterized precursors, show strong luminescence on their own. They have been used to generate new luminescent MIFs. Such new MIFs may be useful toward future inorganic (LEDs) or organic (OLEDs) light-emitting diodes, respectively. The electronic communication along their infinite coordination structures is desirable for color tuning and enhanced conductivity functions, compared to the small molecules used in such technologies, which rely on intermolecular interactions for these functions.

ACKNOWLEDGEMENTS

I would like to thank Dr. Mohammad Omary first and foremost for his guidance as my Ph.D. advisor over these years and for his help through my various synthetic and analytical problems that I encountered while generating this document. I would like to thank the members of my committee for their feedback on this dissertation. I'd like to thank the Omary group members for their help, support and friendship during my time here at the University of North Texas. Special thanks goes to Dr. Vladimir Nesterov for helping me with crystal growth and the subsequent work on solving the structures of those crystals, and to Simona Galli (Insubria) in particular for her work on the products in Chapter 4. I'd also like to thank our various collaborators, Xiaoping Wang (ORNL), Hong-Cai Zhou (TAMU), and Omar Yaghi (California – Berkeley) for their help and guidance during my projects.

I'd like to thank my parents, Gary and Shirley Ivy, for their support through my time in school during my pursuits of higher learning. And last but not least I'd like to thank Sarah Strittmatter for her constant encouragement, support, and patience while working on my Ph.D.

TABLE OF CONTENTS

Page

LIST OF TABLES

Page

LIST OF FIGURES

Page

# CHAPTER 1

# INTRODUCTION

## 1.1 MOFs and Porous Materials*

### 1.1.1 Metal Organic Frameworks

Porous materials with inorganic, organic, or metal-organic compositions have been subject to intense investigations in fundamental and applied research projects. These materials are typified by zeolites (alumina silicates), activated carbons, and metal-organic frameworks ("MOFs"). MOFs (and the derivatives thereof) in particular stand out in terms of their ability to design highly uniform structures, with excellent control over pore size and chemical functional groups that may facilitate specific applications, customized for specific guest molecules. The applications for which such versatile porous materials could be used include size- and shape-selective catalysis, separations, gas storage, ion-exchange, sensors, and optoelectronics. In particular, stable MOFs with permanent highly-porous channels or cavities have been explored as effective, economic, and safe on-board vehicular gas (hydrogen or methane) storage materials for fuel-cell-driven automobiles, $CO_2$ capture and/or storage, gas separation, sensing and/or remediation of hazardous gases or liquids, etc.

Extensive efforts have been devoted to the rational design and construction of new MOFs including zeolitic imidazolate frameworks (ZIFs) with zeolite-like, well-defined, stable, and extra-large micro- or meso- size pore channels exhibiting higher or selective gas affinity properties.

*Parts of this section are reproduced from the following sources: (a) Omary, M. A.; Ivy, J. F. "Metal-Inorganic Frameworks", United State Patent and Trademark Office. U.S. Provisional Patent Application Number: 62/332,292. Filing Date: May 5, 2016. UNT Technology Number: 12MO-2016-01; UNTP.P0001US.P1. (b) Omary, M. A.; Ivy, J. F. "Metal-Inorganic Frameworks", United State Patent and Trademark Office. U.S. Non-Provisional Patent Application Number: 15587053. Filing Date: May 4, 2017. UNT Technology Number: 12MO-2016-01; UNTP.P0001US/11704341.

Pioneered by Yaghi et al., a vast number of organic ligands with a variety of donor groups and over 40 metal cations have been explored in MOF construction.[1]

The idea of structured, porous materials has been extended to fully organic systems with covalent bonds between linkers rather than ionic bonds to metal clusters. These covalent-organic frameworks (COFs) use reversable, thermodynamically controlled linkages to form uniform pores out of organic linkers.[2,3] Metal-inorganic frameworks (MIFs), on the other hand, represent a new concept developed in this dissertation project whereby metal atoms or clusters are connected by inorganic complexes.

High volumetric capacity is an important property for gas storage applications. Particularly for $H_2$ and $CH_4$ storage in automobiles, the volumetric capacity is arguably more important than the gravimetric capacity. Due to their high porosity, the best MOFs known to date have disappointingly low densities (e.g., 0.43, 0.51, and 0.62 g/mL) leading to low $H_2$ and $CH_4$ volumetric uptake[4,5] with a few exceptions.[6] Due to the additive size and function of the metal, inorganic or organic ligand, and ligand substituents within their inorganic complex linker, MIFs offer the potential to achieve significantly higher and more efficient hydrogen uptake and volumetric storage capacity than MOFs do at both cryogenic and near-ambient temperatures.

Nanostructured carbon materials (e.g., carbon nanotubes, graphite nanofibers, activated carbon, and graphite) and porous MOFs have become of interest to researchers as potential hydrogen adsorbents. However, it has been shown that nanostructured carbons have slow uptake, exhibit irreversible adsorption, and contain reduced transition metals as impurities. Meanwhile, known MOFs have low volumetric $H_2$ uptake due to their low densities and weak affinity to hydrogen molecules. In addition, the porous nature and high surface areas of MOFs

give rise to rather weak $H_2$ adsorption energies (~ 5 kJ/mol), whereas vehicular use requires ~15kJ/mol.[7,8]

Oil, natural gas, and petroleum products (hydrocarbons) are some of the most important energy sources in the world. As long as oil is prospected, transported, stored, and used, there will be a risk of spillage that may result in significant environmental damage and vast economic loss. It is estimated that the oil spill clean-up costs worldwide amount to over $10 billion dollars annually. The adverse impacts to ecosystems and the long-term effects of environmental pollution by these and other releases call for an urgent need to develop a wide range of materials for cleaning up oil from impacted areas, especially because the effectiveness of oil treatment varies with time, type of oil and spill, location and weather conditions. There are many adsorbents in use for oil spill cleanup, including sand, organo-clays and cotton fibers. These adsorbents, however, have strong affinity to water, limiting their effectiveness in cleanup operations. Therefore, the development of waterproof sorbents that are effective even at very low concentrations of oil residue remains an urgent challenge.

MOFs are promising adsorbents for many guest molecules, although reports concerning adsorption of hydrocarbons (organic vapor) in MOFs remain scarce compared to their $H_2$, $CO_2$, CO, and inert gas adsorption. Thus, the search for MOF and MIF materials with the desirable combination of good thermal stability, high selectivity, and excellent recyclability is a major challenge and of great technological importance for oil spill cleanup, hydrocarbon storage in a solid matrix for safer transportation, catalysis, water purification, component and isomer separation from gasoline mixtures, and environmental remediation of greenhouse gases.

MIFs, when considered in this aspect, will have higher metal concentration than MOFs.

With this higher metal content, there will also be more coordinating sites on the inorganic linkers, allowing for stronger adsorption of gases. These metal sites will also prove to be more tunable than those in MOFs, that have already been used for catalysis.[9,10]

### 1.1.2 Fluorinated Porous Materials*

It has been shown that M/DOBDC (MODBC = 2,5-dioxido-1,4-benzenedicarboxylate MOFs show a significant decrease in $CO_2$ capture capacity under humid conditions.[11] Hydrophobic MOFs could be an attractive alternative, due to their ability to withstand humid conditions and suppress competitive adsorption of water. Several studies in the literature have investigated the effects of fluorination and hydrophobicity in MOFs. FMIF-1 is a fluorous metal–organic framework first synthesized in the Omary lab by Yang et al.[12] It is formed by the reaction of a perfluorinated ligand (3,5-bis(trifluoromethyl)-1,2,4-triazolate ($Tz^-$)) with an $Ag^+$ precursor, leading to $\{Ag_2[Ag_4Tz_6]\}$. FMIF-1 and polymorphs/structural isomers thereof exhibit a perfluorinated structure, and the many $CF_3$ groups lining their channels and small pockets imbue them with hydrophobicity. FMOFs, herein recategorized as F-MIFs, have proven to be efficient adsorbents for high volumetric uptake of $H_2$, $O_2$, $N_2$, $CH_4$, $C_6$-$C_8$ hydrocarbons, and $CO_2$. While previous attempts by other groups failed to counteract the higher material density resulting from fluorination in partially fluorinated MOFs, the perfluorinated FMOFs/F-MIFs have attained the desired high

*Parts of this section are reproduced from the following publications: A)Galli, Simona; Cimino, Alessandro; Ivy, Joshua F.; Giacobbe, Carlotta; Arvapally, Ravi K.; Vismara, Rebecca; Checchia, Stefano; Rawshdeh, Mustafa A.; Cardenas, Christian T.; Maspero, Angelo; and Omary , Mohammad A. "Fluorous Metal-Organic Frameworks and Non-Porous Coordination Polymers as Low-κ Dialectrics: A Case Study", Submitted for Publication; B) P. Z. Moghadam, J. F. Ivy, R. K. Arvapally, A. M. dos Santos, J. C. Pearson, L. Zhang, E. Tylianakis, P. Ghosh, I. W. H. Oswald, U. Kaipa, X. Wang, A. K. Wilson, R. Q. Snurr and M. A. Omary, "Adsorption and molecular siting of CO2, water, and other gases in the superhydrophobic, flexible pores of FMOF-1 from experiment and simulation" *Chem. Sci.*, 2017, **8**, 3989

volumetric gas storage.

### 1.1.3 Fluorinated Zeolitic Imidazolate Frameworks

Zeolitic imidazolate frameworks (ZIFs) are a particular class of metal-organic frameworks that imitate the general pore structure of zeolite materials.[13,14] They typically consist of a zinc metal center coordinated to several imidazolate groups. In the case of ZIF-8, 2-methylimidazole coordinates with Zn(II) to form a highly porous framework ( Figure 1.1). This product has been shown to be hydrophobic, as measured by water adsorption isotherms.[15] Ortiz et al. used Monte Carlo simulations to show the hydrophobicity or hydrophilicity of a series of ZIF materials.[16] They analyzed ZIF-8 with the original imidazolate functional groups as well some isostructural ZIFs with added hydrophobic or hydrophilic groups on imidazolate linkers, and found that altering functional groups can be used for tuning the hydrophobicity of a ZIF material.

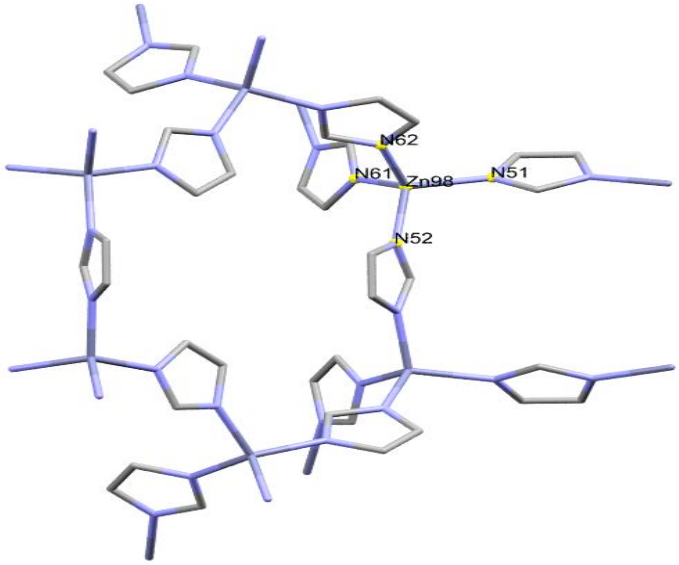


**Figure 1.1: ZIF-8**

Lalonde et al. used solvent-assisted linker exchange (SALE) to introduce ligands with fluorinated functional groups into a ZIF framework.[17] By selectively replacing 5-

chlorobenzimidazolate with = 5-(trifluoromethyl)benzimidazole, they added fluorine groups into ZIF materials. However, the authors showed little difference in the water adsorption profile compared to the unmodified version. There were other functionalized ligands in the framework, namely 2-nitroimidazole, which correlated to hydrophilicity. More recently, Liu et al. synthesized a ZIF out of a fluorine-functionalized ZIF-90 imidazole ligand.[18] They reported superhydrophobicity in the ZIF, at the cost of losing surface area to the bulky pentafluoroaniline group.

Fluorine groups have been shown to affect the hydrophobicity in a coordination polymer, either porous or nonporous. Perfluorination of the linkers have shown to increase hydrophobicity dramatically versus its nonfluorinated analog, and partially fluorinated linkers have even shown to increase hydrophilicity in some instances. As an extension to existing studies, fluorinated ligands are being used to synthesize new ZIFs, or F-ZIFs. We expect these materials to exclude water similarly to FMIF-1, granting them all the benefits of the FMIF with higher surface area and volumetric adsorption capacity.

## 1.2 Photophysical Properties *

### 1.2.1 Use MOF/Polymer Regime to Improve Conductivity vs Small Molecules

In the past two decades, metal-organic frameworks (MOFs), also addressed as

* Parts of this section are reproduced from the following publications: A) Omary, M. A.; Cimino, A.; Almotawa, R.; Maspero, A.; Giacobbe, C.; Palmisano, G.; Yang, C.; Ivy, J. F.; Williams, C.; Rawashdeh-Omary, M. A.; Galli, S. "Are MOFs et al. really the next best thing since sliced bread? A case study for electronic device apps", Prepr. – Am. Chem. Soc., Div. Ener. Fuels 2015, 60, 391-392, B) Galli, Simona; Cimino, Alessandro; Ivy, Joshua F.; Giacobbe, Carlotta; Arvapally, Ravi K.; Vismara, Rebecca; Checchia, Stefano; Rawshdeh, Mustafa A.; Cardenas, Christian T.; Maspero, Angelo; and Omary , Mohammad A. "Fluorous Metal-Organic Frameworks and Non-Porous Coordination Polymers as Low-κ Dialectrics: A Case Study", Submitted for Publication

coordination polymers (CPs), have emerged as a new class of materials implicated in industrially relevant applications ranging from the more traditional ones of gas storage, gas separation and heterogeneous catalysis, to the latest ones involving electronic devices, cancer treatment, and sensing – among a multitude of proposed applications for MOFs and related molecular porous solids (ZIFs, COFs, PCNs, etc.).[19] Depending upon metal/central atoms and organic linkers adopted, key properties – such as pore size and functionalization, specific surface area, guest binding capability and catalytic activity – of MOFs et al. can be potentially modulated.

MIFs and FMIFs specifically can be appropriately tuned to further increase low- κ centers in its structure beyond FMIF-1, which shows a good, if only initial, proof-of concept.

### 1.2.2 Nonporous MIF Advantages

Opposed to MOFs that can be designed to exhibit significant porosity, which typically implies discarding the non-porous or less porous species in favor of "superstar" materials, one would be in a "win/win situation" upon the isolation of porous or non-porous coordination polymers, which genuinely self-assemble due to their coordination propensities. Our collaborative efforts are currently focused on functional non-porous coordination polymers (FN-PCPs), which we wish to communicate herein some of their advantages vs. MOFs and other related porous molecular solids. Thanks to their high density, FN-PCPs could be used in electronic, photonic, and magnetic devices, given that the semiconducting, luminescent, light-harvesting, and magnetic functions are proportional to the number of charge carriers (polarons), excitons (luminophores or chromophores), and magnetons, respectively, per unit area of a thin film-based device. The absence of porosity might be very advantageous also for the fabrication of low-κ

dielectrics for integrated circuit (IC) devices or corrosion protection. In spite of this, only a few reports, regarding exclusively MOFs but not FN-PCPs, have been published to date to focusing on dielectric properties.[20,21]

The aim of the present work is to illustrate the high versatility of self-assembled FN-PCPs, the functional properties of which are strictly correlated to their composition and crystal structure, so as to prescribe the embodiment obtained "as is" for its best application(s). While self-assembly could yield MOFs and related porous materials, we aim to show how it is feasible to systematically bias the effort toward non-porous analogues. Moreover, even when porous solids are obtained, they can be "stuffed" with active guest molecules that will improve their use for electronic device-related applications.

Recent theoretical and experimental investigations have drawn the attention to non-fluorous and fluorous metal-organic frameworks as low-κ materials.[22-24] Fluorous metal-organic frameworks (FMOFs), fluorous metal inorganic frameworks (FMIFs) and fluorous non-porous coordination polymers (FN-PCPs) are potentially promising alternatives to current low-κ dielectrics as they possess a number of desirable traits in one material, namely: i) Controlled and reproducible chemical composition; ii) reproducible crystal structure, which allows controlled and correspondingly reproducible physio-chemical properties, which is not always the case with amorphous materials; iii) low adsorptivity of high-κ species.

Absence of porosity, as in FN-PCPs, inhibits the adsorption of water. In both FMOFs and FN-PCPs, fluorination promotes an intrinsic increase in hydrophobicity. Despite its permanent porosity, FMIF-1 is superhydrophobic, as demonstrated by experimental contact angles of 158°. Recently, three perfluorinated copper(II)-based FMOFs have been reported to exhibit

hydrophobic behavior with contact angles in the range 108-151°.[25] Superhydrophobic FMOFs allow a platform for further reduction of κ without allowing water to access their pores and increase the effective κ value.

High material density, especially in FN-PCPs, imparts a high concentration of low-κ centers, which concomitantly helps decrease the concentration of high-κ centers and increase transistor density. Below is a table of results of κ measurements, showing that these FMOFs and FMIFs are superior to the next-best case of hydrophobic MOF, ZIF-8.

| Compound | $\kappa$ at $2\times10^6$ Hz (ambient RH) | $\kappa$ at $2\times10^6$ Hz (~saturated RH) |
|---|---|---|
| FMIF-1[a] | 1.89(1) [1.63(1)] | n.a. |
| FN-PCP-1 | 2.57(3) | 2.64(4) |
| $[Ag_2(BTB)]$ | 3.79(1) | n.a. |
| FMOF-3 | 2.44(3) | 2.51(3) |
| lc-[Cu(BTB)(DMF)] | 2.94(8) | n.a. |
| ZIF-8 | 1.95(3) | 5.90 |

**Figure 1.2: Values of κ at 2 V And 2×106 Hz for FMOF-1 (Pressed at 69 and 103 bar), FN-PCP-1, [Ag2(BTB)], FMOF-3, lc-[Cu(BTB)(DMF)], and ZIF-8 Under Ambient and Near Saturated Humidity Levels. Values for pellet pressed at 103 bar in square brackets.**

## 1.3 Overview of Dissertation

This dissertation represents part of the work performed by the author during his graduate studies at UNT. The candidate has coauthored several other publications, including co-inventing the MIF compositional patents, that have been published or submitted for publication[26-30] but are not described in the subsequent dissertation chapters.

### 1.3.1 FMOF-1 Revisited: Carbon Capture and Luminescent Derivatives

This chapter sets forth to describe isosteric heat of adsorption studies of FMIF1 for $CO_2$ at

near ambient temperatures, suggesting promise for carbon capture and storage. We then successfully exchanged some of these Ag(I) centers with Au(I) to form an isostructural Au-FMIF-1. In the second part of this chapter, a family of luminescent extended solids are observed. The first family is based on the FMIF-1 materials 3,5-bis(trifluoromethyl)-1,2,4-triazolate (tz) and silver(I).

Compounds of 3,5-bis(trifluoromethyl)-1,2,4-triazole and Ag(I) have produced multiple structures previously, most notably the fluorous metal-organic frameworks FMIF-1 and FMOF-2. While the focus has been upon gas adsorption properties, no published work yet exists about materials of this type that exhibit photoluminescence. Upon combining these materials with diimine bridging ligands, 4,4'-bipyridine, pyrazine, and a Pt(II) complex containing two oppositely-situated non-coordinating pyridines, we showed novel luminescent properties not seen with this class of silver-triazolate material. This strategy attained luminescent products better-positioned for photonic devices than porous materials due to greater exciton density.

### 1.3.2 Coordination Polymers of $Pt(P_2O_5)_4$ (Pt(POP))

Pt-based Inorganic building blocks were used to generate a new series of MIFs. Zinc, zirconium, nickel and manganese were used to form these new inorganic polymers. They were analyzed by low pressure nitrogen adsorption, diffuse reflectance, and photoluminescence spectroscopy. Zr and Zn-based MIFs showed enhanced luminescence properties compared to the solid starting material. Mn and Ni were accordingly shown to quench luminescence. MIFs show promise as functional materials for the stabilization of otherwise unstable luminescent materials.

These first-generation materials show potential for further use as porous materials to be used as doped white-light emitters.

### 1.3.3 Homoleptic Platinum Complexes and Their Coordination Polymers

Chapter 4 overviews the design and application of new MIF linkers. Pt complexes based upon (pyridyl)azolates, functionalized with carboxylic acid groups, have been synthesized. These complexes, and their esterized precursors, show strong luminescence on their own. They have been used to generate new luminescent MIFs which may be useful toward future inorganic (LEDs) or organic (OLEDs) light-emitting diodes. The electronic communication along their infinite coordination structures is desirable for color tuning and enhanced conductivity functions, compared to the small molecules used in such technologies, which rely on intermolecular interactions for these functions.

# CHAPTER 2

# FMOF-1 REVISITED: CARBON CAPTURE AND LUMINESCENT DERIVATIVES*

## 2.1 Introduction

Metal organic frameworks are a class of materials that have gained increasingly more attention and popularity over the past 15 years. The beginning of this surge in popularity arguably happened with the publication of MOF-5 by Li et al.[31] This material exhibited remarkable temperature stability and surface area, having been formed with metal centers bound together by dicarboxylate ligands. Since then, the field has grown dramatically, with research going into applications such as hydrogen storage[32], catalysis[9], and carbon capture.[33]

A metal organic framework is generally composed of an organic linker attached to a metal cluster, typically by a metal-oxygen or metal-nitrogen bond.[34] They are differentiated from the broader class of coordination polymers by their porosity.[35] The porosity of MOFs vary widely and are mostly dependent on the size and shape of the linker. Interpenetration is also a common concern with the synthesis of MOFs, where a framework grows within the pores of another.[36,37] Generally, this is most common in MOFs with large linkers that are not exceptionally bulky and thus have large pores. While in some cases this interaction is favorable, allowing for uses such as interesting gas separations, it almost always results in a decrease of pore volume and surface area.[38]

* Portions of this chapter have been reproduced from two publications that the candidate has co-authored: A) P. Z. Moghadam, J. F. Ivy, R. K. Arvapally, A. M. dos Santos, J. C. Pearson, L. Zhang, E. Tylianakis, P. Ghosh, I. W. H. Oswald, U. Kaipa, X. Wang, A. K. Wilson, R. Q. Snurr and M. A. Omary, "Adsorption and molecular siting of CO2, water, and other gases in the superhydrophobic, flexible pores of FMOF-1 from experiment and simulation" *Chem. Sci.*, 2017, **8**, 3989, B) Omary, M. A.; Cimino, A.; Almotawa, R.; Maspero, A.; Giacobbe, C.; Palmisano, G.; Yang, C.; Ivy, J. F.; Williams, C.; Rawashdeh-Omary, M. A.; Galli, S. "Are MOFs et al. really the next best thing since sliced bread? A case study for electronic device apps", Prepr. – Am. Chem. Soc., Div. Ener. Fuels 2015, 60, 391-392.

In early MOF materials, there were issues with atmospheric stability; this is still an problem with many MOF materials, particularly those with open metal sites.[10,39] It can be difficult to fully activate open metal sites due to strong solvent molecule binding at the site, and just as difficult to retain that activated state outside of an inert environment. However, the open metal sites do provide stronger gas adsorption and is seen as a potential way to increase effective surface area.[40]

Metal organic frameworks have grown to prominence as a potential material for use in the capture and storage of carbon dioxide.[33,41] Capture of carbon dioxide or mitigation of its production and release into the atmosphere is likely to be the most important environmental task to perform over the next century. Extensive reports have been made by the Intergovernmental Panel on Climate Change on the current effects of greenhouse emissions and possible means of mitigation.[42] Mitigation of $CO_2$ emissions will be a multi-step process involving reducing emissions from sources as well as capture and storage of current production. MOFs in the future may prove to be good candidates for capture as well as storage of carbon dioxide.

Capturing carbon from flue gas is an important challenge, as fossil fuel combustion continues to be a primary source of energy. The search for adsorbents capable of capturing large amounts of $CO_2$ has led to many studies of adsorption in MOFs, which show promise for a number of separation applications including $CO_2$ capture at the low partial pressures relevant to flue gas.[34,43,44] In an early example, Yazaydin et al. screened 14 MOFs and concluded that the M/DOBDC series shows exceptionally high $CO_2$ capacity at room temperature.[45] This can be attributed to the high density of open metal sites, and other studies on $CO_2$ capture in MOFs have shown similar results. After the CO2 is captured, it must be stored or used afterward. One option

is permanent subterranean storage as a pressurized liquid. Alternatively, it could be converted and used as other chemical products. Darensbourg et al. recently reported $CO_2$ capture in a MOF, HKUST-1, to perform a copolymerization with propylene oxide with a 49.9% conversion rate.[41]

FMOF-1 is a material intensively studied in this lab, and one that has multiple special properties that could help it adsorb industrial $CO_2$ from flue gas produced from power plants. It has been shown to have good stability in heat and aqueous environments; in fact, the material is quite hydrophobic. Its reported surface area is 810 $m^2/g$ and shows a type IV adsorption pattern with nitrogen, oxygen and hydrogen.[12] The reason for these two steps is because there are two adsorption sites in the material; large channels surrounded by smaller pockets (Figure 2.1). During adsorption studies the small pockets fill first, followed by the larger channels. This gives FMOF-1 a type IV isotherm with the absorption of most gasses.

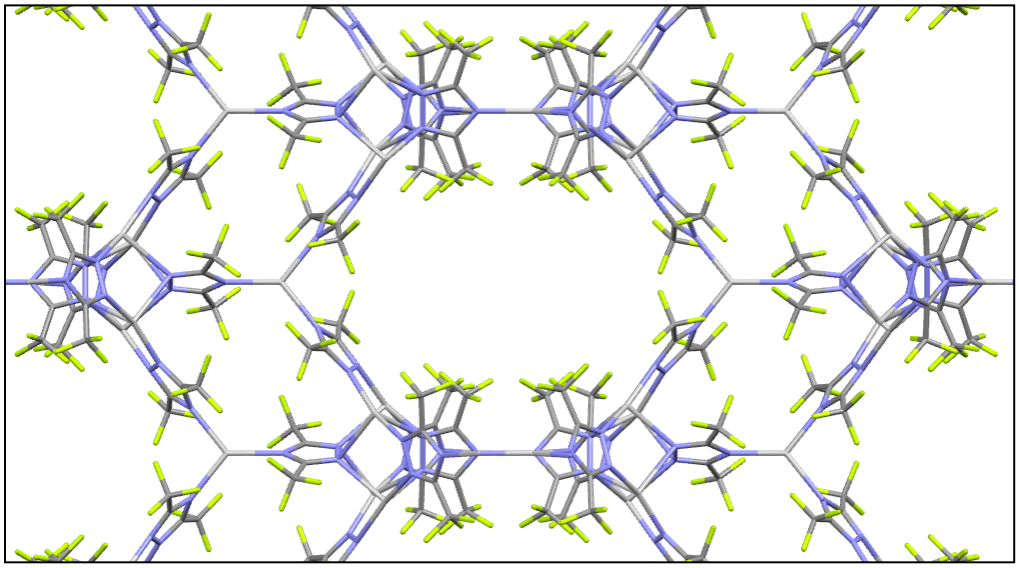

**Figure 2.1: Cross section of FMOF-1 showing the larger channels and smaller cavities**

To date, there has been little published work on FMOF-1's ability to adsorb and capture carbon dioxide. The first part of this chapter focuses on attaining FMOF-1 high pressure isotherms

of $CO_2$ and subsequently using them to determine the isosteric heat of adsorption of $CO_2$ within the material. Attaining this metric will help us to evaluate FMOF-1's capability to capture and effectively hold $CO_2$ at various levels of uptake.

## 2.2 Experimental

### 2.2.1 FMOF-1

FMOF-1 was prepared according to previously reported methods.[12,46,47]

### 2.2.2 $Ag_6(bpy)_3(tz)_2(NO_3)_4$ FMOF-bpy($NO_3$) Synthesis

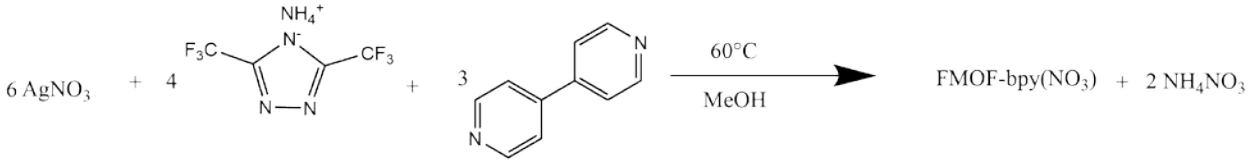


In a 50mL round-bottom flask, 10mL MeOH and 0.1665g (0.10mmol) silver nitrate were combined and stirred while heating for 30 minutes at 60°C until the silver nitrate was dissolved. Bipyridine (0.0765g, 0.049mmol) and 3,5-bis-trifluoromethyl-1,2,4-triazole (0.100g, 0.45mmol) (tz) was then added to the flask and left stirring overnight. The solid at the end of the reaction was then filtered out, washed with methanol and water, and dried in a vacuum oven at 60°C overnight. Yield 0.14g (0.079mmol), 48%. Elemental analysis: C 25.75%, H 1.37%, N 12.65%, F 12.87%. Found: C 26.75%, H 1.08%, N 12.53%, F 13.15%

### 2.2.3 $Ag_3(pyz)_2(tz)(NO_3)_2$ FMOF-pyz($NO_3$) Synthesis

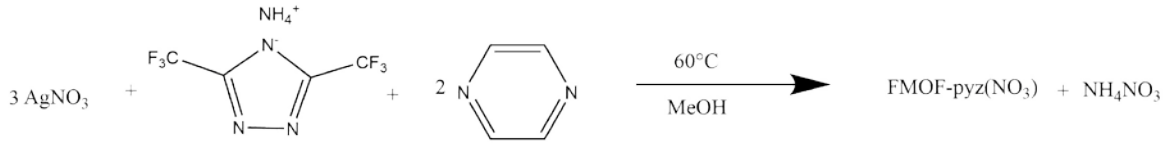

In a 50mL round-bottom flask, 10mL MeOH and 0.1663g (0.01 mmol) silver nitrate were combined and stirred while heating for 30 minutes at 60°C until the silver nitrate was dissolved. Pyrazine (0.045g, 0.56mmol) and 0.100g (0.45mmol) tz was then added to the flask and left stirring overnight. The solid at the end of the reaction was then filtered out, washed with methanol and water, and dried in a vacuum oven at 60°C overnight. Yield 0.20g (0.25mmol), 75%. Elemental analysis: Expected: C 25.76%, H 1.00%, N 15.53%, F 14.04%; Found: C 17.49%, H 0.65%, N15.40%, F 13.05%.

### 2.2.4 FMOF-bpy Synthesis

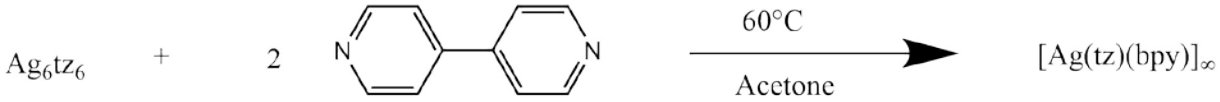


To a solution of 0.100g (0.05mmol) FMOF-1 in 10 mL acetone, a solution of 0.050g (0.3mmol) 4,4' bipyridine in 5mL acetone was added while stirring. The solution was left stirring at 60°C for 2 hours. After 2 hours, the solution was cooled and filtered with a fritted funnel, and rinsed with acetone before drying in a vacuum oven overnight at 60°C. Yield 0.0894g (0.095mmol), 60%.

Material was recrystallized by dissolving FMOF-1 in acetonitrile, and then layering a solution of 4,4’ bipyridine in acetone on top. Crystals of FMOF-bpy grew slowly overnight on the interface for analysis.

### 2.2.5 FMOF-PTA Synthesis

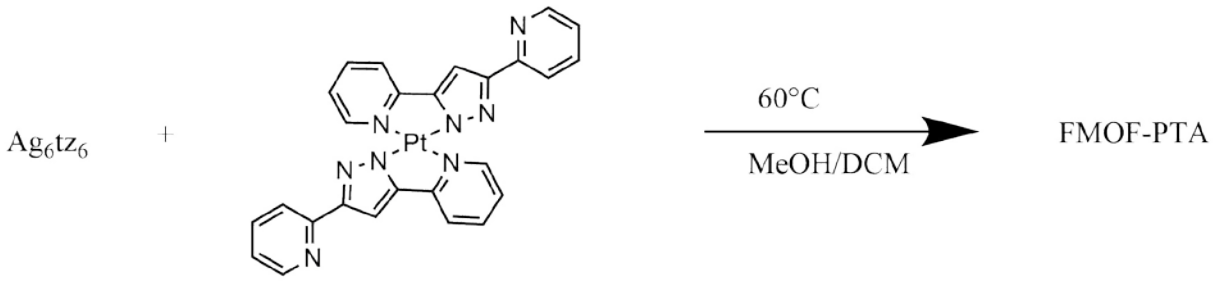


In 10mL methanol, 0.073g (0.04mmol) FMOF-1 material was dissolved while heating to 40°C. $Pt(ptp)_2$ (0.025g, 0.04mmol) was added to the FMOF-1 solution along with 2mL dichloromethane. A bright red precipitate immediately formed and was filtered from solution. The solid was washed with water and methanol, then dried overnight in a vacuum oven at 60°C. Yield: 0.07g (0.028mmol), 70%. Elemental analysis: C 22.96%, H 0.64%, N 15.62%, F 27.24%; Found: C 24.80%, H 0.62%, N 14.59%, F 27.78%

## 2.3 FMOF-1 $CO_2$ Adsorption Measurements

### 2.3.1 FMOF-1 Activation and Structure Confirmation

Before taking isosteric heats of adsorption measurements on FMOF-1 samples, there must first be several quality checks to ensure the sample is well formed and that the pores have been properly evacuated. The best way to prove proper formation of the material is through powder x-ray diffraction (PXRD). While single crystals can easily be grown, FMOF-1 starting materials can coordinate to the solvent molecules to form new materials or even grow into a structural isomer. Since we have a reliable, published crystal structure for the material at room temperature, we can use a calculated powder pattern to compare to an experimental PXRD diffraction pattern. Since FMOF-1 is a flexible framework that changes its crystal parameters in different temperatures and even under different environments, patterns generated from crystal

structures taken at 100K under standard operating conditions may not match exactly.[46] Comparison of the FMOF-1 sample used during isosteric heat of adsorption measurements are shown in Figure 2.2.

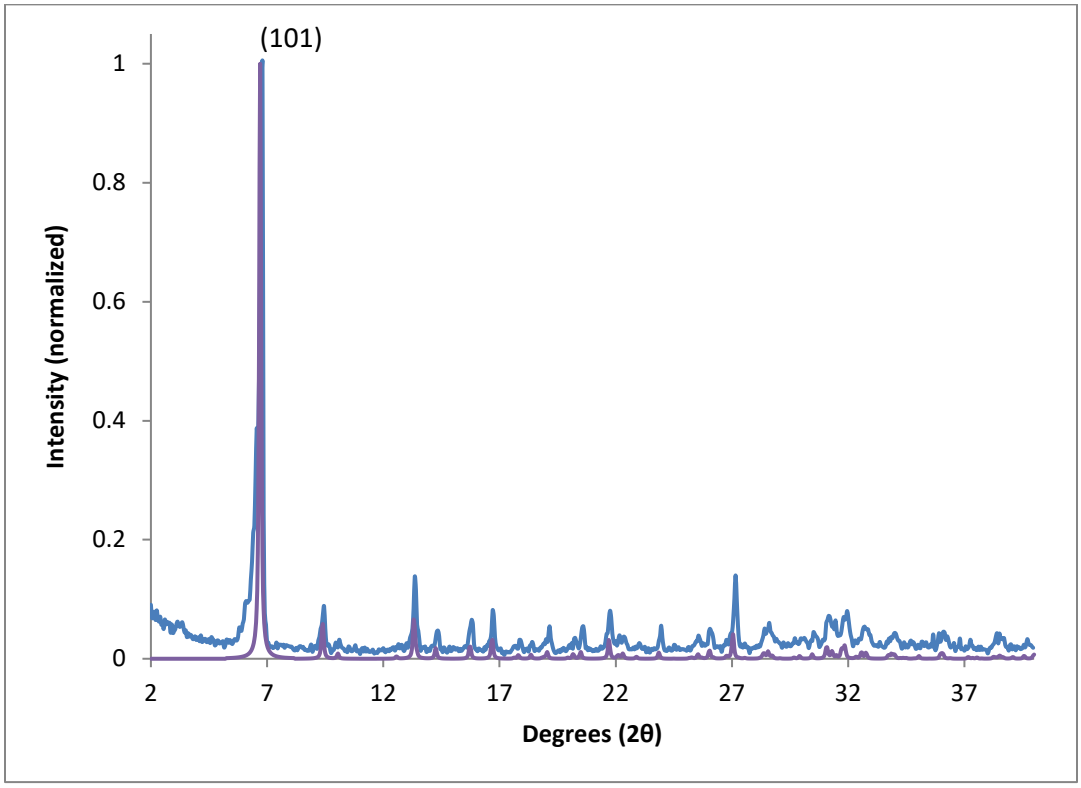


**Figure 2.2: PXRD of FMOF-1 sample (blue) vs calculated pattern from FMOF-1 room temperature crystal structure (red).**

An example of another product grown from FMOF-1 starting materials and one found as a side-product of FMOF-1 powder synthesis is FMOF-TOP. This material is initially formed upon the combination of tz and $AgNO_3$ in methanol. It must be filtered out from solution and is completely nonporous, but attempts at recrystallization of the material were unsuccessful; it was only soluble in solvents such as pyridine or acetonitrile which both coordinate so the silver triazolate complex upon recrystallization, generating a completely novel material. However,

recrystallizing FMOF-1 with zinc nitrate provided us with a crystal structure of a nitrate-coordinated silver triazolate structure (Figure 2.3).

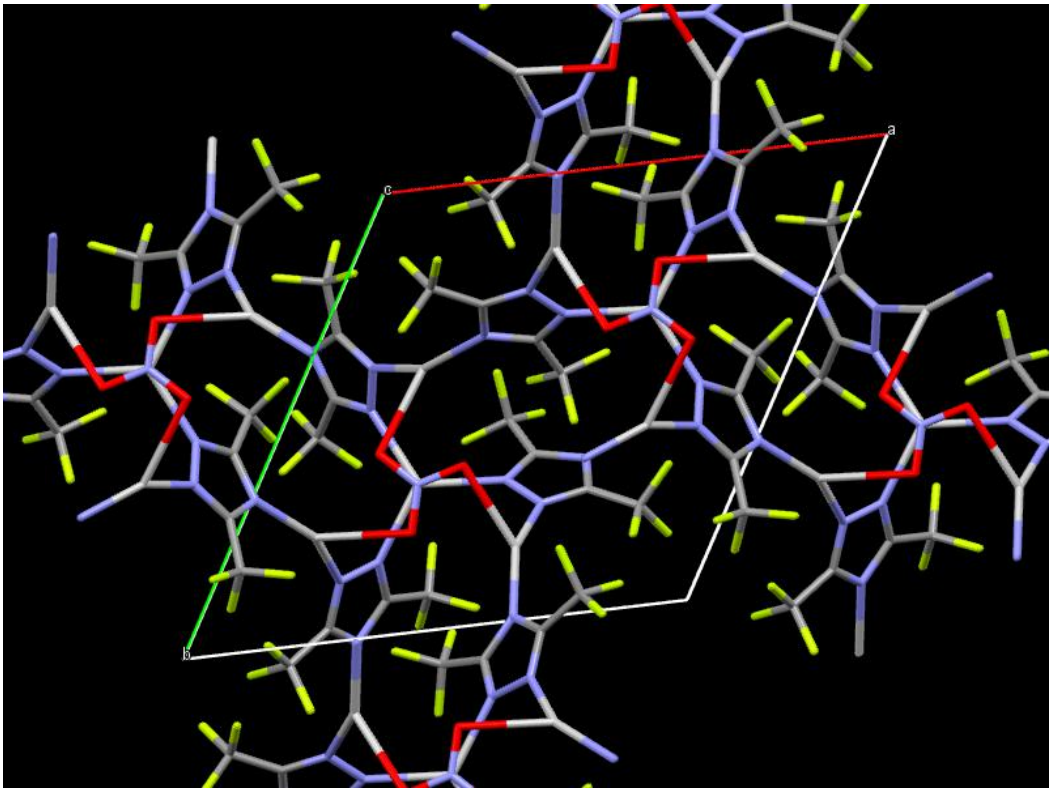


**Figure 2.3: Crystal structure of FMOF-TOP**

Upon analysis of FMOF-TOP's powder pattern, parameters were found that were similar to the simulated powder pattern from the crystal. The powder was found to have a hexagonal crystal lattice, and calculated volume and parameters versus that of the crystal are summarized in Table 2.1 crystal and powder calculated parameters and volume in nm.. Comparison of the calculated pattern from the crystal versus the experimental pattern from the powder is shown in Figure 2.4. There were small variations in the cell lengths and volume, but that is to be expected due to the difference in temperatures at which the crystal and powder measurements are taken (100K and 293K, respectively). This discovery gave us further insight into the reactivity of FMOF-1 and its various forms.

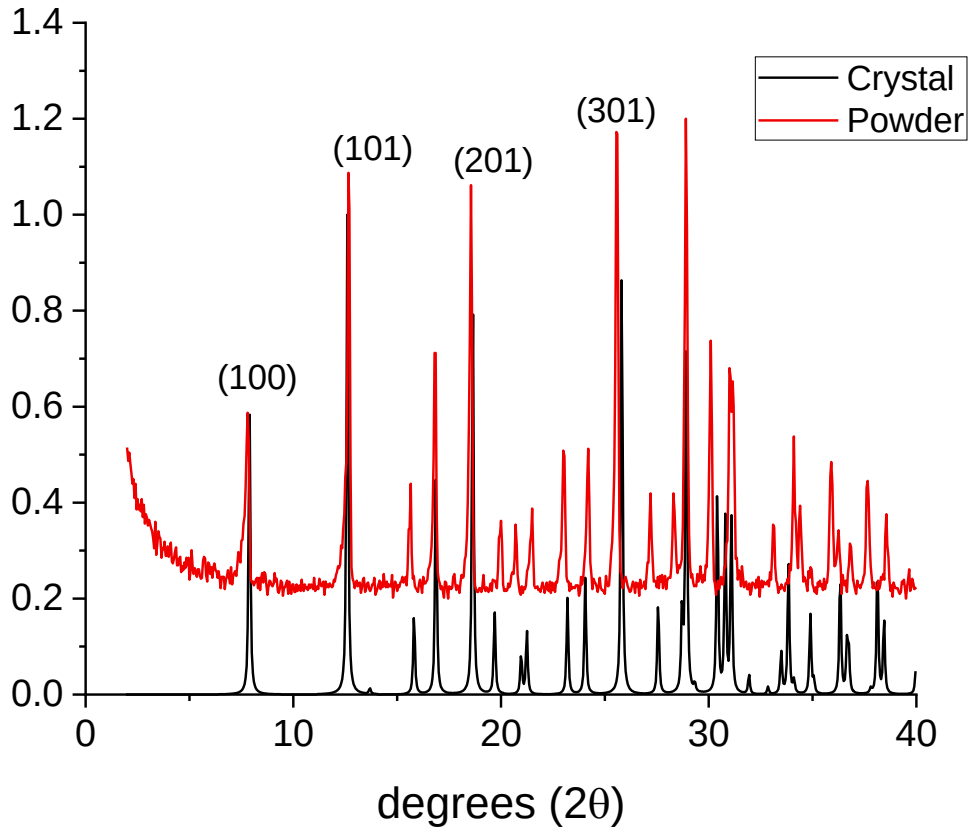


**Figure 2.4: FMIF-TOP powder pattern versus crystal structure**

**Table 2.1: Crystal and powder calculated parameters and volume in nm.**

| | Crystal | Powder |
|---|---|---|
| a= | 1.293 | 1.309 |
| c= | 0.901 | 0.8895 |
| V= | 1.3049 | 1.319906 |

### 2.3.2 FMOF-1 Isosteric Heat of Adsorption Measurement*

Once the structure of FMOF-1 is confirmed, a nitrogen isotherm is taken of the sample to ensure the material has been properly activated and to calculate BET surface area. To do this, we

* This section is based upon: P. Z. Moghadam, J. F. Ivy, R. K. Arvapally, A. M. dos Santos, J. C. Pearson, L. Zhang, E. Tylianakis, P. Ghosh, I. W. H. Oswald, U. Kaipa, X. Wang, A. K. Wilson, R. Q. Snurr and M. A. Omary, "Adsorption and molecular siting of

used a Micromeritics ASAP 2020 low pressure volumetric instrument. The values obtained here can be compared to theoretical calculations from the crystal structure or through previous experimental data from crystalline samples that have been published.[12] Figure 2.5 shows the $N_2$ isotherm of one of the powder samples used in these experiments. The published BET surface area of an FMOF-1 sample was 810.5 $m^2/g$, which is close to the current sample calculated at 733.9 $m^2/g$.[12] Once PXRD and surface area measurements are found to be equivalent to published data, our sample is confirmed to be correct and $CO_2$ isotherms can be collected.

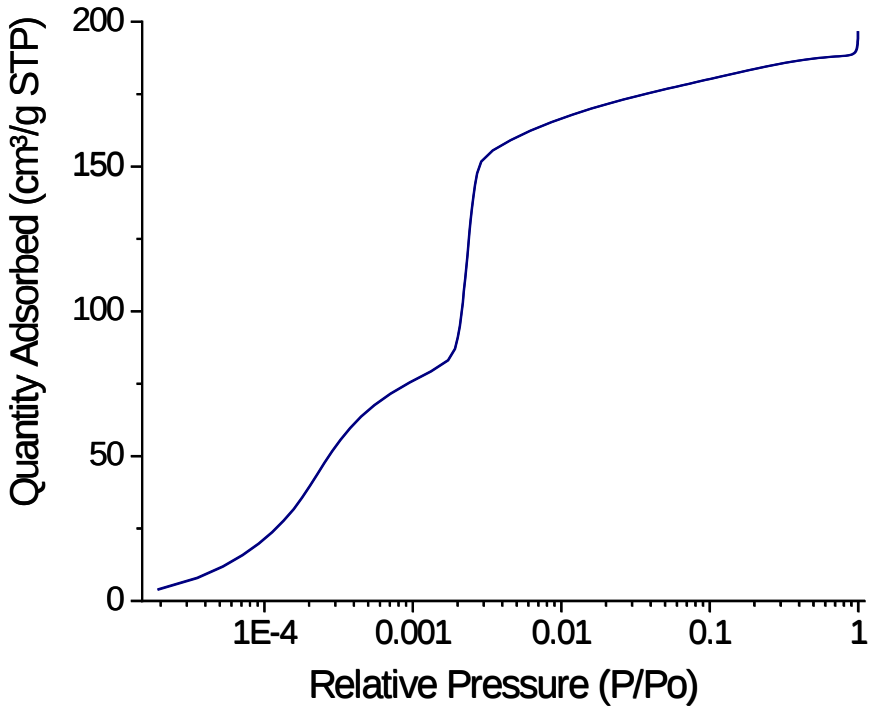


**Figure 2.5: Nitrogen isotherm up to one atmosphere and BET surface area, plotted logarithmically**

Isotherms were taken in five-degree intervals from 288K to 313K (Figure 2.6). While using

CO2, water, and other gases in the superhydrophobic, flexible pores of FMOF-1 from experiment and simulation" *Chem. Sci.*, 2017, **8**, 3989

only three isotherms is typically adequate, some inconsistencies between initial experiments suggested a higher degree of accuracy should be taken. With the extra experiments we were able to have more accurate trend lines for the enthalpy calculations that followed. Overall, the isotherms had a decreasing trend as the temperature increased, and some of the experiments in the midrange showed some potential character for a second step within the isotherm.

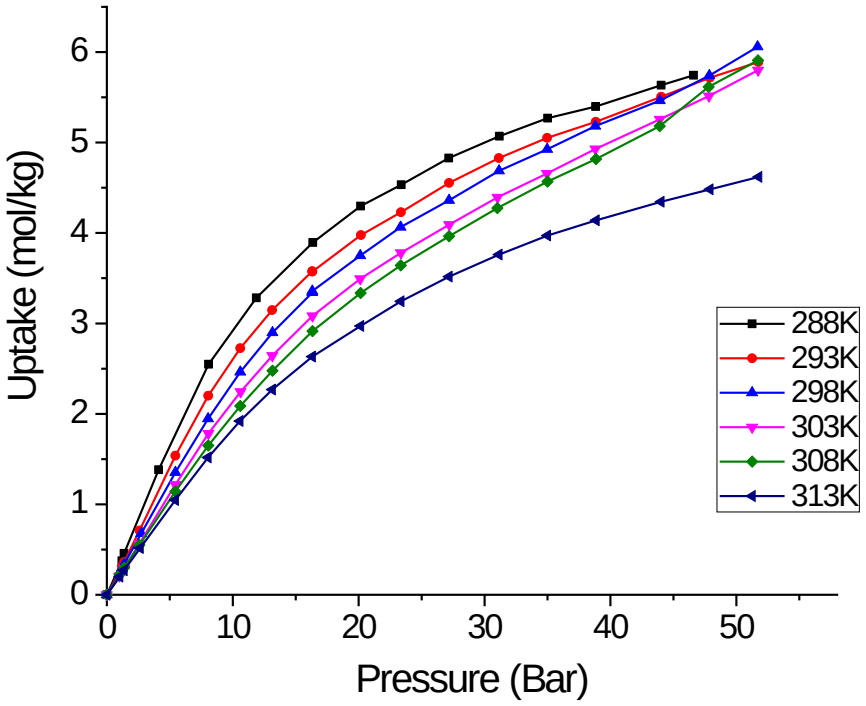


**Figure 2.6: $CO_2$ Isotherms of FMOF-1 used for isosteric heat of adsorption calculations**

Since our instrument is gravimetric the exact pressure can vary by up to several hundred torr between isotherm measurements, depending on the temperature and rate of adsorption by our material. However, we need comparable pressures and temperatures to determine heat of adsorption at specific pressures. To ensure accurate comparisons, the isotherms were traced by least squares polynomial functions and checked visually and by coefficients of determination.

The number of polynomials in the function were increased until $R^2$ was at least 0.999 and there were no significant points of deviation from the isotherm, especially where the volumes would be taken.

The data were plotted to get $CO_2$ uptake as a function of pressure. The isotherms were plotted as a function of uptake vs pressure, with pressure on the x-axis to provide an equation to calculate the theoretical uptake of each isotherm at each temperature per the model. A graph of these inversed functions can be seen in Figure 2.7 along with the least squares functions and $R^2$ values.

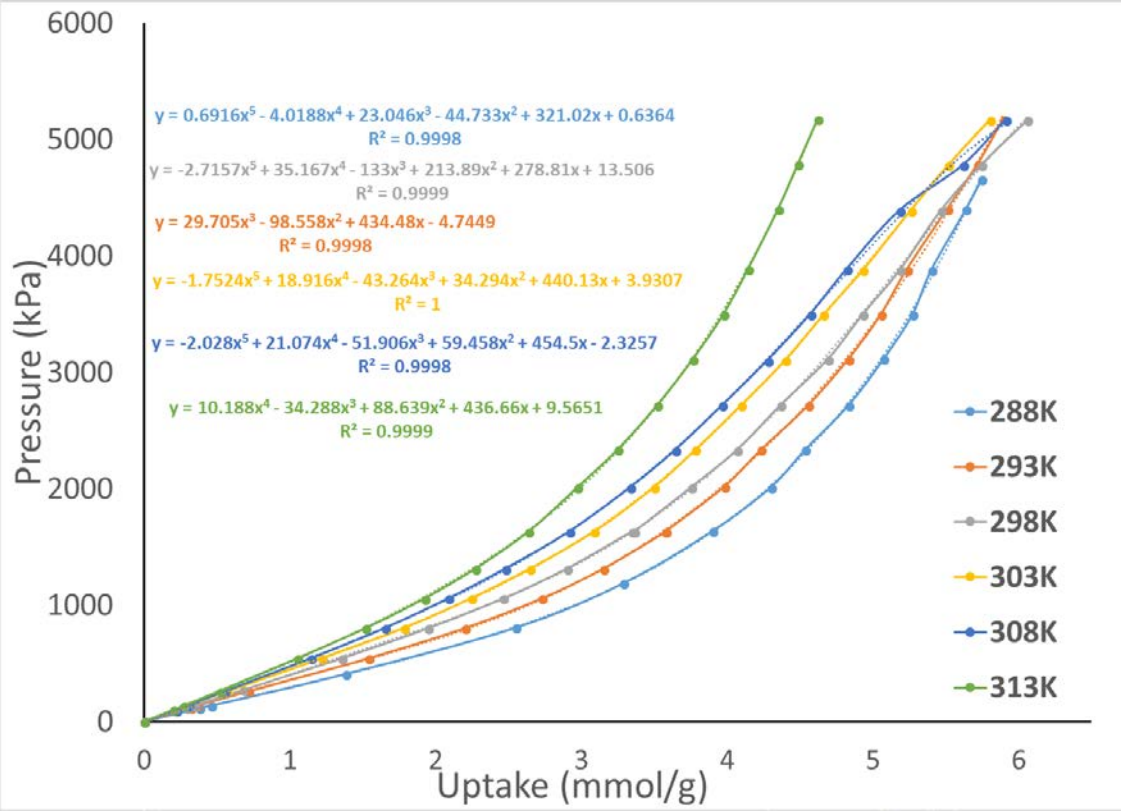


**Figure 2.7: Inverse isotherms used for $Q_{st}$ calculations, along with least their squares regression**

From these equations, we calculated approximate pressures at which each isotherm would reach specific pressures and plotted each set of uptake values as ln P over 1/T (Figure 2.8).

These were selected so that the slope would be directly related to the heat of adsorption for that temperature. The Clausius-Clapeyron equation which describes this relationship is summarized in eq. 2.1.

$$\ln(P) = -R\Delta H(\frac{1}{T}) \quad \text{(Eq. 2.1)}$$

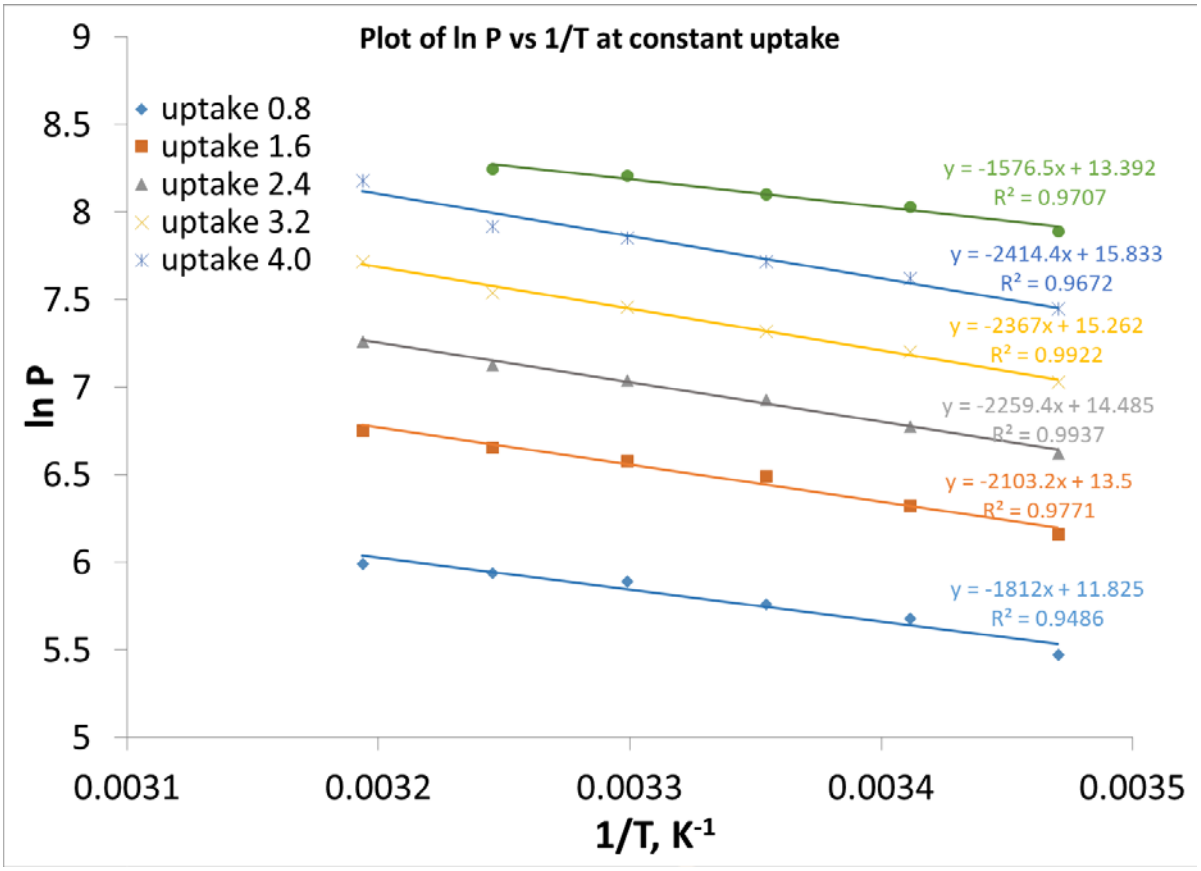


**Figure 2.8: Calculated uptake values of FMOF-1 isotherms, plotted in natural lof of pressure of inverse temperature. Linear regression equations and $R^2$ values shown on the side next to each uptake set.**

The slope of each pressure's linear least-squares line was transformed to calculate the isosteric heat of adsorption at that uptake, averaged between the individual temperatures.[48] The result is shown in Figure 2.8. The heat of adsorption was calculated to be 15-20 kJ/mol. Simmons et al. presented an excellent summary of common MOF materials and their heats of adsorption for $CO_2$.[49] The BET surface areas, gravimetric capacities and $Q_{st}$ values of a few select materials

are shown in Table 2.2. A quick comparison shows that FMOF-1 falls in the middle of the pack in terms of heat of adsorption and on the lower end of gravimetric surface areas and capacity. However, looking at the volumetric surface areas FMOF-1 is superior to the others. Also, most of the materials with higher heats of adsorption are those with open metal sites. While these are very beneficial for adsorption, they are also susceptible to binding strongly with water and generally special care must be taken to prevent this before sorption experiments. Overall, FMOF-1 has strong potential as a temporary storage option such as inside a gas cylinder, or a means of increasing carbon dioxide capacity while maintaining lower operational pressures. The heat of adsorption allows the carbon dioxide to freely desorb without heating of the material.

**Table 2.2: List of BET surface areas and heats of adsorption of $CO_2$ for various metal organic frameworks. Unless otherwise noted or FMOF-1, data comes from Simmins et al.[49]**

| Framework | BET Surface Area ($m^2\ g^{-1}$) [$m^2\ cm^{-3}$] | Capacity (wt. %) | Qst (kJ $mol^{-1}$) |
|---|---|---|---|
| MOF-5 | 3500 [700] | 48.8[33] | 15 |
| Mg-MOF-74 | 1332[33,50] [600] | 31.4 | 45 |
| ZIF-8 | 1980 [693] | 39[33] | 17 |
| HKUST-1 | 1690 [591] | 32[33] | 28.1 |
| FMOF-1 | 810.5[12] [1442] | 22.3 | 20 |

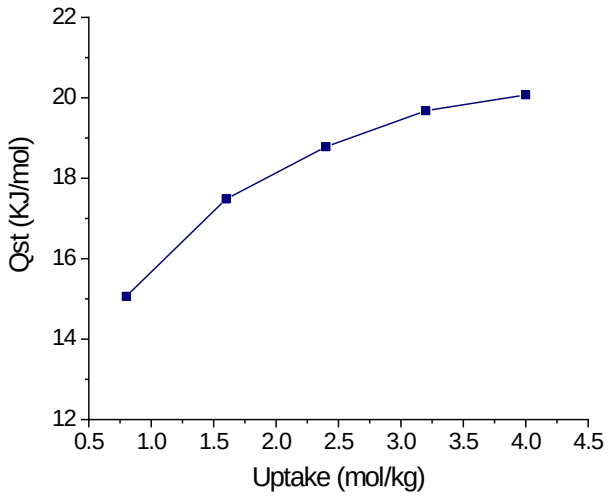


**Figure 2.9: Heat of adsorption of carbon dioxide for FMOF-1 as a function of uptake.**

### 2.3.3 Toth Plots

Toth plots are generally great at modelling Type I isotherms.[51] However, FMOF-1 has two different pore sizes, which presents as a type IV or two-step isotherm for small molecules, as is seen in with nitrogen. Moghadam et al. recently ran simulations in collaboration with the Omary group on the $CO_2$ adsorption of FMOF-1 and showed that the small pores in FMOF-1 do not play a role in the modeled adsorption.[26] These models show good agreement with FMOF-1 experimental values up to 30 bar. However, deviations from the standard Toth model begin to show as the pressures increase to 50 bar, and a second shoulder in the isotherm appears to present itself at about 40 bar (Figure 2.10). Extrapolation of this data to 100 bar should at best represent the lower limit of $CO_2$ adsorption at that pressure (Figure 2.11).

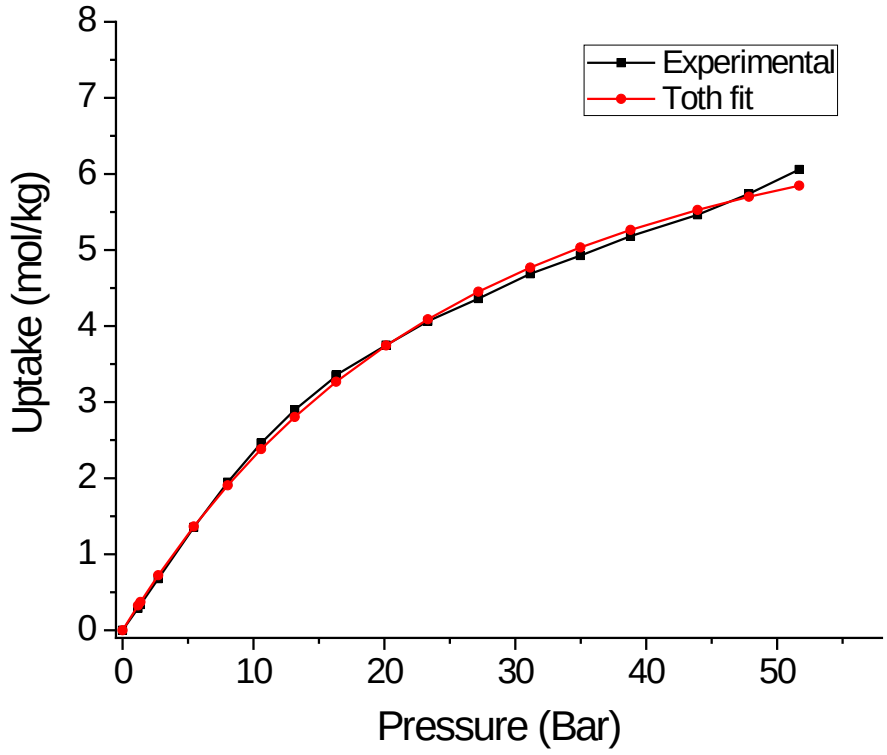


**Figure 2.10: Toth fitting of FMOF-1 $CO_2$ isotherm at 298K**

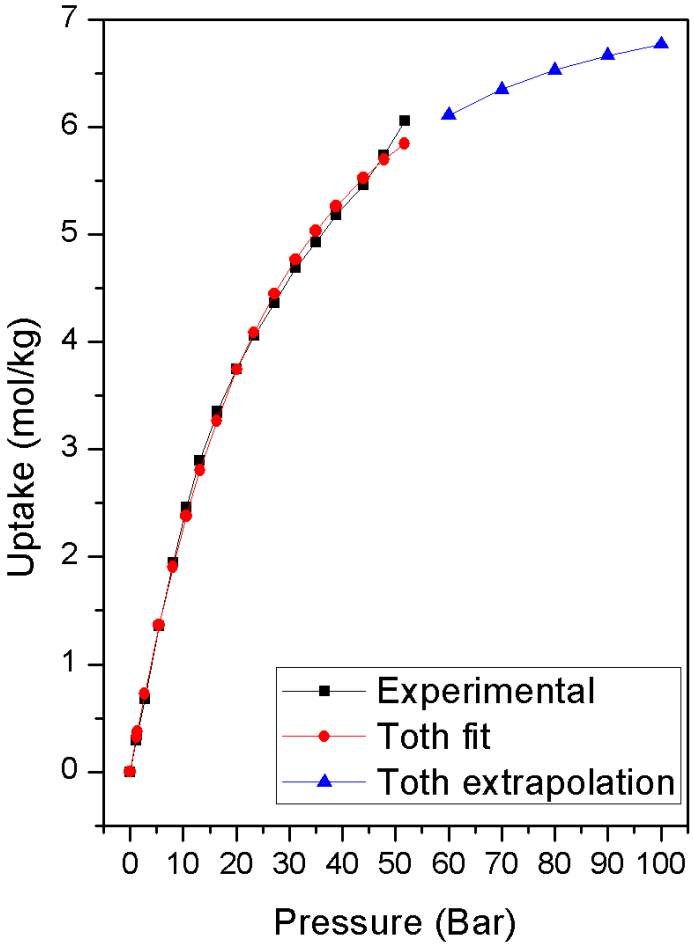


**Figure 2.11: Toth extrapolation of the FMOF-1 $CO_2$ isotherm at 25°C**

## 2.4 Luminescent Complexes of FMIF-1 Derived Extended Solids

The use of silver complexes in luminescence studies is well established.[52-56] In general, silver compounds are poor emitters, though strong emission has been seen from carbene and diphenylposphine silver (I) systems.[26] Wang et al. synthesized a polymeric material from silver (I) and 1,3-bis(4-pyridyl)propane and 2,2'bipyridyl-4,4'-dicarboxylic acid that exhibited shifted

emissions from the ligand. However, the emission was not attributed to silver-silver interactions, despite the metal centers being close enough to have Van der Waals interaction.

One interesting property that has allowed us to experiment with FMIF-1 and its derivatives is its ability to dissolve and crash out of solution with relative ease. A mixing of ligands in the synthetic procedure was attempted initially to introduce new properties within the silver triazolate extended structure, and we started with two imine linkers: pyrazine and 4,4'-bipyridine. From these ligands we were able to form three different coordination polymers, all with yellow room-temperature luminescence. Following this success, we used a third linking material, $Pt(ptp)_2$ (ptp = bis-3,5-di(pyridine-2-yl)-1,2,4-triazolate), or PTA to link silver triazolate clusters to form a novel nonporous coordination polymer with vibrant red luminescence.

### 2.4.1 Structure Elucidation of FMOF-Derived Extended Solids

The first reactions run used the FMOF-1 starting materials, silver nitrate and 3,5-bis-trifluouromethyl-1,2,4-triazole, and either pyrazine or 4,4'-bipyridine. The resulting products were both off-white powders that fell out of the reaction solution, reminiscent of how FMOF-TOP is formed in the FMOF-1 synthesis. Because of this, it was suspected that a nitrate ion was present in the extended framework. Since these both have the same problems with crystallization as FMOF-TOP, no crystal structure has been achieved to date. To confirm the presence of nitrate, IR spectra were taken. There is a distinct, strong absorption at around $1400cm^{-1}$ corresponding to $NO_3$ (Figure 2.12, Figure 2.13).

By using elemental analysis, the composition of each of the three polymers was determined. The results of this are summarized in table 2.3. FMOF-BPY showed reasonable

agreement with the formula $Ag_6(tz3)_2(bpy)_3(NO_3)_4$, and FMOF-PYZ $Ag_3(tz3)(pyz)_2(NO_3)_2$. The third, FMOF-PTA, appears to have a formula of $Ag_6Pt(tz)_6(ptp)_2$, or functionally the same formula of PTA and FMOF-1 units combined.

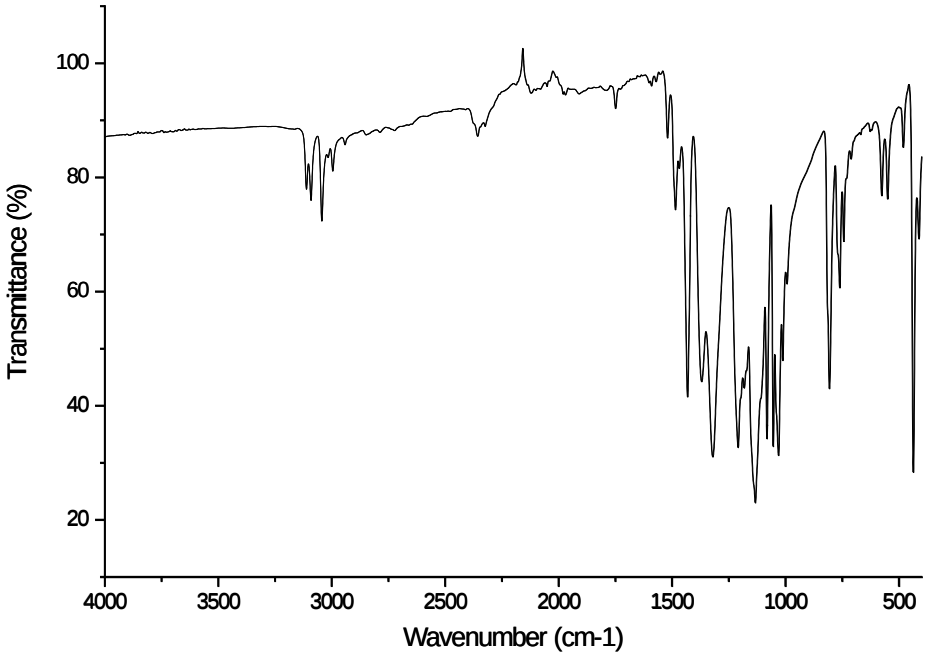


**Figure 2.12: FTIR spectrum of FMOF-pyz**

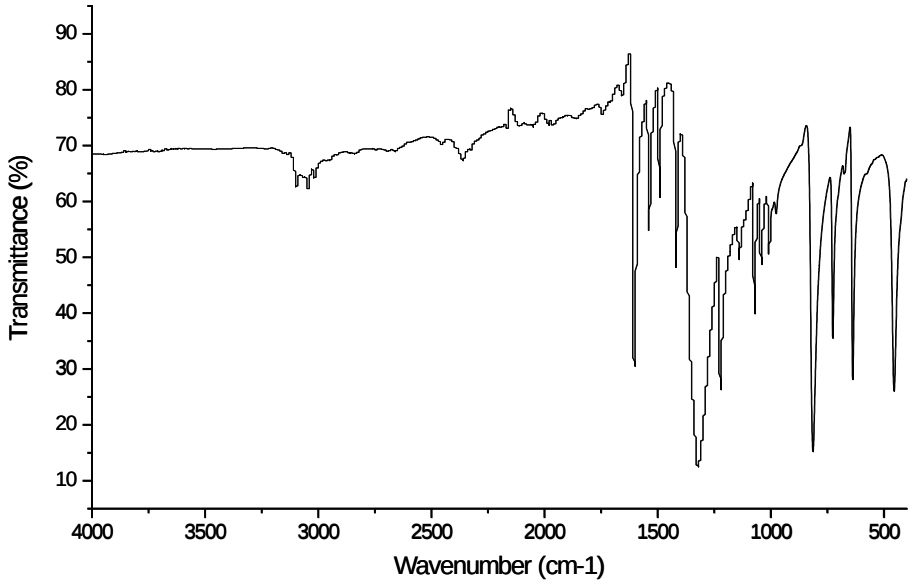


**Figure 2.13: FTIR spectrum of FMOF-bpy**

**Table 2.3: Elemental analysis of luminescent FMOF-based complexes**

| | Empirical formula | C | H | N | F |
|---|---|---|---|---|---|
| FMOF-pyz(NO3) | $C_{12}H_8Ag_3F_6N_9O_6$ | 17.75% | 1.00% | 15.53% | 14.04% |
| | Found: | 17.49% | 0.65% | 15.40% | 13.05% |
| FMOF-bpy(NO3) | $C_{38}H_{24}Ag_6F_{12}N_{16}O_{12}$ | 25.76% | 1.37% | 12.65% | 12.87% |
| | Found: | 26.75% | 1.08% | 12.53% | 13.15% |
| FMOF-PTA | $C_{48}H_{16}Ag_6F_{36}N_{28}Pt$ | 22.96% | 0.64% | 15.62% | 27.24% |
| | Found: | 24.80% | 0.62% | 14.59% | 27.78% |

During attempts to crystallize FMOF-bpy$NO_3$, a related material and structure was discovered. The crystal grown was of good quality and was analyzed by single crystal X-ray spectroscopy. Crystal structure and crystallographic data are presented below (Figure 2.15 and Table 2.4). The Ag – Ag distance in this crystal is 3.29Å, allowing for potential argentophilic interactions. the powder samples of FMOF-pyz($NO_3$) and FMOF-bpy($NO_3$) were analyzed by PXRD, though currently it is only useful in confirming crystallinity of the sample, and confirming the composition is different than that of FMOF-1. A PXRD of FMOF-1 and FMOF-bipyridine are included in Figure 2.14 for comparison. By comparison there is no FMOF-1 in these species, and there is a marked difference between these species and the previously solved structure of FMOF-TOP.

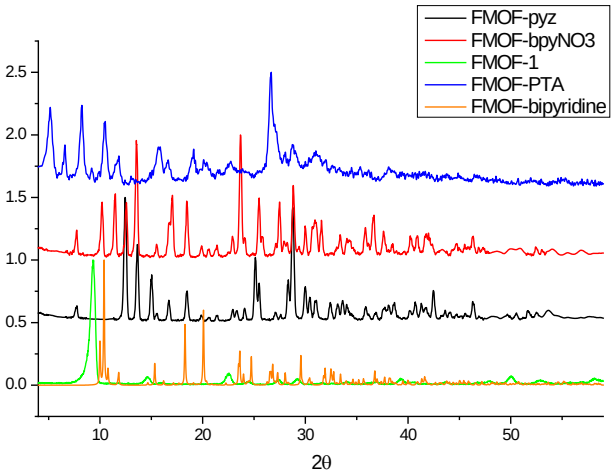


**Figure 2.14: Normalized PXRD spectra of various FMOF-X species**

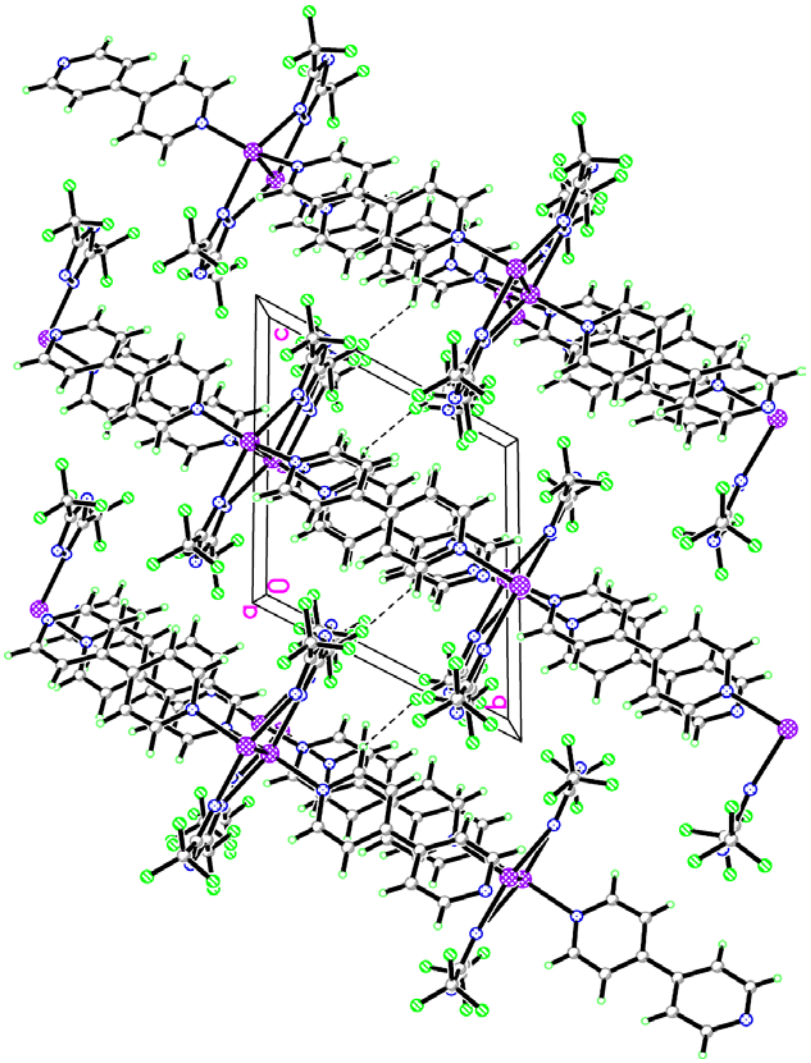

**Figure 2.15: FMOF-bipyridine Crystal Structure**

**Table 2.4: Crystallographic data for FMOF-bipyridine**

| | | |
|---|---|---|
| Empirical formula | C14 H8 Ag F6 N5 | |
| Formula weight | 468.12 | |
| Temperature | 100(2) K | |
| Wavelength | 0.71073 Å | |
| Crystal system | Triclinic | |
| Space group | P -1 | |
| Unit cell dimensions | a = 9.0273(10) Å | a= 113.551(2)°. |
| | b = 9.8800(11) Å | b= 103.167(2)°. |
| | c = 10.3709(19) Å | g = 104.1440(10)°. |
| Volume | 765.14(18) Å3 | |
| Z | 2 | |
| Density (calculated) | 2.032 Mg/m3 | |

| | |
|---|---|
| Absorption coefficient | 1.394 mm-1 |
| F(000) | 456 |
| Crystal size | 0.28 x 0.09 x 0.05 mm3 |
| Theta range for data collection | 2.30 to 27.06°. |
| Index ranges | -11<=h<=11, -12<=k<=12, -13<=l<=13 |
| Reflections collected | 9280 |
| Independent reflections | 3354 [R(int) = 0.0162] |
| Completeness to theta = 27.06° | 99.50% |
| Absorption correction | Semi-empirical from equivalents |
| Max. and min. transmission | 0.9348 and 0.6979 |
| Refinement method | Full-matrix least-squares on F2 |
| Data / restraints / parameters | 3354 / 0 / 235 |
| Goodness-of-fit on F2 | 1.025 |
| Final R indices [I>2sigma(I)] | R1 = 0.0181, wR2 = 0.0449 |
| R indices (all data) | R1 = 0.0198, wR2 = 0.0459 |
| Largest diff. peak and hole | 0.528 and -0.490 e.Å-3 |

### 2.4.2 Photoluminescent Properties of FMOF-Derived Extended Solids

All three of the previously discussed samples show photoluminescent properties. At room temperature, all three show broad yellow emission. This is likely due to Ag(I) ions that are close together in the AgTz cluster; the broad, unstructured emission of the complexes even at low temperatures is indicative of a metal-centered emission. This interaction can be seen in FMOF-bpy, a 1-dimensional wire structure made from the silver triazolate unit with bipyridine bridging the gap between each (Figure 2.15, Table 2.4).

FMOF-bpy shows a broad emission centered around 570 nm (Figure 2.16 FMOF-bipyiridine photoluminescence at room temperature). The excitation spectrum shows a shoulder at 365 nm. The crystalline FMOF-bipyridine showed only narrowing of the emission band without any shift when cooling to 77K. This is to be expected, as the structure is rigid with few degrees of freedom. Distance between the Ag-Ag centers is 3.29Å, placing the two within each other's Van der Waal's radius (3.44Å). This is not seen in FMOF-1, as the Ag-Ag distances are 3.470Å. This

observation can be applied to FMOF-bpy($NO_3$) and FMOF-pyz($NO_3$), as they show very similar excitation and emission profiles.

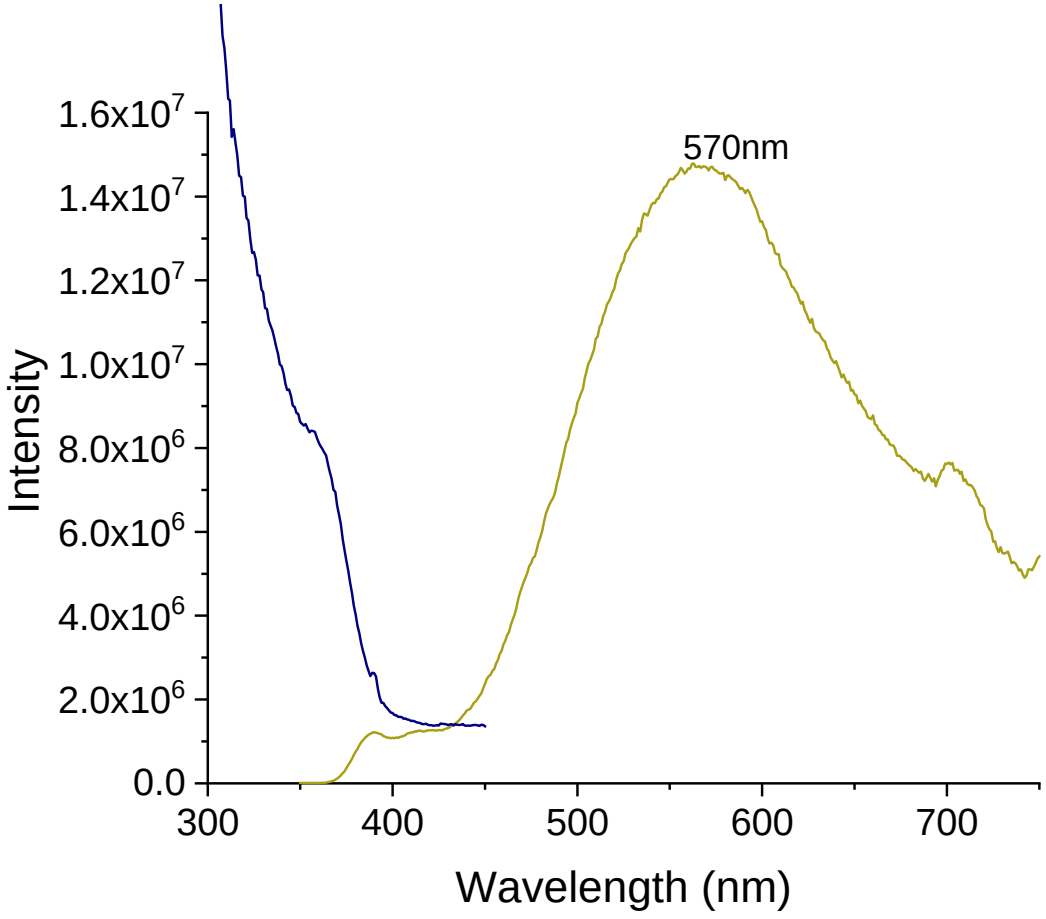


**Figure 2.16: FMOF-bipyiridine photoluminescence at room temperature**

Upon analysis at cryogenic temperatures, the two powder samples of FMOF-bpy($NO_3$) and FMOF-pyz($NO_3$) differentiate themselves from one another. The bipyridine-based material showed the largest shift of 1710 $cm^{-1}$ from 585nm emission to 650nm (Figure 2.17). The pyrazine-based material showed a 1090 $cm^{-1}$ blue shift from 585 to 550nm (Figure 2.18). These thermochromic shifts are likely due to a structural shift in the material itself; similar to how FMOF-1 has shown structural shifts upon cooling.[15] FMOF-TOP, which is possibly an even closer analog due to its incorporation of the nitrate anion, also shows some small but potentially

significant crystallographic shift at lower temperatures, as evidenced by the experimental versus simulated PXRD patterns.

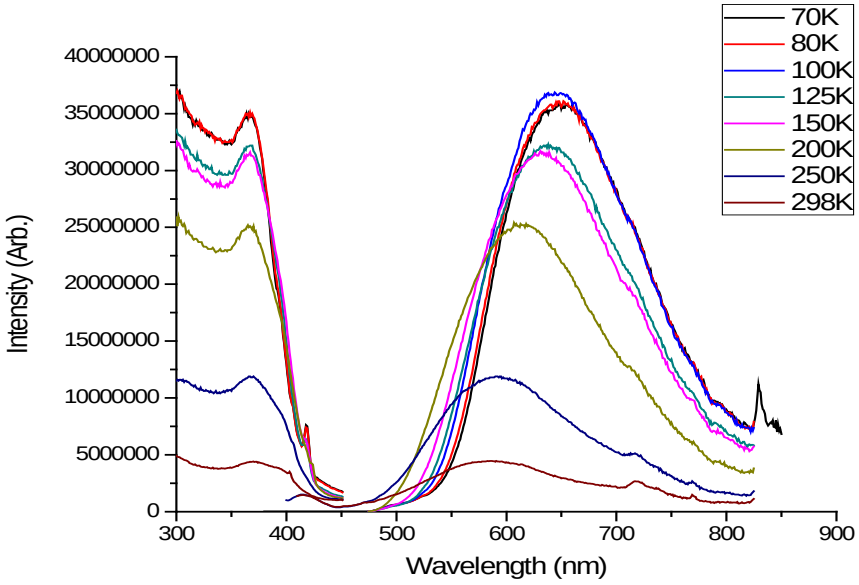


**Figure 2.17: FMOF-bpy($NO_3$) Temperature dependent spectra**

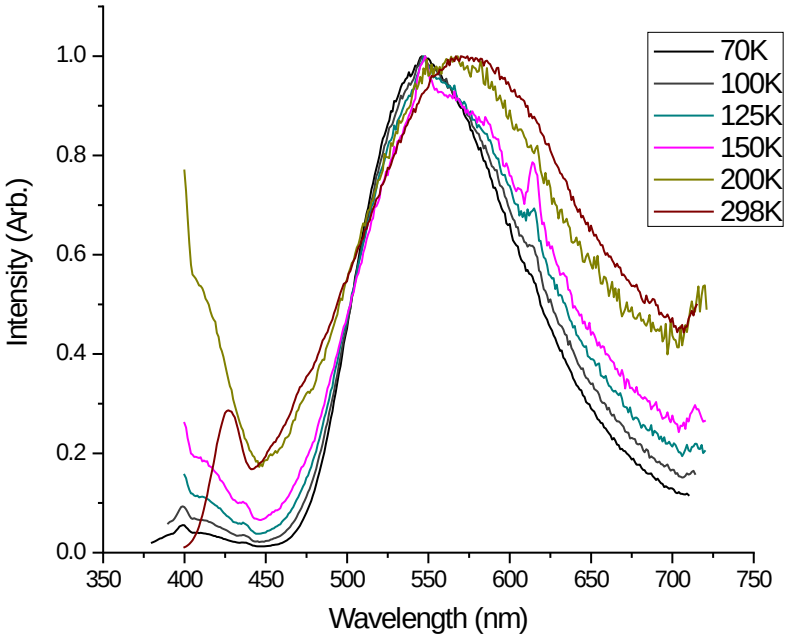


**Figure 2.18: FMOF-pyz($NO_3$) temperature-based luminescence.**

Quantum yields from all three materials increase dramatically upon cooling to cryogenic temperatures as well. FMOF-pyz($NO_3$) shows the largest increase of over two orders of magnitude from 0.37% to 49.51%. FMOF-bpy($NO_3$) increased from 0.69% to 4.66%, and FMOF-bipyridine saw a 4-fold increase from 2.55% to 10.86%. The dramatic increase in quantum yield at cryogenic temperature means there is significant nonradiative decay at room temperature that is quenched. In the case of FMOF-pyz($NO_3$) and FMOF-bpy($NO_3$), the increase could also be due to the silver centers coming closer together, allowing for a more facile transition into an excited state. The emissions of these samples are phosphorescence, as evidenced by their lifetimes. This is to be expected; as seen in other silver complexes, dramatic increases in luminescence tends to happen when the materials are cooled to cryogenic temperatures.

**Table 2.5: Quantum yield and lifetimes of the maximum peaks of each FMOF-derived luminescent species**

| | Quantum yield | | Lifetime |
|---|---|---|---|
| | RT | 77K | 77K |
| FMOF-pyz($NO_3$) | 0.37% | 49.51% | 8.27µs |
| FMOF-bpy($NO_3$) | 0.61% | 4.66% | 1.17µs |
| FMOF-bipyridine | 2.55% | 10.86% | 9.62µs |

Using a similar method, FMOF-1 and platinum(II) 3,5bis(2-pyridyl)-1,2,4-triazolate ($Pt(ptp)_2$) were combined to form a new coordination polymer. This material has a square-planar structure with the platinum center coordinated to one of the pyridyl groups and one nitrogen on the triazole on each of the two ligands. This material shows a shifting emission between monomer and excimer in solution, with a broad emission of the solid at 600nm.[57-59] When combined with FMOF materials, the result is an insoluble solid that has a peak emission around 660nm at room temperature. Its absorption band which reaches a maximum at 580nm and extends throughout the visible spectrum into the UV. Quantum yield at room temperature is

26.8% with an excitation of 575nm. At 77K, with an excitation max of 700 nm, quantum yield is 19.8%. Seeing a drop in the quantum yield as a system cools is uncommon; usually, this drop in temperature increases the rigidity of the complex, allowing for more stable excited states. In this compound, as the emission shifts further into the IR region, it is moving closer to the energy of vibrational relaxations, actually opening up more nonradiative relaxation pathways.

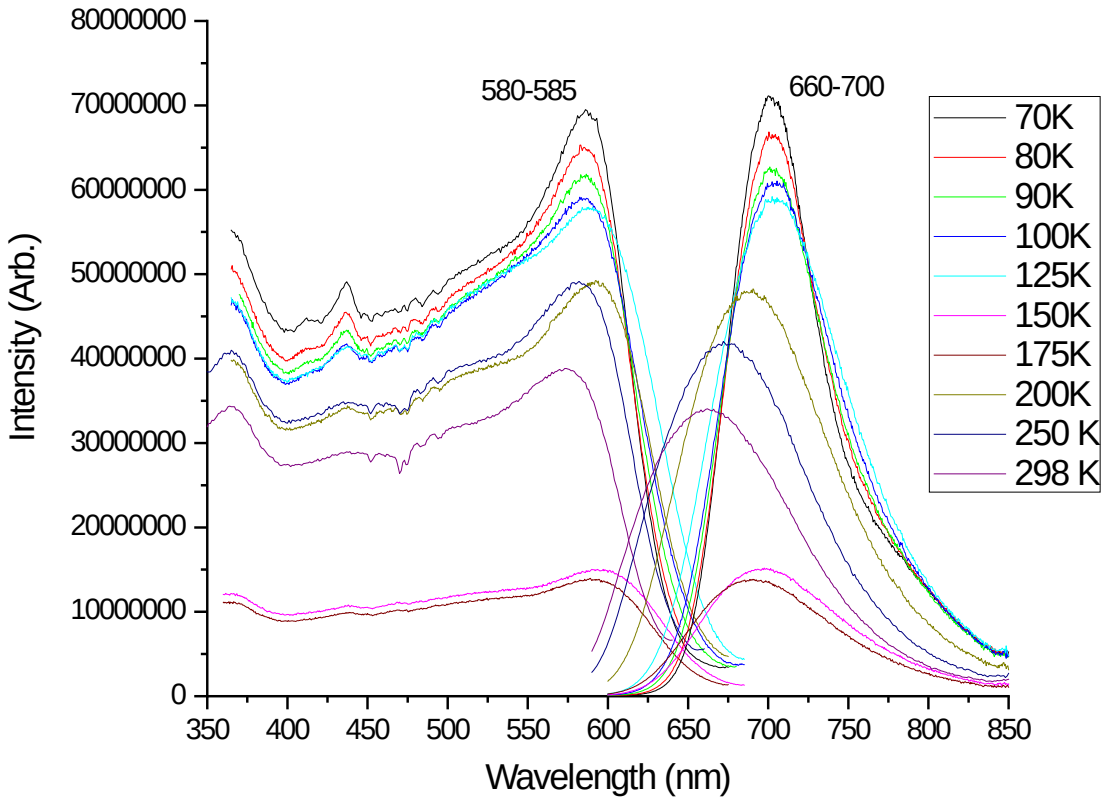


**Figure 2.19: Temperature Dependent Photoluminescence of FMOF-PTA**

The adsorption profile of FMOF-PTA shows very little nitrogen uptake. It shows the form of a typical Type II isotherm characteristic of a material with good affinity for the adsorbate, with a significant uptake at the higher-pressure stage of the adsorption isotherm. The small shoulder in the low-pressure region of the isotherm corresponds to monolayer adsorption. The dramatic

increase in adsorption at the later part of the isotherm ($P/P_0 > 0.8$) denotes a strong affinity of the material for the gas. This may show promise as use for a sensor, if it can be shown that an adsorbing species can quench or alter the solid state luminescence of the material. Adsorption profiles of FMOF-bpy($NO_3$) and FMOF-pyz($NO_3$) both show minimal nitrogen adsorption profiles to one another with no adsorption in the microporous region, meaning there is no porosity in these materials. The final dramatic spike in adsorption is merely multilayer into bulk deposition of the gas onto the solid as it reaches the saturation pressure.

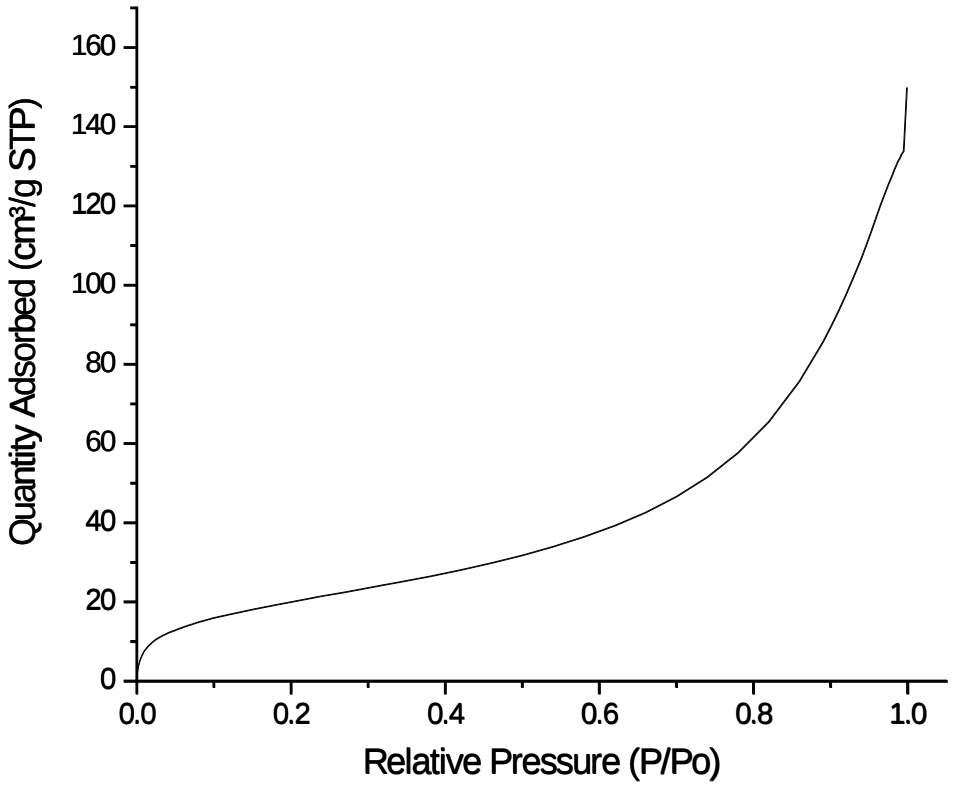


**Figure 2.20: FMOF-PTA nitrogen adsorption curve**

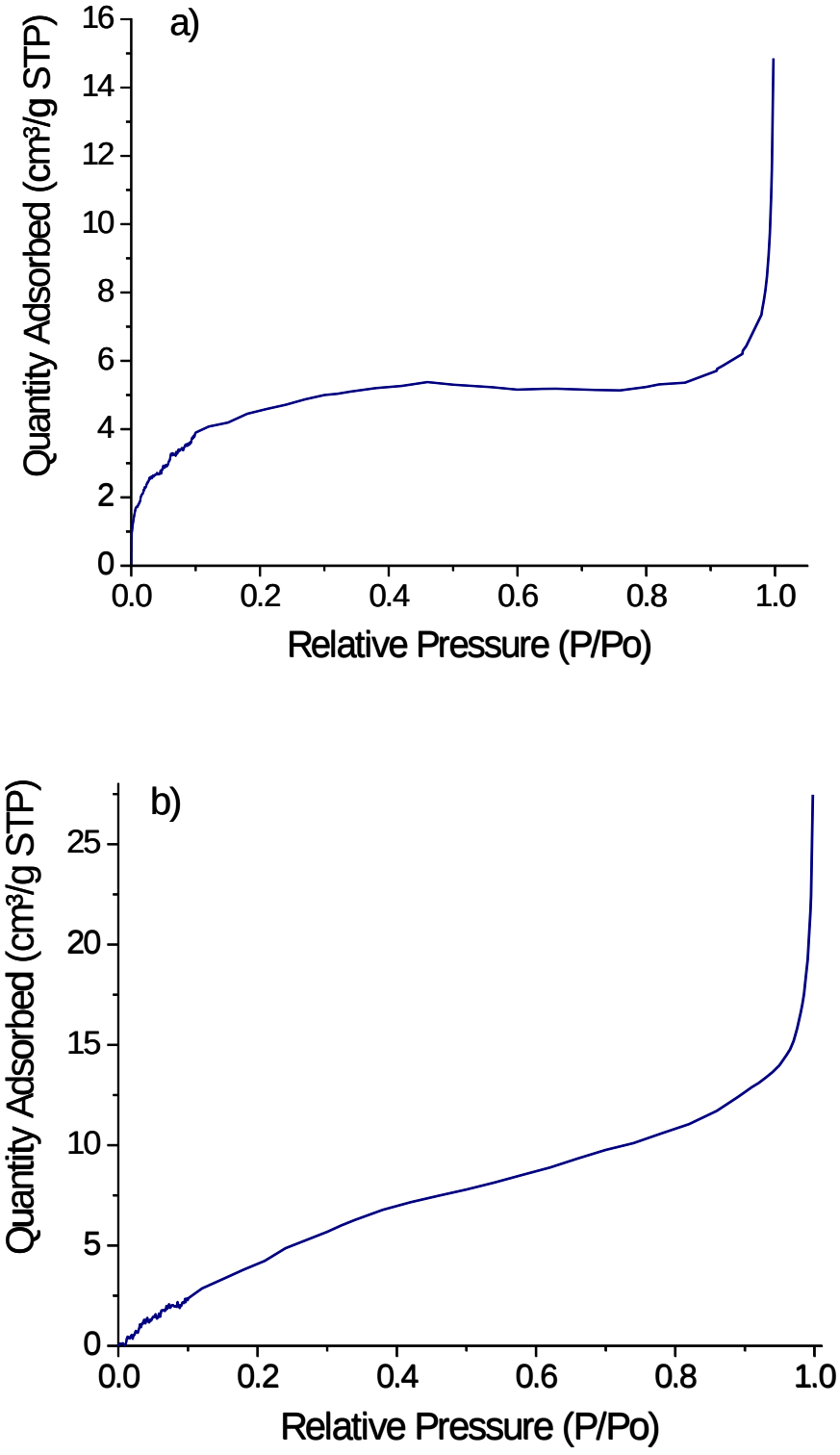


**Figure 2.21: Nitrogen isotherms of a) FMOF-bpy($NO_3$) and b) FMOF-pyz($NO_3$)**

## 2.5 Au-FMIF-1

FMOF-1 is formed from $[Ag_4tz_6]^{-2}$ clusters (tz = 3,5-trifluoromethyl-1,2,4-triazole) and 2 $Ag^+$ metal centers. In theory, we should be able to replace the $Ag^+$ metal centers that bridge the clusters with another, singly charged metal cation. The first attempt to do this is by replacing it with a metal in its own group, in this case gold (I). Since the source used for the gold is Au-THT-chloride (THT = tetrahydrothiophene), replacement of the $Ag^+$ centers with $Au^+$ should stoichiometrically form AgCl as a product, which would drop out of the reaction solution (Figure 2.22). The precipitate should act as both a confirmation of reaction and should push the ion exchange to completion. The resulting Au-FMIF-1 would stay in solution and could be similarly precipitated out of solution or recrystallized.

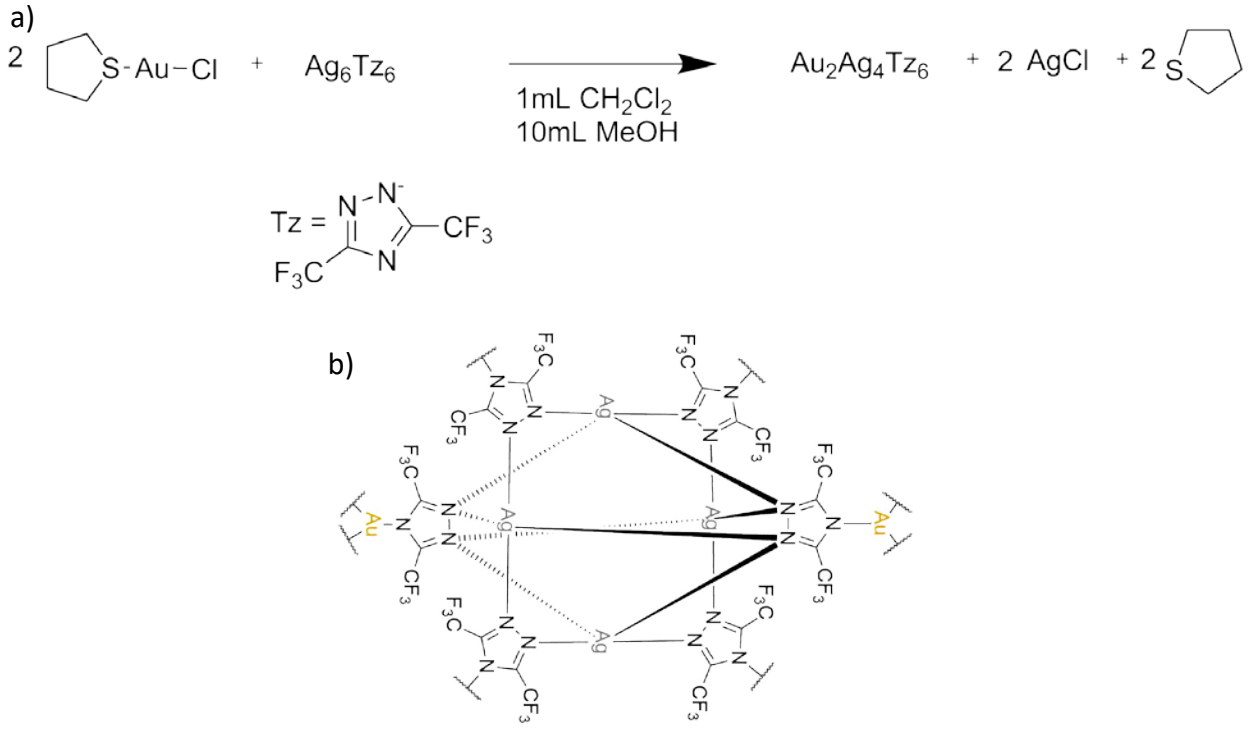


**Figure 2.22: a) Au-FMIF-1 reaction schematic. B) Au-FMIF-1 proposed structure.**

Initial PXRD analysis shows a main peak at 6.68°, which corresponds to the same primary peak of FMOF-1 at room temperature. Since the intent of this experiment is to replace silver

cations with gold, we would not expect the structure of the material to change dramatically. In fact, showing that this material is isostructural is encouraging (Figure 2.23). Since this PXRD was taken using crystals of Au-FMIF-1, the differences in relative intensities could be due to a preferred orientation of the sample and does not necessarily indicate a second material in the sample.

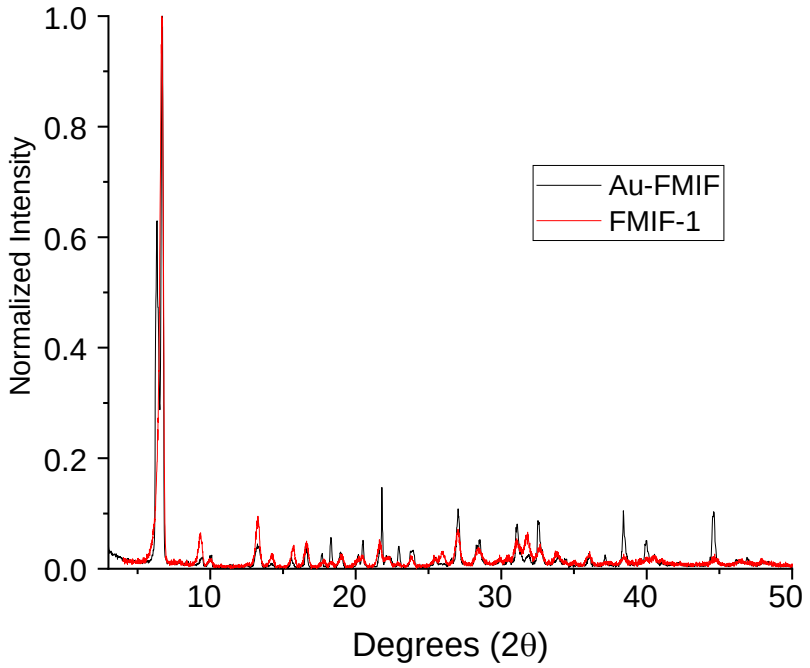


**Figure 2.23: Normalized PXRD of FMOF-1 vs Au-FMIF-1**

The Au-FMIF-1 nitrogen isotherm also shows an adsorption isotherm similar to that of FMOF-1 (Figure 2.24). As the material should be isostructural to that of FMOF-1, we would expect to see the two-step isotherm, with a volumetric surface area slightly lower due to the increased density from having gold cations in the structure.

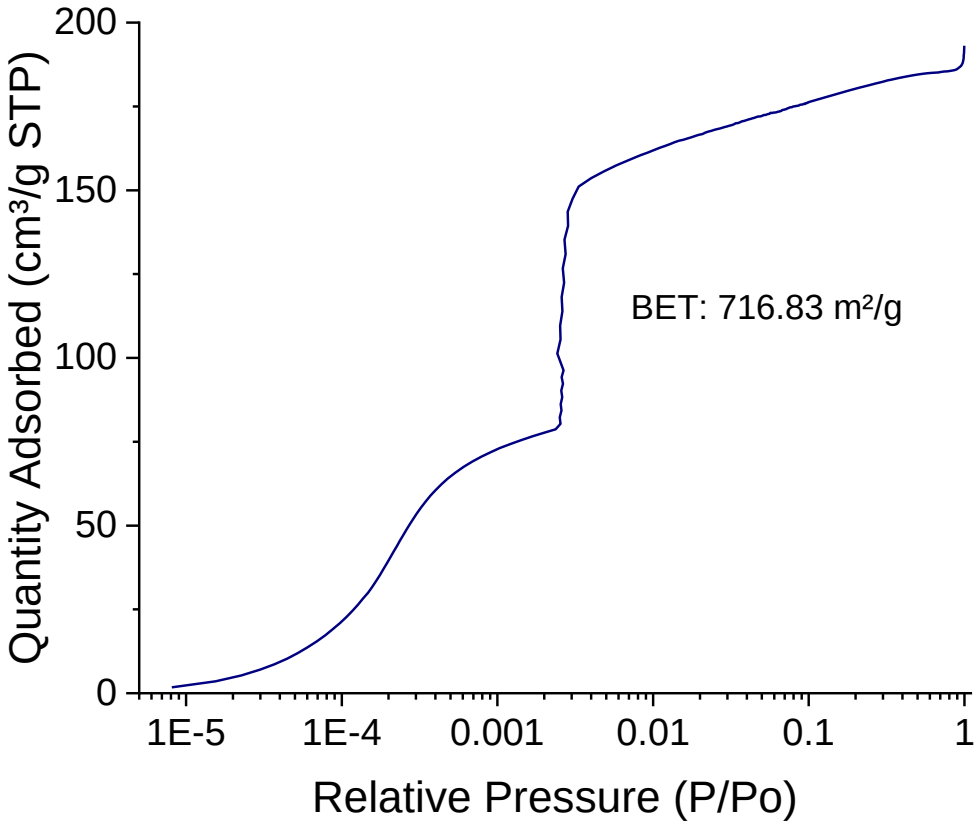


**Figure 2.24: Au-FMIF Isotherm**

In order to determine how the gold cations were incorporating into FMIF-1, we ran an experiment using electrospray ionization mass spectrometry (ESI). We ran samples of both FMOF-1 and Au-FMIF-1 to compare their differences. Both samples were dissolved in methanol and then injected into the instrument. In the FMOF-1 spectrum, we can see 3 distinct peaks: m/z 204, which correlates to the Tz linker; 515, which is the $AgTz_2^-$ fragment; and 828, which correlates to the $Ag_2Tz_3^-$ and the $Ag_4Tz_6^{2-}$ fragments (Figure 2.25). Upon close-up inspection of the 515 peak, you can see a doublet (Figure 2.26) correlating to the isotopic abundances of silver at 107 and 109 amu. The 828 in Figure 2.27 is more convoluted, having signals from two different masses, but the major triplet shown is consistent for both the $Ag_2Tz_3^-$ and $Ag_4Tz_6^{2-}$ clusters.

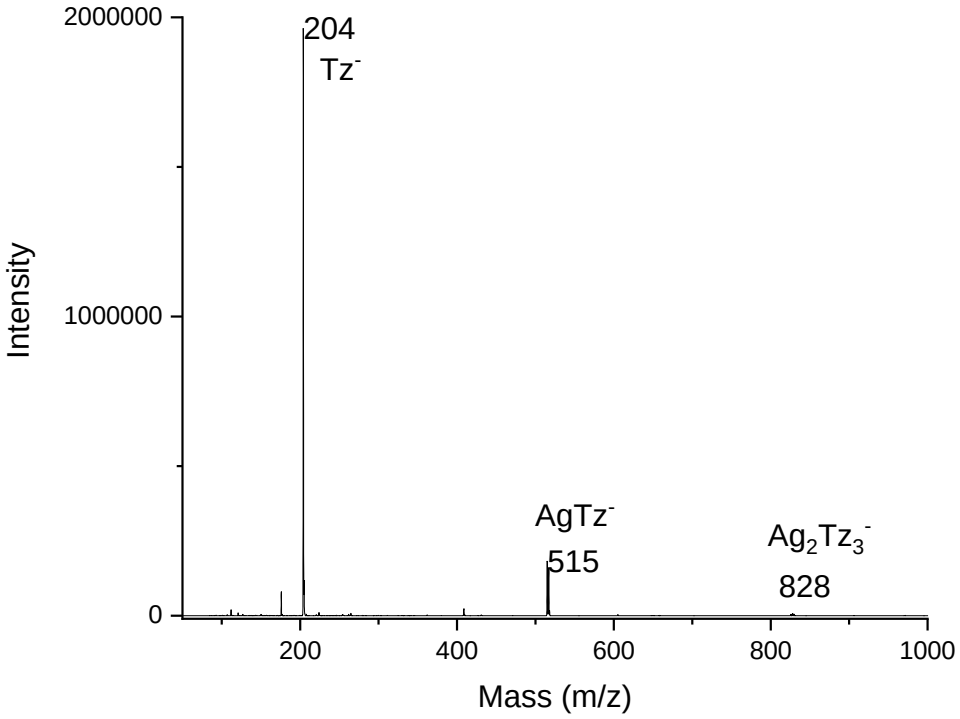


**Figure 2.25: Negative m/z spectrum of FMOF-1**

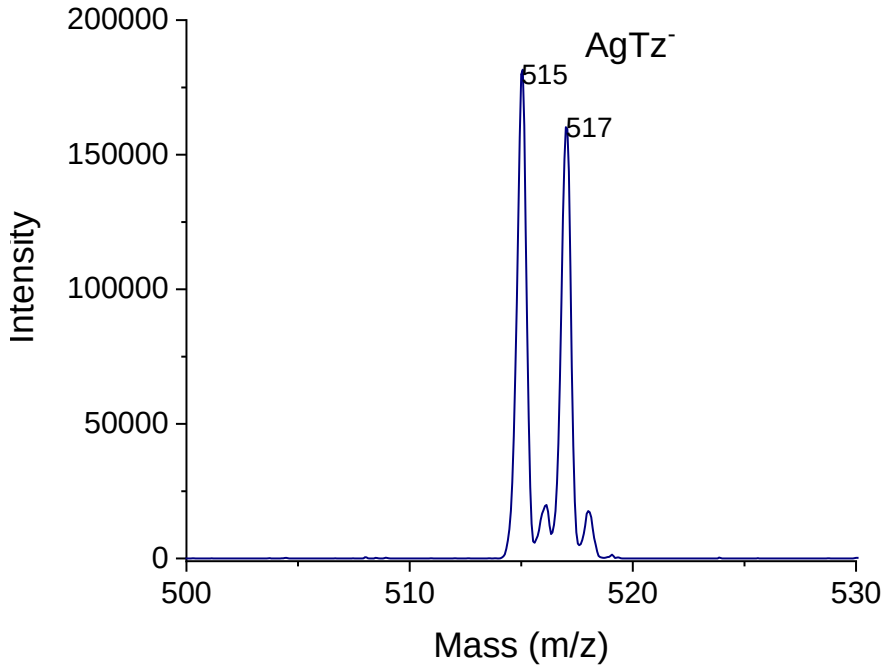


**Figure 2.26: Fragment of the 515 m/z peak of FMOF-1**

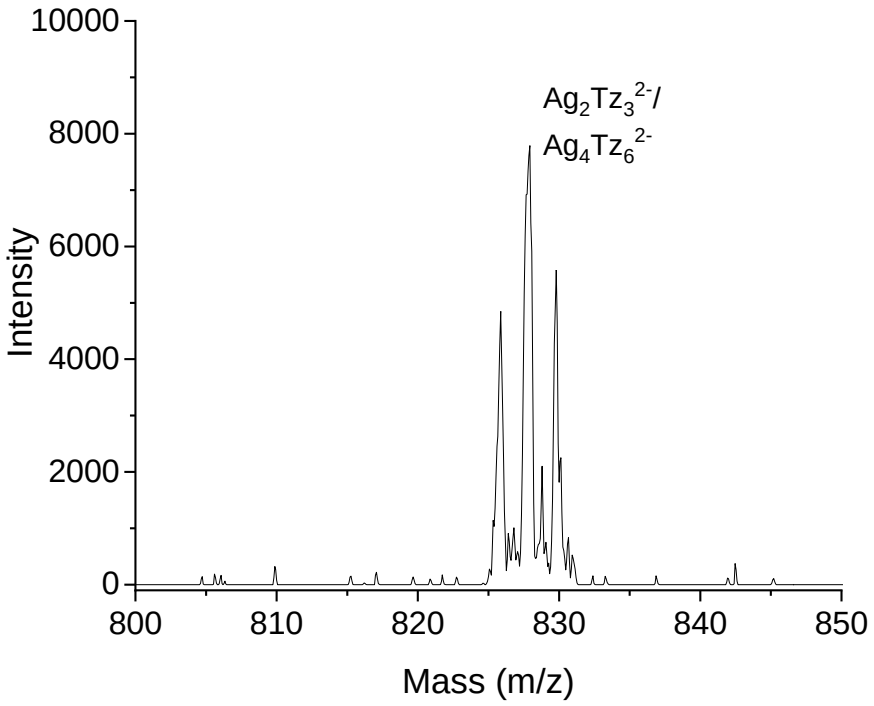


**Figure 2.27: Fragment of the 827 m/z peak of FMIF-1**

When viewing the negative ESI spectrum of Au-FMIF-1, we see similar results. As seen in Figure 2.28, there are significant peaks at 204, 515 and 827, similar to FMOF-1. It is expected these peaks would still be in the system, as we are only partially replacing the silver (I) centers in the framework. Two new peaks show up in the system; at 605 and 917 m/z, correlating to $AuTz_2^-$ and $AgAuTz_3^-$ clusters, respectively (Figure 2.28 and Figure 2.29). Looking at the peak splitting of the signal at 917, we can ascertain that it is exclusively of the binuclear Au-Ag fragment, rather than an $Au_2Ag_2Tz_6^{2-}$fragment; two silver atoms in the system would lead to a triplet signal due to the isotopic abundance of silver.

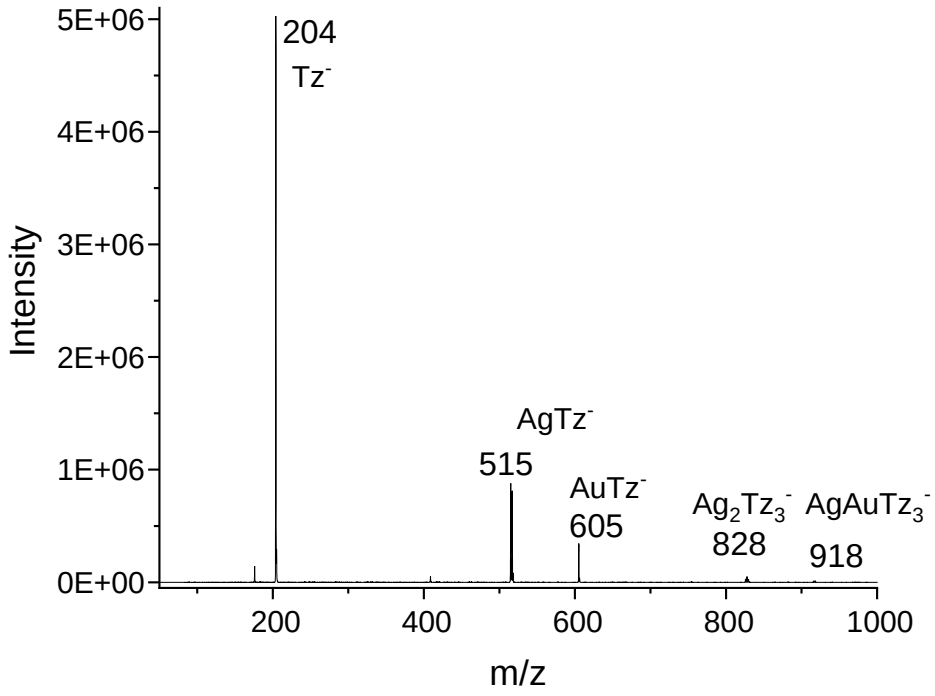


**Figure 2.28: m/z spectrum of Au-FMIF-1**

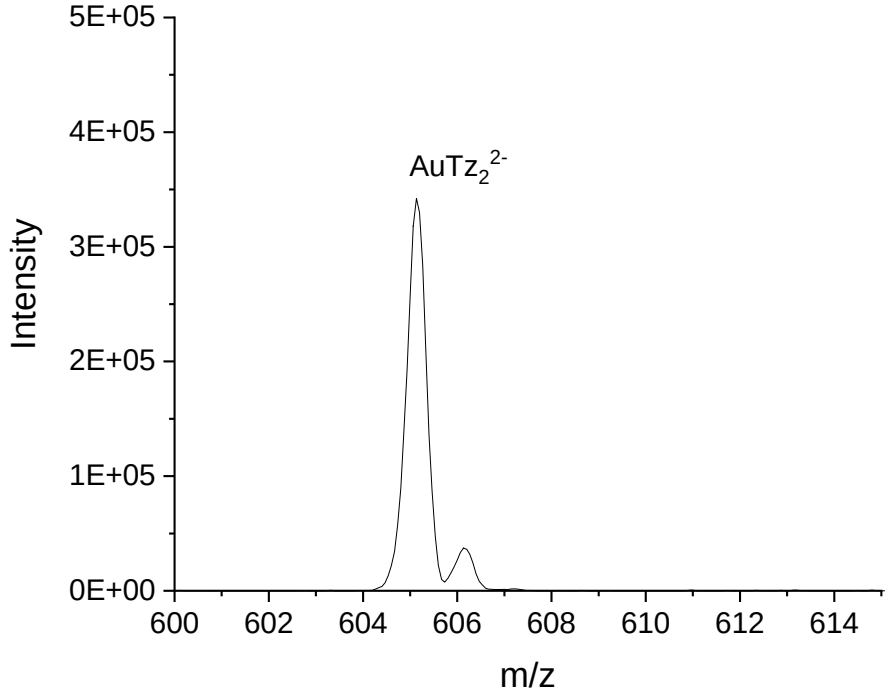


**Figure 2.29: Au-FMIF-1 605 m/z peak.**

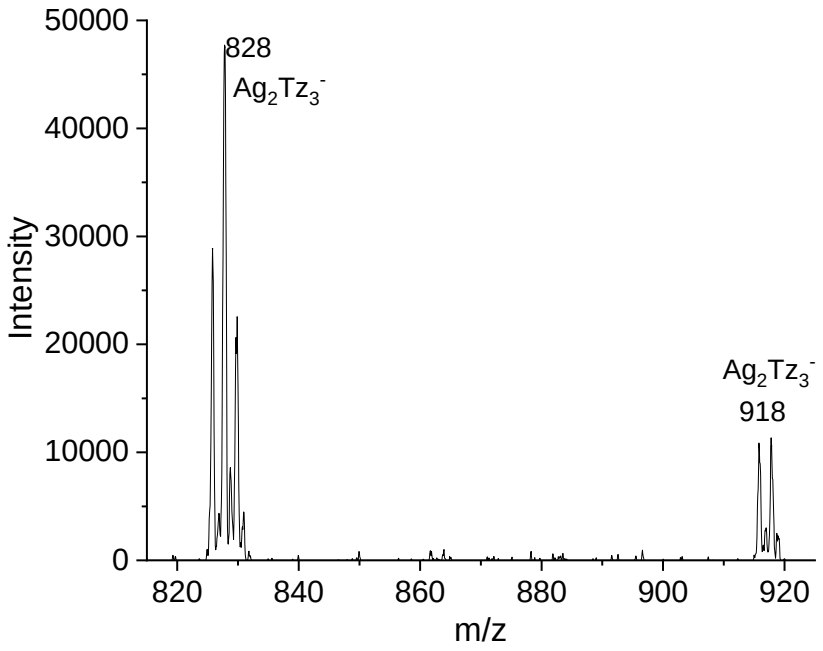


**Figure 2.30: Au-FMIF-1 827 and 915/917 m/z peak**

There is also a considerable difference in the fragmentation spectrum of the FMOF-1 peaks and the Au-FMIF-1 peaks. In Figure 2.31 we see the fragmentation pattern of m/z 514. We see only a m/z 204 peak for the free $Tz^-$ ligand, and then a second peak of 175.93 for $C_4F_6N^-$, where the $Tz^-$ ligand loses dinitrogen. This means that the silver (I) cations dissociate from the ligand fairly easily in solution, which is primarily evidenced by the exceptional solubility of the framework.

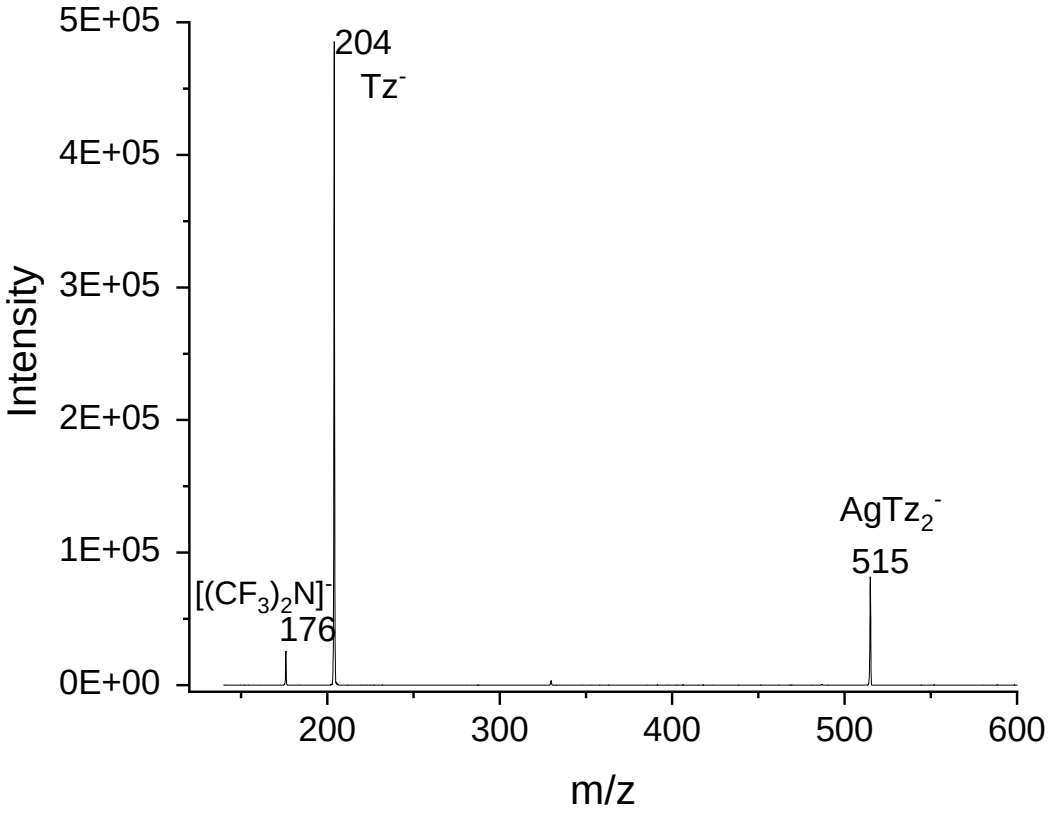


**Figure 2.31: Fragmentation of the 514 m/x peak of FMOF-1**

In Figure 2.32 the fragmentation of the analogous Au-FMIF-1 607 m/z peak is shown. Rather than seeing a large free ligand peak, we instead see fragmentation of one of the ligands while still attached to the gold cation. This paired with the increased energy needed to show the fragmentation peaks shows a much stronger bond between the metal and ligands compared to silver.

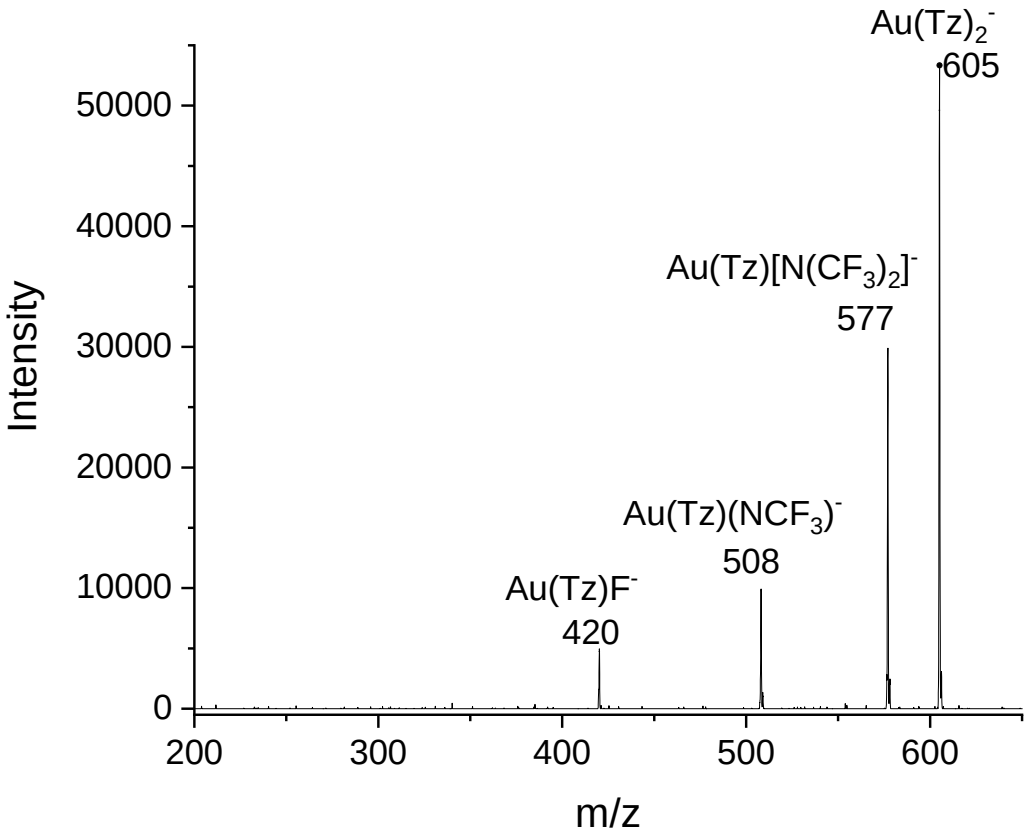


**Figure 2.32: Fragmentation of the 605 m/z peak of Au-FMIF**

## 2.6 Conclusion

FMOF-1 was studied to determine its $CO_2$ isosteric heat of adsorption, and found it to be about 20kJ/mol. This isosteric heat is good for potential applications in temporary storage of carbon dioxide gas. Further iterations of this hydrophobic material, designed to have a stronger affinity to carbon dioxide, could be used in applications such as sequestering of $CO_2$ from flue gas emissions. We have shown the synthesis of a series of new solids based on FMIF-1. By combining either the starting materials or the final FMIF-1 product with pyrazine or 4,4'-bipyridine, we were able to form a new series of luminescent complexes. FMOF-pyz($NO_3$) and FMOF-bpy($NO_3$)

displayed thermochromic behavior, shifting from 585 nm to 550 and 650 nm, respectively. The nitrate-free complex FMOF-bpy, however, does not show this phenomenon, but shows a quantum yield of 10% at room temperature. Finally, we have shown we can exchange some of the silver cations in FMOF-1 for gold, as shown in the new Au-FMIF-1. This is a partially substituted complex, as we see gold and silver mixed clusters in its ESI-MS spectrum. This material may prove to be useful as a catalyst due to the gold centers present in the material. By selectively replacing certain silver (I) cations in the framework, we have shown that the FMOF-1 material can be described as a metal-inorganic framework and can thus be recategorized as FMIF-1.

# CHAPTER 3

# CARBON-FREE METAL INORGANIC FRAMEWORKS: COORDINATION POLYMERS OF "PLATINUM POP" WITH GREATLY SYNSETIZED LUMINESCENCE ENHANCED SHELFLIFE

## 3.1 Introduction

The complex known as Pt-POP, or $[Pt_2(P_2O_5H_2)_4]^{4-}$, was first published almost 40 years ago (Figure 3.1). This material was interesting due to its intense luminescence in aqueous solution, attributed to interaction between the diplatinum centers. [60-62] The authors noted intense luminescence in an aqueous solution with absorption bands at 367 and 452 nm, and a primary emission at 514 nm. Other studies on this material attributed the absorption bands at 367nm and 452 nm to singlet and triplet transitions, respectively.[62,63] Quantum yields of the solution were reported to be around 50%.[64-66] These numbers, however, are only attained in de-aerated solutions, as oxygen will quench the emission of Pt-POP. DFT studies on this material have been performed to verify the primary transitions attributed to luminescence, further confirming the attribution of excited state to a dσ* -> pσ transition.[67,68]

The POP structure has been modified previously by other groups seeking to tune the luminescence of the material. When changing the ligand from a P-O-P bridged structure to a P-C-P bridge, the triplet lifetime dramatically decreases to 55ns from 9.5μs.[69,70] More recently, terminal hydrogens of the Pt-POP complex were exchanged with $BF_2$ groups. While absorption properties of the new complex stayed largely the same, it slowed the intersystem crossing of the singlet to triplet states, causing the singlet emission to become more prominent.[68,71]

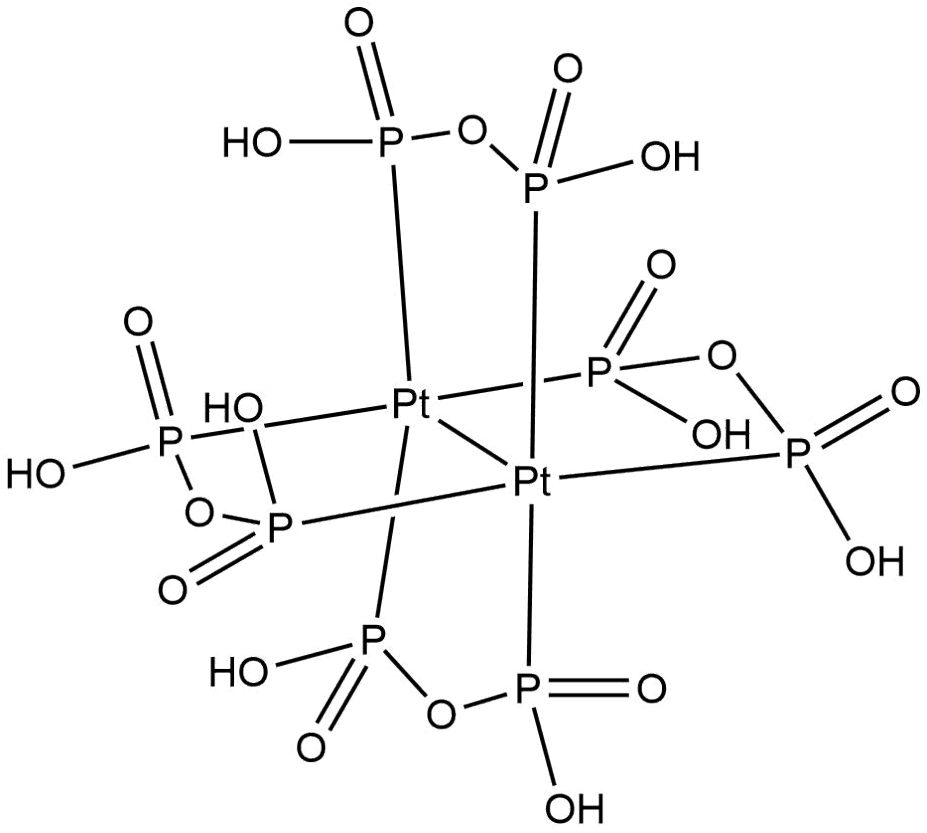


**Figure 3.1: Structure of Pt-POP**

Aside from altering counterions for soluble Pt-POP, not much work has been done to study heterometallic interactions with the complex. Recently, some work was published studying exciplexes of Pt-POP and $Ag^{+}$ in solution and corroborated later by DFT studies.[72,73] The physical experiment and subsequent theoretical study found that when excited, the Pt(II) centers and the metal cation would form a short-lived bond.

Solid PtPOP with sodium or potassium counterions has relatively low quantum yield (0.02) compared to the material in aqueous solution. PtPOP also has problems with stability; if left in an uncontrolled environment for an extended period of time, it will begin to decompose from a yellow solid to a black material (Figure 3.2). By turning this material into an extended solid, the

goal is to increase the relative stability of the material while improving its luminescent properties in the solid state.

Metal-organic frameworks (MOFs) have had issues with stability since the first material, MOF-5, was popularized.[74-76] These stability pathways typically involve water interacting with the metal-oxygen bond between the metal center and the ligand. By moving to inorganic complexes in metal-inorganic frameworks (MIFs), we hope to improve this stability problem with stronger bonds between the new inorganic linker and the bridging metal clusters. Further, by targeting specifically $d^{10}$ and $d^{0}$ metals zinc and zirconium, we aim to apply the reticular chemistry principles of MOFs to make systematically designed extended solids that still retain the luminescent properties of the MIF linkers.

By making larger, insoluble chains of the material we hope to reduce the decomposition time while also increasing the optoelectronic properties of the solid. Zirconium(IV) (MIF-1) and zinc(II) (MIF-2) were used due to both their success in other applications relating to coordination polymers and MOFs, and to their optoelectronic properties. Also attempted were nickel(II) (MIF-3), and manganese(II) (MIF-4). Generally, these materials were made solvothermally and had yellow-green or orange physical appearances.

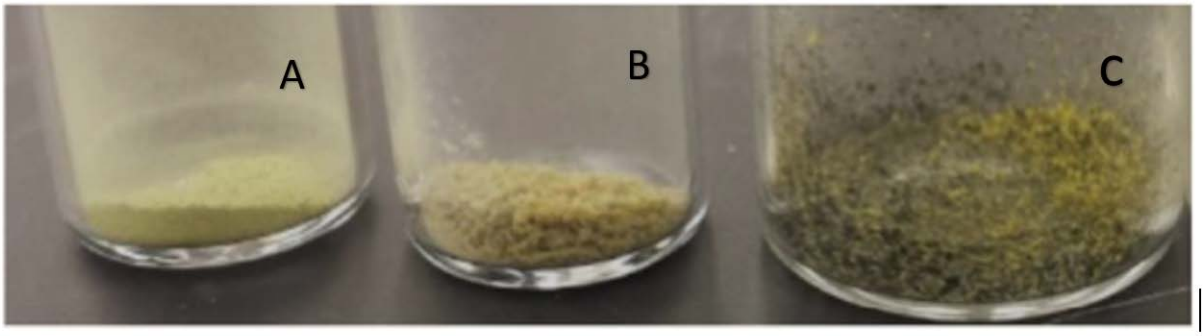


**Figure 3.2: Pictures of A) MIF-2, B) MIF-1, and C) NaPtPOP.**

## 3.2 Materials and Methods

### 3.2.1 MIF-1 (ZrPtPOP)

$Na_4$PtPOP (0.100g, $9.46x10^{-5}$ mol) was dissolved in 15 mL of a 5:1 DMF:HCl solution and bubbled with argon for 10 minutes. Zirconium chloride (0.104g, $4.46x10^{-4}$ mol) was dissolved separately in 15 mL of 5:1 dimethylformamide (DMF):HCl, then added dropwise to the NaPtPOP solution. A yellow-green precipitate formed immediately. The solid was collected on a fritted funnel and washed with DMF, then acetone, and dried in a vacuum oven at 40°C overnight to yield 0.07g of MIF-1.

### 3.2.2 MIF-2 (ZnPtPOP)

NaPtPOP (0.1g, $9.46x10^{-5}$ mol) was dissolved in 15mL deionized water inside a 40mL scintillation vial while degassing with argon. Zinc nitrate hexahydrate (0.1126g, $3.78x10^{-4}$ mol) was dissolved in 15mL DMF, then slowly added to the water solution. The solution was bubbled with argon for another 10 mins, then placed in a 45°C oven overnight. A yellow powder formed overnight, which was filtered then washed with water and acetone, and then dried in a vacuum oven overnight at 40°C. Yield 0.0525g of MIF-2.

### 3.2.3 MIF-3 (NiPtPOP)

NaPtPOP (0.050g, $4.73x10^{-5}$ mol) was initially dissolved in 3mL deionized water while degassing with argon. DMF (5mL) was added to the solution after the PtPOP fully dissolved, followed by 0.024g ($1.0x10^{-4}$ mol) Nickel chloride hexahydrate. Solution was degassed for 10 more minutes after everything had dissolved, then heated in an oven for 72 hours at 40°C to form

a yellow precipitate. The solid was washed with water, then methanol and dried in a vacuum oven overnight at 40°C. Yield 0.012g of MIF-3.

### 3.2.4 MIF-4 (MnPtPOP)

NaPtPOP (0.050g, $4.73 \times 10^{-5}$ mol) was initially dissolved in 3mL deionized water while degassing with argon. DMF (5mL) was added to the solution after the PtPOP fully dissolved, followed by 0.024g manganese (II) nitrate hydrate ($8.9 \times 10^{-5}$). The solution was degassed for 10 minutes after all solids had dissolved, then capped and heated in an oven for 72 hours at 40°C to form a yellow precipitate. The precipitate was washed with water, then acetone, and dried overnight in a 40°C vacuum oven. Yield 0.018g of MIF-4.

## 3.3 Structure Elucidation

All materials observed in this project have been amorphous solids, as seen in Figure 3.3. The single large, broad peak is due to the background of the glass slide substrate. Despite significant quantities of the material used for these PXRD analyses, no peaks can be deciphered from the patterns. Since there is no order in the structures, scattering of X-rays is random.

One possible reason for this is exemplified by the MIF-1 material. Typically, in MOFs with zirconium, we see a $Zr_6O_4(OH_4)$ cluster form (Figure 3.4), which links together the ligands to make the framework. In the example of MIF-1, the Pt-POP structure (Figure 3.1) is simply too bulky for it to coordinate completely with this cluster. It would be likely, then, that the coordination of the Pt-POP happens through ($-PO_2$), and then coordinates to one or two of the zirconium centers within a cluster. The Pt-POP can coordinate with two to eight of these clusters on its own, and

each cluster could coordinate with two to six or eight linkers. Due to the bulk, some of the potential coordinating sites would go unused, and those that are used would be random, resulting in a non-uniform material.

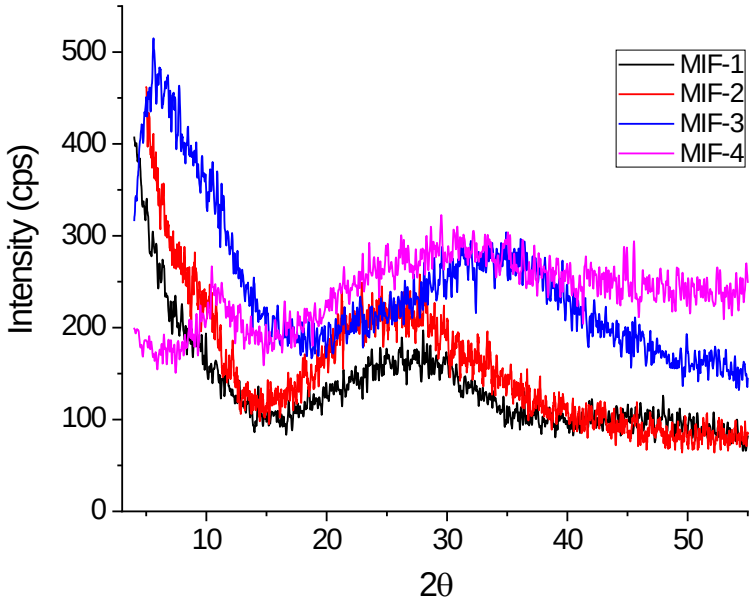


**Figure 3.3: PXRD analysis of Pt-POP based species. All materials were amorphous**

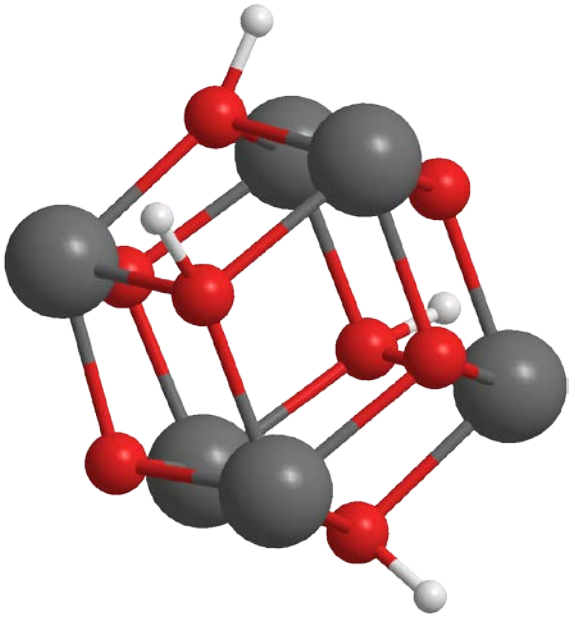

**Figure 3.4: $Zr_4O_6(OH)_6$ cluster**

Nitrogen isotherms were run for each of these materials (Figure 3.5). MIF-2 and MIF-4 both showed negligible adsorption, however MIF-1 showed some significant porosity. MIF-2, MIF-3, and MIF-4 are all of isotherm type II, whereas MIF-1 shows a type I isotherm. The low porosity MIFs showed primarily adsorption on the outside surface of particles, while MIF-1 shows a larger adsorption in the micro and mesoporous region (0-0.3 $P/P_0$). The adsorption below 0.1 $P/P_0$, denotes microporous character in the sample. The calculated BET surface area of MIF-1 is 266.5 $m^2/g$, while the others showed negligible adsorption.

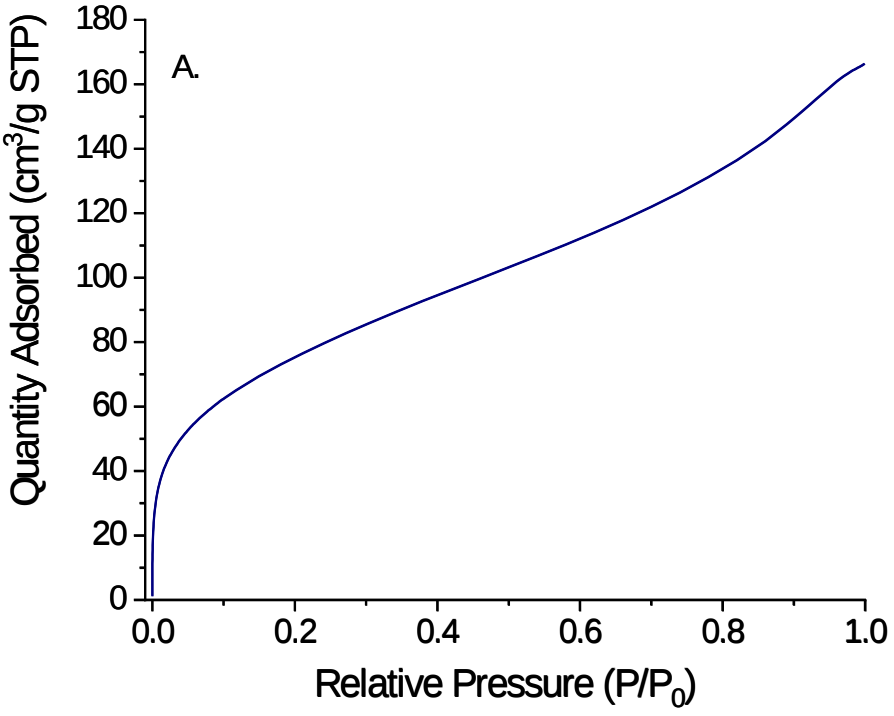

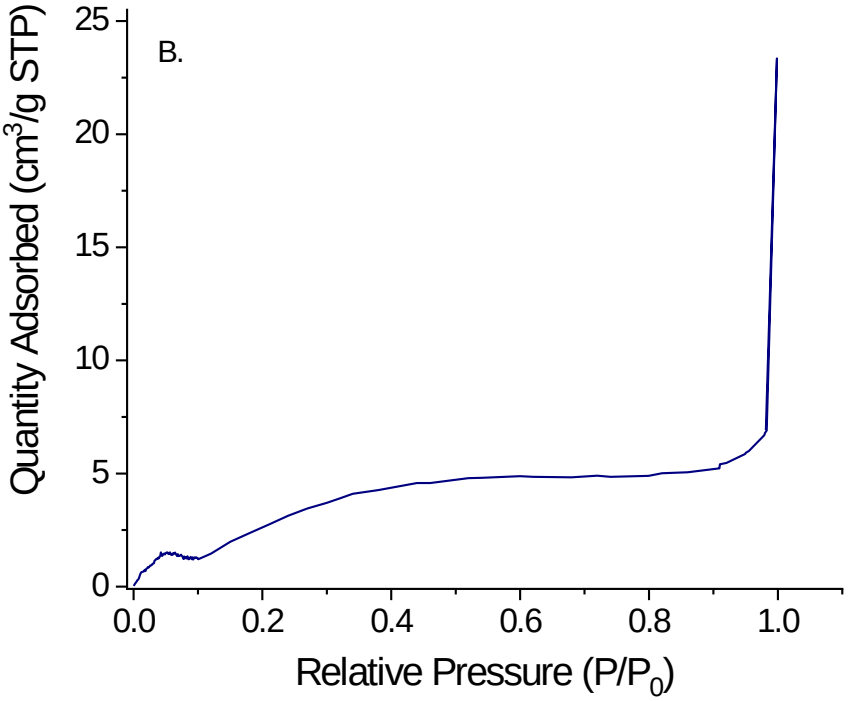
B.
Quantity Adsorbed (cm3/g STP)
0
5
10
15
20
25
0.0
0.2
0.4
0.6
0.8
1.0
Relative Pressure (P/P0)

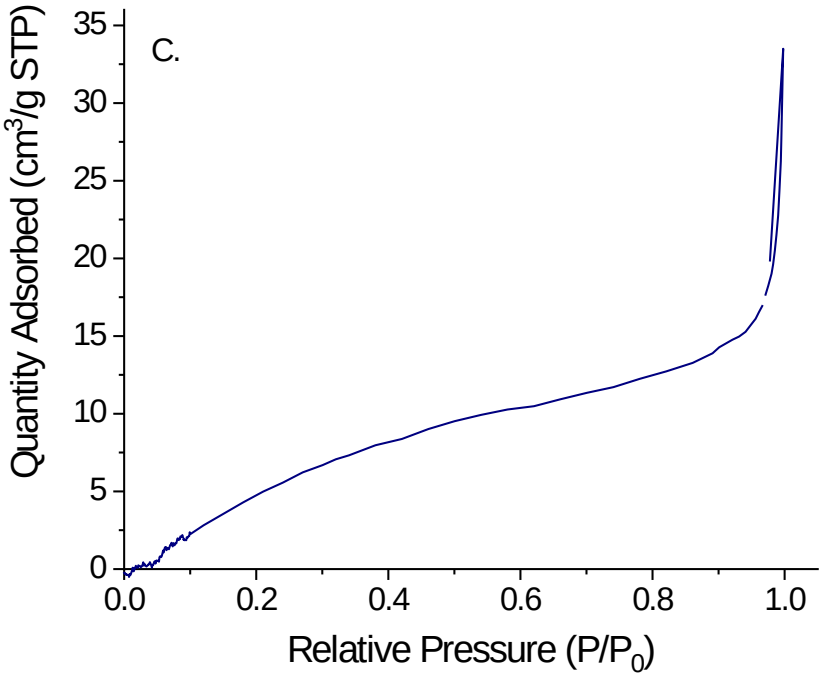
C.
Quantity Adsorbed (cm3/g STP)
0
5
10
15
20
25
30
35
0.0
0.2
0.4
0.6
0.8
1.0
Relative Pressure (P/P0)

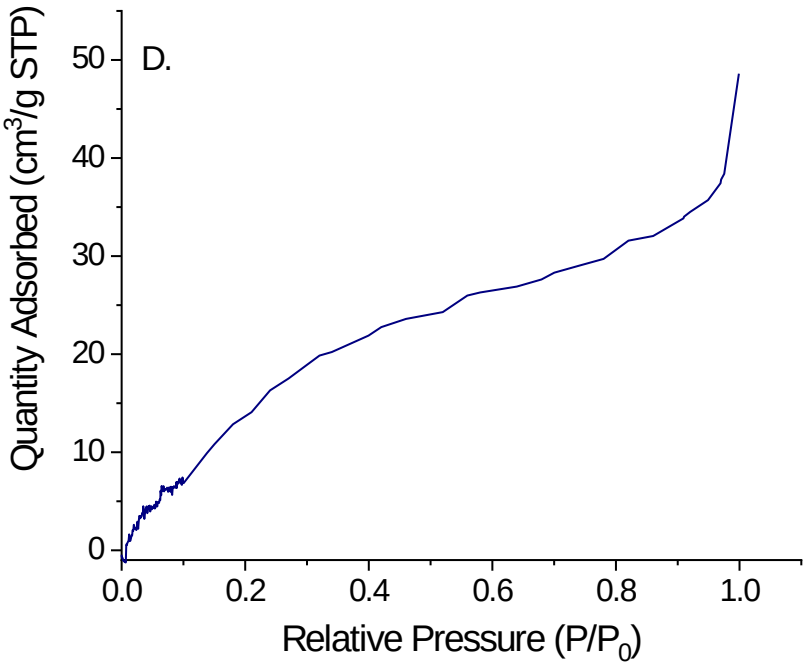


**Figure 3.5: Nitrogen isotherms for the four "MIF" species with calculated BET surface area A) MIF-1 (266.5 $m^2/g$). B) MIF-2 (21.4$m^2/g$), C) MIF-3 (35.5$m^2/g$), and D) MIF-4 (82.3 $m^2/g$) all show nonporous or low mesoporous character.**

MIF-1, when analyzed by a differential H-K plot, shows a broad range of pore sizes, centered around 10Å (Figure 3.6). This broad distribution of pore size extending into the mesoporous region is consistent with the material existing as an amorphous extended solid. The uniformity of pore sizes typically seen in MOFs is a product of their high crystallinity; not having that ordered structure would mean that pore sizes would have a wide distribution. Regardless, the H-K plot shows significant microporous adsorption pore sizes.

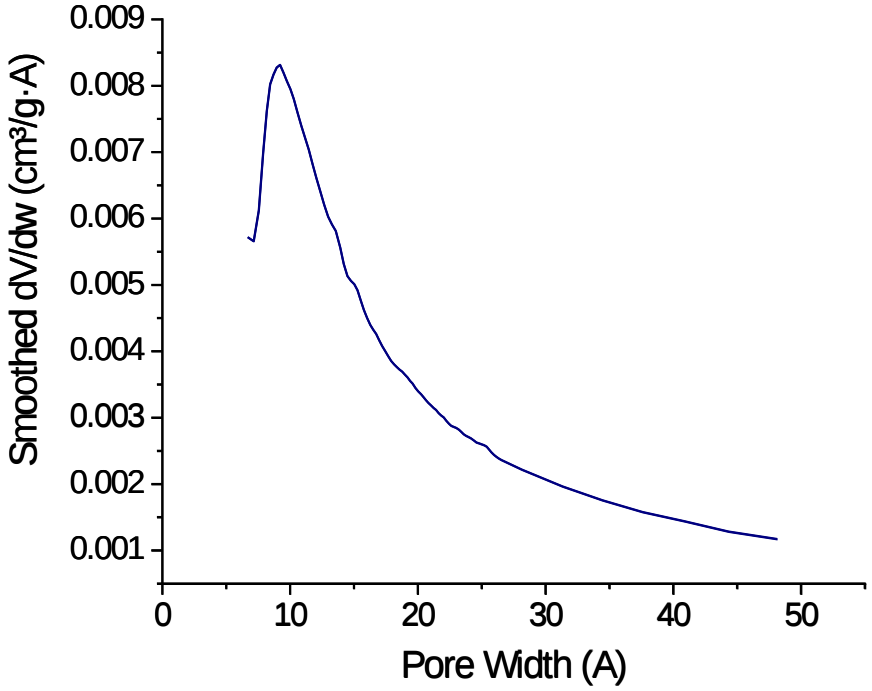


**Figure 3.6: H-K plot of MIF-1 showing the average pore width of the material in the microporous region.**

## 3.4 Diffuse Reflectance

Below in Figure 3.7 is diffuse reflectance spectra attained from four of the MIFs. All the species have strong absorbance in the blue-UV region, giving them their yellow appearance. The nickel MIF shows a larger range than the others, giving it an orange appearance. This wider absorption is likely due to additional d-d transitions brought by the $Ni^{2+}$ centers in the complex. MIF-1, 2 and 4 all have maximum absorbance around 360 nm, corresponding to the $S_0 \rightarrow S_1$ excitation of Pt-POP.

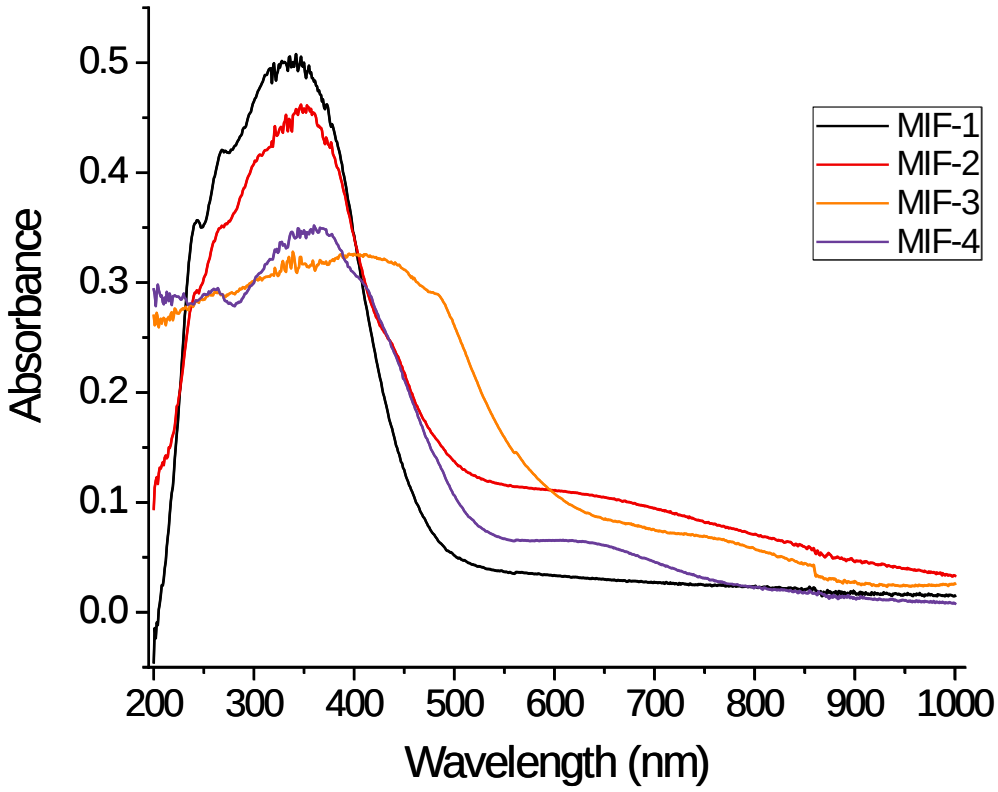


**Figure 3.7; Diffuse reflectance of MIF species**

Band gap energies were calculated from the diffuse reflectance data (Table 3.1). MIF-3 shows the lowest band gap of the three, with a calculated energy of 2.04 eV. MIF-3 therefore has a wide optical absorption profile and may have some uses as a semi-conductor despite having poor photoluminescence.

**Table 3.1: Calculated band gaps of MIF species**

| Species | MIF-1 (Zr) | MIF-2 (Zn) | MIF-3 (Ni) | MIF-4 (Mn) |
|---|---|---|---|---|
| Bandgap (calculated) | 2.52 eV | 2.42 eV | 2.04 eV | 2.33 eV |

## 3.5 Luminescence

Two of the four samples exhibit significant luminescence at ambient temperatures, MIF-1 and MIF-2. Due to their empty (or full) d-shells, MIF-1 and MIF-2, made with Zr(IV) and Zn(II), do not exhibit any quenching from the coordinating metal. There should be little electronic interaction between the metal and PtPOP species, hence preserving its luminescence without nonradiative quenching pathways to a low-lying ligand field state. However, Mn(II) is $d^5$ and Ni(II) is $d^8$, both high spin. Because of this, these metal complexes will have a quenching effect instead, whereby ligand field states at longer wavelengths in the red and near IR regions are prevalent in such paramagnetic species. Indeed, these materials are nonluminescent, or greatly quenched compared to the $Zn^{2+}$ and $Zr^{4+}$-based complexes, and even the NaPtPOP starting material.

Luminescence from these MIFs still come from the Pt-Pt interactions in the $Pt_2(P_2O_5)_4$ structure. The shifts in emission bands could either be due to metal interactions on the open face of the platinum or else from binding of the free oxygen atoms on the PtPOP complex. While PtPOP in solution has a strong and bright green luminescence, these solid-state species have more yellow emissions. This red shift is due to modulation between the Pt(II) centers and the Zr(IV) or Zn(II) coordinating metals. By adding these $d^0$ or $d^{10}$ metal centers, we allow communication to happen between the discrete PtPOP molecules and the larger metal-oxide coordination system. We can also see the opposite of this in the nonluminescent systems, where the luminescent is quenched via communication to the paramagnetic Ni(II) and Mn(II) centers.

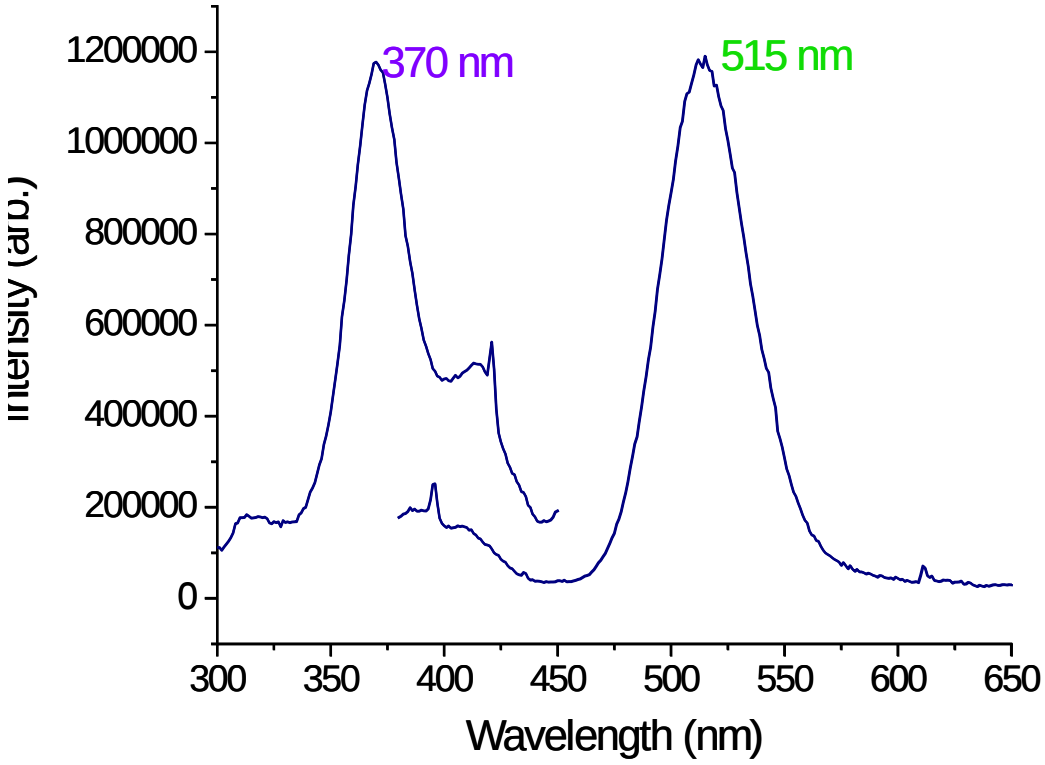


**Figure 3.8: Room temperature luminescence spectrum of NaPtPOP**

Figure 3.8 shows the solid spectrum of NaPtPOP. It shows a peak max of 370nm, like that of the Pt-POP in solution, attributed to the $S_0 \rightarrow S_1$ transition, with a minor contribution from the $S_0 \rightarrow T_1$ transition at approximately 425nm.[64] Its primary emission is at 515 nm, attributed to the $T_1 \rightarrow S_0$ triplet emission. MIF-1 shows two excitation peaks with an emission that is red-shifted from Pt-POP (Figure 3.9). The primary excitation attributed to the $S_0 \rightarrow T_1$ transition is also red shifted to 450 nm and, significantly, represents the main excitation route.

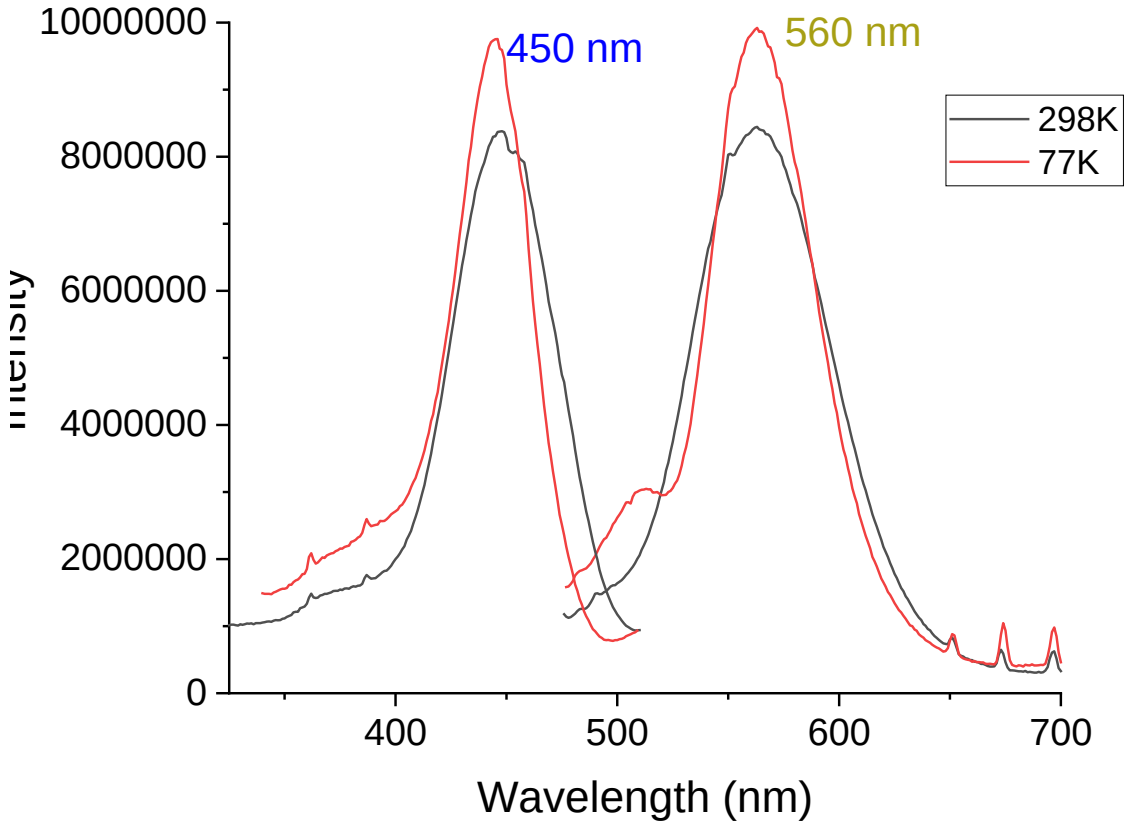


**Figure 3.9: Room temperature and 77K spectrum of MIF-1**

A temperature dependence study was done on MIF-1 (Figure 3.10). The dominant excitation and emission peaks stay in the 450-560 nm range throughout all temperatures with a doubling of intensity from room temperature to 77K. As the sample cools, however, a second emission peak begins to show up at 520 nm. These multiple emission peaks could be due to multiple Pt-POP environments within the amorphous structure of the MIF, as this second, higher energy emission peak is very close to the NaPtPOP emission. As the material is amorphous, it is difficult to correlate these peaks to specific phenomena.

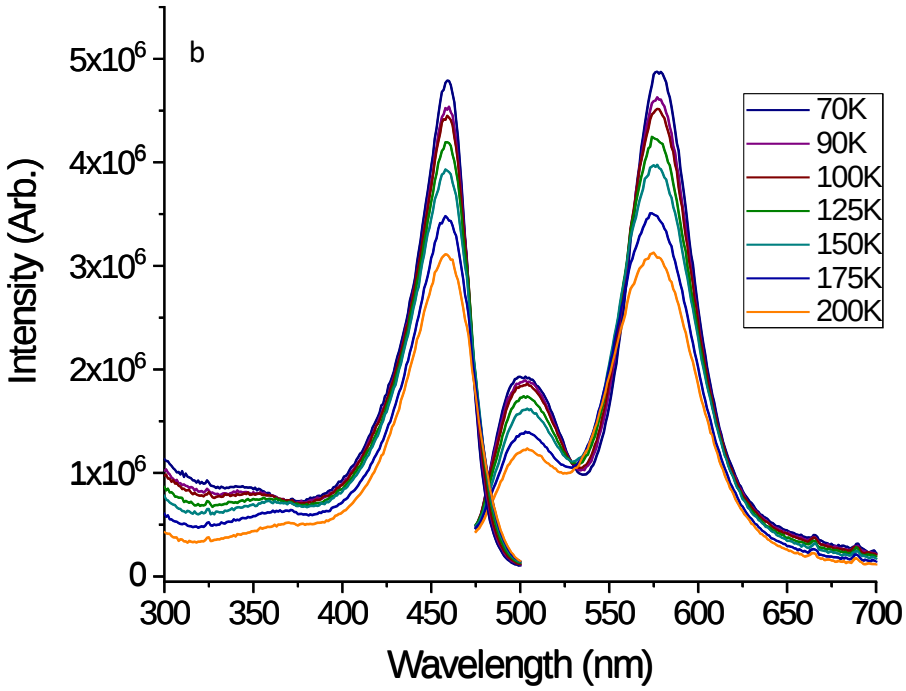


**Figure 3.10: Temperature dependence of MIF-1 absorption and emission.B) Excitation/emission pairs of 450/575 nm**

MIF-2 shows a similar profile to MIF-1. The absorption at 375 nm is markedly higher than MIF-1, showing that the excitation to a singlet state is more accessible, though the triplet excitation is still dominant. At 77K, the MIF-2 absorption spectrum begins to show multiple other, smaller peaks. Unlike MIF-1 however, there is much less variance of emission over temperature changes and a second emission peak does not occur. These peaks could again be caused by the Pt-POP environments, or even assisted by the zinc (II) metal that it is coordinating with.

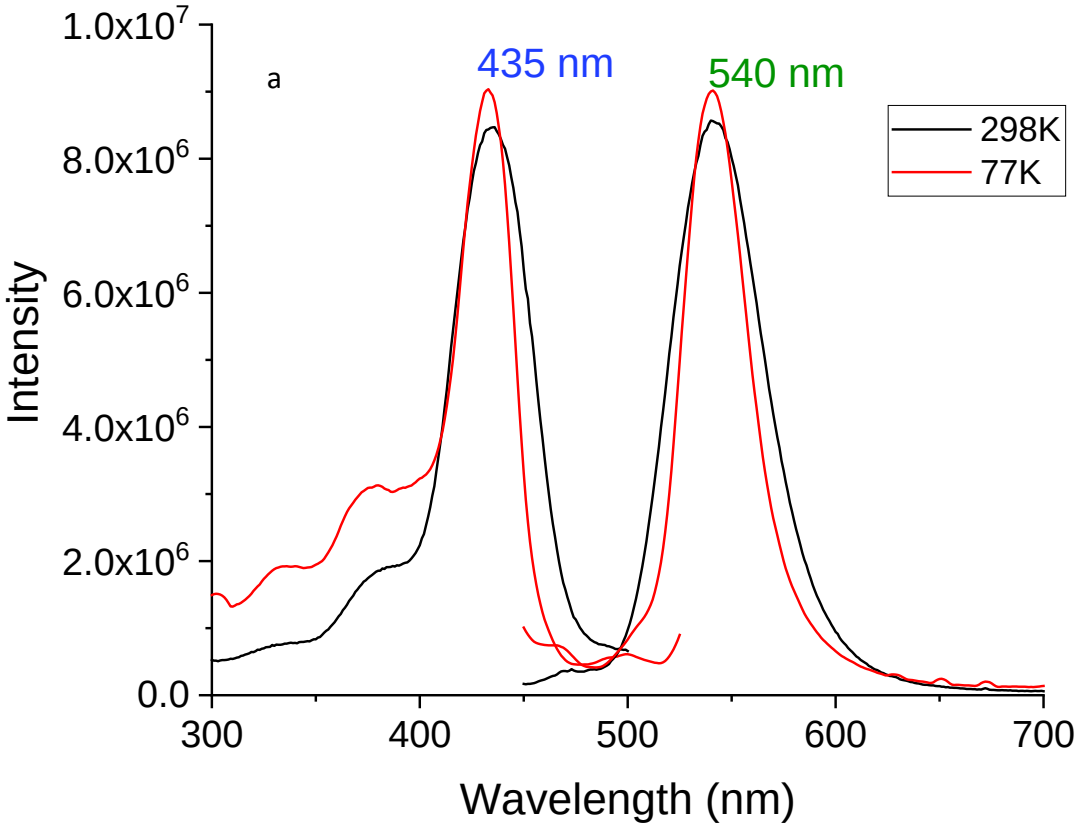


**Figure 3.11: Room temperature and 77K spectrum of MIF-2**

Overall, the two MIF materials would be expected to have similar excitation and emission profiles, since the phenomenon comes from the interactions in the diplatinum complex, rather than what is happening outside of it. While MIF-1 has a heavier atom binding the phosphors together, potentially increasing its relative lifetime and triplet state stability relative to MIF-2, the $P_2O_5$ ligands bound to the platinum makes for a fairly rigid structure.

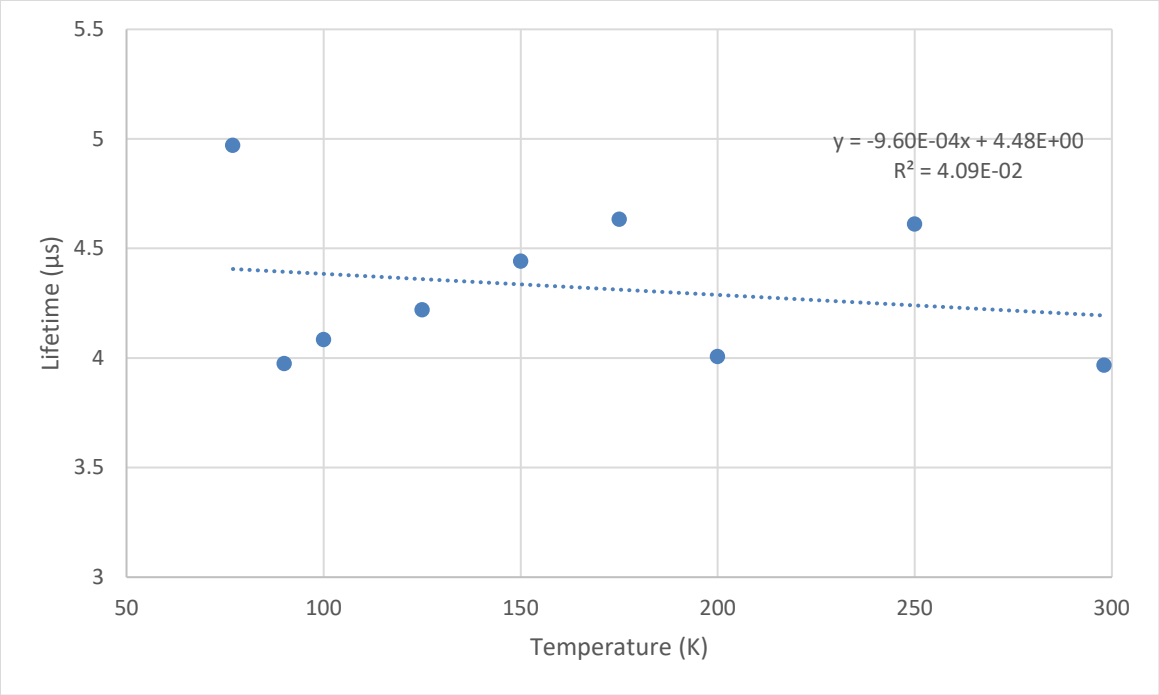


**Figure 3.12: Lifetimes of MIF-2**

MIF-2 lifetime showed to be 3.9 µs at room temperature (Figure 3.12). This is compared to a reported lifetime of NaPtPOP of 2.8 µs[77]. At 77K this lifetime remains largely constant, and it seems to be largely independent of temperature. These results are consistent with the much higher PLQY of MIF-2 versus NaPtPOP. The constant lifetime also suggests that even at room temperature, MIF-2 is emitting fairly efficiently and at a high PLQY, as one could infer that there is little nonradiative decay to be reduced.

Compared to NaPtPOP solid, the quantum yield of MIF-1 and 2 are significantly enhanced. Each sample had a primary excitation peak at 435-440 nm. MIF-1 showed a full order of magnitude improvement in quantum yield over NaPtPOP at room temperature. This marked difference could be due to the increased stability of the MIF materials compared to the starting material, as the same deteriorating processes that happen with the starting material happen

slower, if at all, to MIF-1 and MIF-2 due to a less favorable environment for redox processes to occur at the platinum centers.

**Table 3.2: Quantum yields and lifetimes of various PtPOP-based solids**

| | Quantum Yield | | |
|---|---|---|---|
| Sample | MIF-1 | MIF-2 | PtPOP solid |
| Excitation | 440 nm | 435 nm | 370nm |
| Quantum Yield | 0.2090 | 0.1220 | 0.02 |
| Lifetime (298K) (μs) | 3.5 | 3.9 | 2.8 |
| Lifetime (77K) (μs) | 7.4 | 4.97 | |

The degradation of PtPOP comes from an interaction between PtPOP and free oxygen molecules to cause oxidative degradation to Pt(IV) or light to cause photoreduction to Pt(0). By replacing the simple counterion of $Na^+$ with the larger coordination systems of Zr and Zn, we are able to restrict the steric pathway by which oxygen is able to attack the Pt(II) system. This situation is akin to the stabilization of phosphines upon coordination to transition metal ions which usually prevents their oxidation to phosphine oxide. This way we are able to have a more stable extended solid whereby the quenching effects of oxygen are mitigated; as a consequence, these extended solids not as able to sense oxygen as PtPOP in solution as previous studies have shown.

## 3.6 Conclusions

Using Pt-POP as a base material, we made a series of inorganic extended solids. Two samples, MIF-1 and MIF-2 were luminescent with red-shifted emissions compared to the parent material, with emission peaks at 560 and 540 nm, respectively, compared to $Na_4$PtPOP's peak emission at 515nm. Quantum yields were also enhanced in the solid state, with the luminescent

MIF materials showing up to a 10-fold improvement in quantum yield versus the starting material. We showed that there is electronic communication between the Pt-POP centers and the metal centers with MIF-3 and MIF-4, where the manganese (II) and nickel (II) quenched the luminescence of Pt-POP. These materials are shelf stable under ambient conditions for dramatically longer than that of the $Na_4$Pt-POP material. MIF-1 shows porosity with a measured BET surface area of 266.5 $m^2/g$. This porosity allows for further studies and applications for the material as a sensor or a means of sequestering chemical agents. Further studies using Pt-POP as a MIF linker will work on making crystalline samples, rather than the amorphous solids shown in this chapter. This will likely involve introducing secondary linkers to make multivariate MIFs, or MOF/MIF hybrids.

# CHAPTER 4

# HIGHLY LUMINESCENCT PYRIDYL AZOLATE COMPLEXES AND THEIR METAL INORGANIC FRAMEWORK COORDINATION POLYMERS

## 4.1 Photoluminescence of Extended Solids

Luminescence in MOFs has seen increasing interest in the last five years, and has been reviewed extensively in other works.[78-81] Most commonly, luminescent MOF research focuses on using lanthanide metal centers as emissive sites, using the linker to produce the "antenna effect".[82-84] MOFs based on this concept show the characteristically strong, sharp bands associated with lanthanide emissions. Since the linkers within MOF structures are typically extended pi structures, they tend to show luminescence on their own. This luminescence can be enhanced by increasing rigidity and thus decreasing nonradiative quenching effects. Recently Wei et al. showed an increase from 33% of the free linker to unity quantum yield in a fluorescing MOF by isolating and rigidifying the molecule.[85]

Zhan et al. developed a copper (I) pyrazolate trimer complex to be used in their MOF materials.[86] In their MOF materials they saw a thermochromic behavior brought on by competitive excited states of the Cu trimer and the $Cu_4I_4$ metal cluster that connected the trimers into an extended framework. In FMOF-1 however there has not been a published instance of luminescence to date, though silver-lanthanide interactions in other materials have been reported.[52,87,88] Zhao et al. produced a series of La-Ag MOFs and studied them for their luminescent properties.[88] Several of these materials showed strong luminescence assigned to the lanthanide centers, using the previously mentioned antenna effect to sensitize the metal.

When platinum is interacting with MOFs, it is usually not acting as a structurally-integral coordination site. Typically, Platinum-group metals are attached to chelating sites post-synthetically.[89-91] MOF-253, for example, uses 2,2'-bipyridine-5,5'-carboxylic acid ($H_2$bpydc) as its linker. The carboxylate groups coordinate to metal centers, in the case of MOF-253 aluminum, leaving the bipyridine group open to act as an additional coordinating site. Atoini et al. used this coordinating site to place iridium and platinum complexes inside the MOF structure.[90] They used XPS to confirm the coordination of platinum and iridium, and then compared absorption and emission spectra of the different species. Toyao et al. used a different structure comprising of $H_2$bpydc and zirconium to produce a similar structure Zr-MOF-bpy-$PtCl_2$. They showed that this structure could be used as a hydrogen evolution catalyst using visible light absorption.[92]

Coordination polymers (CPs) with Pt(II) as a heteroatom in the extended structure have been reported. Hara et al. produced a series of CPs using $K_2[Pt(CN)_2(bpydc)]$ as the linker with a series of metals. These compounds showed thermochromic and solvochromic effects.[91,93] A series of Pd-Zn based CPs were synthesized by Miyazaki et al. They observed porosity in two of these CPs, but did not report on any potential luminescence properties.[94]

Square planar platinum complexes have long garnered attention for their luminescent properties.[94-102] It is well established that platinum-platinum distances play a significant role in a complex's luminescent properties. A great example of this comes from studies in which a series of pyrazolate-bridged diplatinum complexes.[99,101,103] These studies controlled the platinum distances using different functional groups on the 3 and 5 positions of the pyrazoles. The first study by Ma et al. also had a mono-platinum analogue to show how an isolated center would act in similar conditions. The single platinum center showed structured, ligand-centered emission at

room temperature in solution, while the diplatinum complexes showed broader, lower-energy emission dependent on the Pt-Pt distance caused by the substituted pyrazole ligands from a $^3$MMLCT excited state.

Previous members of this group have studied potential OLED materials extensively.[104,105] One material, bis(3,5-dipyridyl-1,2,4-triazolato)platinum(II) or $Pt(ptp)_2$, exhibited strong orange luminescence and tunability of the color in solution, found to be linked to monomeric or exomeric emissions. This material is of interest in this work due to the ligand's free imine groups on the coordinating ligand (figure 4.1). This site can be used as a secondary coordination site to establish increased rigidity in the structure and produce novel emission peaks, as was shown in chapter 2.

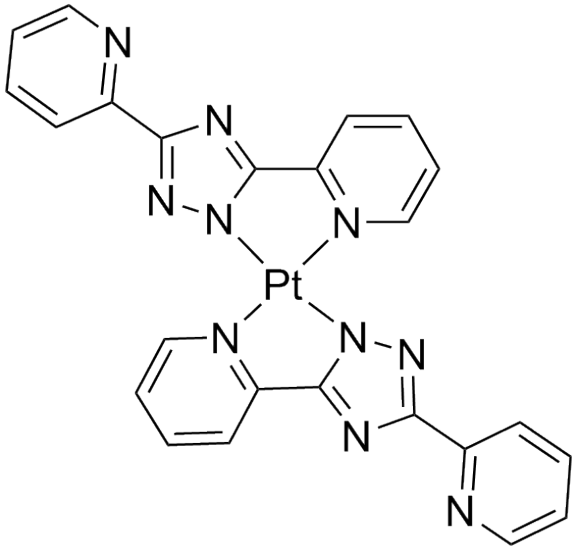


**Figure 4.1: Chemical Structure of Pt(ptp)2**

By creating luminescent extended solids, we hope to develop materials that are brightly luminescent and incredibly stable. Porous materials have their advantages for this application as sensors, since their porous nature allows small molecules access to quench or enhance the emission peaks of the material.[106]

The goal of this project is to synthesize new heterometallic porous coordination polymers using established bright platinum-based square planar complexes. This will be a first in that the Pt(II) centers will hold an integral role in the structure of the coordination polymer, with the whole $PtL_2$ inorganic complex serving as the linker in the CP. Porosity will allow us to load other luminophores into the framework to possibly produce white light, and the exposed metal sites will potentially allow unique gas adsorption or catalytic properties.

Following the trend of using previously established luminescent complexes, an attempt was made to design new similar compounds that are more favorable for making extended solids with carboxylate terminal functional groups. Having these groups will allow us to more reliably use solvothermal synthesis with metal salts like that of published MOF procedures.[34] The structure needs to be symmetrical to function in this way, and for that we chose platinum (II) complexes. Two ligands were made and complexed with platinum.

## 4.2 Materials and Methods

### 4.2.1 Synthesis of $H_2$cpt/Hcept

#### 4.2.1.1 2-pyridylamidrazone

Method was modified from a previously published procedure.[107,108] 2-Cyanopyridine (5.0135g, 0.0481mol) was combined with hydrazine hydrate (2.9ml, 0.048mol) in a 50 mL round-bottom flask. The mixture was gently stirred and heated in 3mL ethanol until all materials dissolved or melted, then stirred at room temperature for 24 hours. Solvents were removed by vacuum, then the remaining solid was recrystallized in toluene. Yield 3.906g (0.0287 mol), 60%. $^1$H NMR (DMSO): $\delta$ = 8.510(d), 8.015(d) 7.689 (t), 7.269(t).

#### 4.2.1.2 3-(ethoxycarbonyl)-5-(pyrid-2'-yl)-1,2,4triazole

Method was modified from a previously published procedure.[107] 2-pyridylamidrazone (3.0g, 0.022mol) and 14.9mL(0.11mol) diethyl oxalate were combined in 15mL ethanol in a dry 50mL round bottom flask and refluxed for 2 hours under nitrogen. The resulting solution was filtered, and the solid $H_2$cpt was collected. The solution was collected and placed in the refrigerator for 3 days, and the off-white precipitate was filtered and collected as 3-(ethoxycarbonyl)-5-(pyrid-2'-yl)-1,2,4-triazole (Hcept). Yield 2.301g, 48% $^1$H NMR (DMSO): 8.724 (d, py), 8.137 (d, py), 8.025 (t, py), 7.561 (t, py), 4.339 (q, $CH_2$), 1.317 (t, $CH_3$)

### 4.2.2 Synthesis of Platinum bis-(3-(ethoxycarbonyl)-5-(pyrid-2'-yl-κ$N_1$)-1,2,4triazole-κ$N_1$) (Pt(cept)$_2$)

0.2513 (1.14mmol) of Hcept were dissolved in 3:1 pyridine:$H_2O$ with 0.2400g $K_2PtCl_4$ (0.576mmol). The solution was placed in a microwave for 3 hours at 90°C while stirring. The resulting pale yellow solid was filtered and washed with water, ethanol, and ether, then dried in a vacuum oven at 60° for 4 hours. Yield 0.1304g (0.207mol), 42%.

### 4.2.3 Synthesis of Platinum bis-(3-carboxy-5-(pyrid-2'-yl-κ$N_1$)-1,2,4triazole-κ$N_1$) Pt(Hcpt)$_2$

Pt(cept)$_2$ (0.100g, 0.159 mmol) was placed in 20mL of 3M aqueous KOH in a 50mL round-bottom flask. The reaction was held at 90°C for 24 hours with a small Vigreux condenser. After 24 hours, the material had dissolved into a yellow solution. 1M HCl was used to adjust the pH to 4, where a yellow-orange product precipitated. This product was collected via filtration, washed with water, and dried under vacuum at 60°C for four hours. The resulting product was a flaky red solid with bright red luminescence. Yield: 0.095g (0.135mmol), 85%.

### 4.2.4 Synthesis of Hcepp

Previously reported synthesis procedure was modified[109].

#### 4.2.4.1 Ethyl picolinoylacetate

In a flame-dried 100mL round-bottom flask, 2.320g (0.034mol) NaOEt was added under inert environment. 44mL absolute EtOH was added and gently heated and stirred until the NaOEt was dissolved. The solution was allowed to cool to room temperature, then 4.22mL (0.031mol) diethyl oxalate was added, followed by 3.48mL (0.031mol) 2-acetylpyridine. The solution was allowed to stir for 18 hours, whereupon the ethanol was removed. The resulting solid was dissolved in water, neutralized by acetic acid, then extracted by 4x25mL diethyl ether. The ether layer was dried over $MgSO_4$, then solvent was removed and the resulting solid dried to afford 5.563g product as a white-brown solid (0.0288 mol, 92.9% yield). Product was used without further purification.

#### 4.2.4.2 3-(ethoxycarbonyl)-5-(pyridine-2-yl)pyrazole (Hcepp).

Crude product of ethyl picolinoylacetate (5.563g, 0.0288 mol), was dissolved in 20mL dry ethanol. 1.67mL of hydrazine monohydrate (85% solution in water, 1 equivalent) was added dropwise to the solution, then the mixture was heated to reflux for 3 hours. The ethanol was removed, and solid crude product was dissolved in 40 mL ether, then washed with 20x2 mL water. The aqueous layer was then extracted twice with 20mL ether, then the organic layers were combined, dried with $MgSO_4$, and then solvent removed. Crude product was a brown solid. This crude product was purified via column in 50/50 hexane/ethyl acetate. Final yield:

1.437g, .0067mol; 23% yield). $^{1}$H NMR: 1.424 (3H, t, $CH_3$) 4.44 (2H, q, $CH_2$), 7.72 (1H, d, py), 7.75 (2H, m, pz + py), 8.79 (1H, d, py), 11.85 (1H, s (broad), N-H).

#### 4.2.4.3 Platinum bis-(3-(ethoxycarbonyl)-5-(pyridine-2-yl- κ*N*$_1$)pyrazole-κ*N*$_1$) (Pt(cepp)$_2$)

0.100g (0.460 mmol) Hcepp and 0.095g (0.230 mmol) $K_2PtCl_4$ were dissolved in 4mL 3:4 Acetone:$H_2O$ solution. The solution was heated by microwave to 70°C for 5 minutes, and then cooled to 4°C to facilitate crashing out of the product. The product was collected by filtration and washed with cold water, acetone and then ether. The final product was dried overnight under vacuum. Yield: 0.05g ($1.21x10^{-4}$mol; 53%).

#### 4.2.4.4 Platinum bis-(3-(ethoxycarbonyl)-5-(pyridine-2-yl- κ*N*$_1$)pyrazole-κ*N*$_1$) (Pt(Hcpp)$_2$)

Pt(cepp)$_2$ (0.050g, 0.121 mmol) was placed in 20mL of 3M aqueous KOH in a 50mL round-bottom flask. The reaction was held at 90°C for 24 hours with a small Vigreux condenser. After 24 hours, the material had dissolved into a yellow solution. 1M HCl was used to adjust the pH to 4, where a yellow product precipitated. The solid was collected via filtration and washed with water, and then diethyl ether. The solid was dried under vacuum over 24 hours, resulting in a brown flaky solid. Yield: 0.044g (0.114 mmol; 94%).

#### 4.2.4.5 MIF-5 (Zn-Pt(cpt)$_2$)

0.050g($8.72x10^{-5}$ mol) Pt(cpt)$_2$ and 0.0760g (0.255mmol) $Zn(NO_3)_2{\cdot}6H_2O$ were dissolved in 20mL $H_2O$, 3mL TEA, and 2.5mL HOAc inside a 30mL scintillation vial, forming a yellow-orange, viscous solution. The vial was placed in an 80°C oven for 4 hours, forming a bright yellow solid.

The solid was rinsed several times with $H_2O$ and then dried under vacuum. Yield 0.0471g ($7.41x10^{-5}$ mol), 85%.

#### 4.2.4.6 Structural Determination of $Pt(cepp)_2$*

A microcrystalline sample of Pt(cept) was lightly ground with agate mortar and pestle. Then, it was deposited in the hollow of a silicon zero-background plate 0.1 mm deep. X-ray powder diffraction data for structure determination were collected at room temperature, in the 2θ range 5-105°, with steps of 0.02° and a total scan time of approximately 12 h, on a Bruker AXS D8 Advance diffractometer equipped with a Cu-Kα tube (λ = 1.5418 Å), a Bruker Lynxeye linear position-sensitive detector, a filter of nickel in the diffracted beam and the following optics: Primary beam Soller slits (2.3°), fixed divergence slit (0.5°), receiving slit (8 mm). The generator was set at 40 kV and 40 mA. A standard peak search followed by profile fitting led to the estimation of the low-to-medium-angle peak maximum positions. Approximate unit cell parameters were derived through the Singular Value Decomposition algorithm[110] implemented in TOPAS-Academic V6.[111] The space group was assigned based on the observed systematic absences. Structure solution was performed with TOPAS-Academic V6 by a combined Monte Carlo/Simulated Annealing approach.[112] The cept ligand was described through a rigid body, imposing idealized bond distances and angles. The background was modelled by a polynomial function. A refined, isotropic thermal parameter was assigned to the metal atoms; lighter atoms were assigned an isotropic thermal parameter 2.0 $Å^2$ higher. The

* Experimental details provided by Dr. Simona Galli, Professor of Chemistry, Dipartimento di Scienza e Alta Tecnologia, Università dell'Insubria

peak shape was described with the fundamental parameters approach. Peak shape anisotropy was described with 1/cos(θ)-dependent spherical harmonics. Crystal structure refinement was carried out by applying the Rietveld method[113] as implemented in TOPAS Academic V6. During the final Rietveld refinement stages, bond distances (except for the C-H distances) of the ligand were refined in restrained ranges, based on a search for similar organic molecules in the Cambridge Structural Database v. 2017.

Main crystallographic details for Pt(cept): triclinic, *P-1*, $a$ = 4.0459(2) Å, $b$ = 9.7420(3) Å, $c$ = 13.8275(4) Å, α = 106.844(2)°, $\beta$ = 97.745(5)°, $\gamma$ = 77.252(5)°, $V$ = 507.27(4) Å$^3$, $Z$ = 2, $d_c$ = 2.06 kg/L, $F$(000) = 368, $R_{Bragg}$ = 3.96%, $R_p$ = 6.29% and $R_{wp}$ = 8.45%, for 4951 data and 57 parameters in the 6-105° (2□) range.

## 4.3 Synthesis and Structural Determination

The first task was the synthesis of the ligands. These were made using minor alterations of previously established procedures for 3-(ethoxycarbonyl)-5-(pyridin-2-yl)-pyrazole ($H_2$cepp)[109] and 3-(ethoxycarbonyl)-5-(pyrid-2'-yl)-1,2,4-triazole ($H_2$cept)[107]. For the sake of this work, all ligands were given systematic names (fig. 4.2). The ester forms of the ligands were used rather than the carboxylic acid analogs to prevent coordination of the carboxylic acid groups to platinum centers.

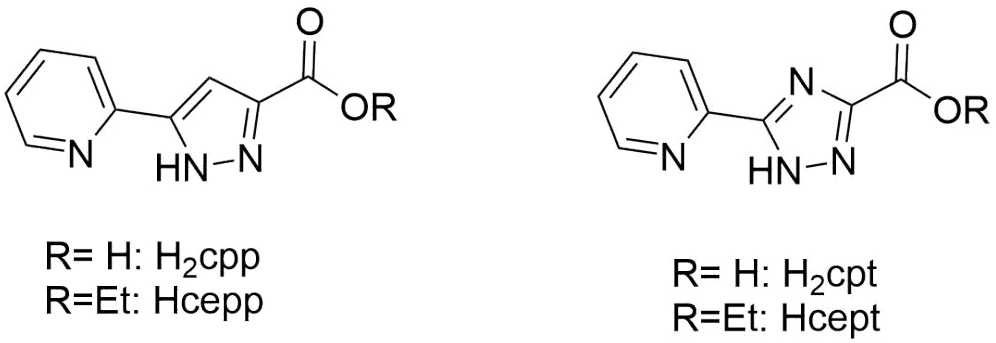


**Figure 4.2: Names of the ligands referred to in this chapter**

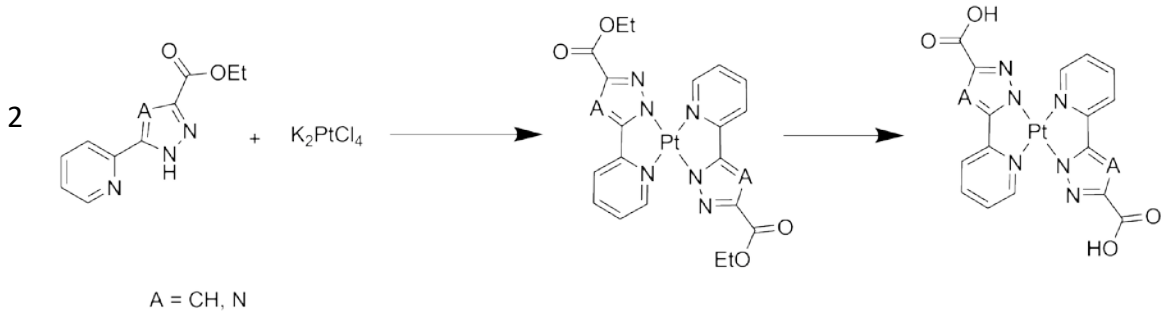


**Figure 4.3: General reaction for making square planar complexes**

Complexation of the ligands to the metals occurred quickly in microwave reactors to form highly crystalline powders of $Pt(cept)_2$ and $Pt(cepp)_2$. Both materials showed to be largely insoluble, and hydrolysis of the complexes had to be performed by allowing a suspension of the solid to stir while heating at 90°C for 24 hours. After some time, the solids dissolved, and the reaction was pushed to completion by distillation of the ethanol product out of the reaction vessel. Previous experiments showed that if this is not done, the product will only partially hydrolyze, forming an orange solid rather than red.

### 4.3.1 $Pt(cepp)_2$

Complexes of $Pt(cepp)_2$ were synthesized. The solids were analyzed by IR, PXRD, and in the case of Pt-cepp, NMR. $Pt(cepp)_2$ NMR was taken in DMSO, and shows a peak dramatically

shifted downfield compared to the free ligand from 8.65 to 10.47 ppm. This peak correlates to the hydrogen next to the nitrogen in the pyridyl ring. This shift occurs due to the deshielding effects of the platinum metal coordinating to the pyridyl ring, changing the electron density of the ligand. You can see smaller deshielding effects (0.2-0.5ppm) on the other aromatic hydrogens, pushing the signals further downfield and causing them to overlap less. The ethyl ester signals, on the other hand, are slightly more shielded showing a upfield shift of 0.05-0.1ppm. This could be due to the ether oxygen taking slightly more double-bonded character versus the free ligand. The hydrolyzed Pt-Hcpp product has similar solubility problems to the triazolate analog, and thus a solution NMR is more difficult.

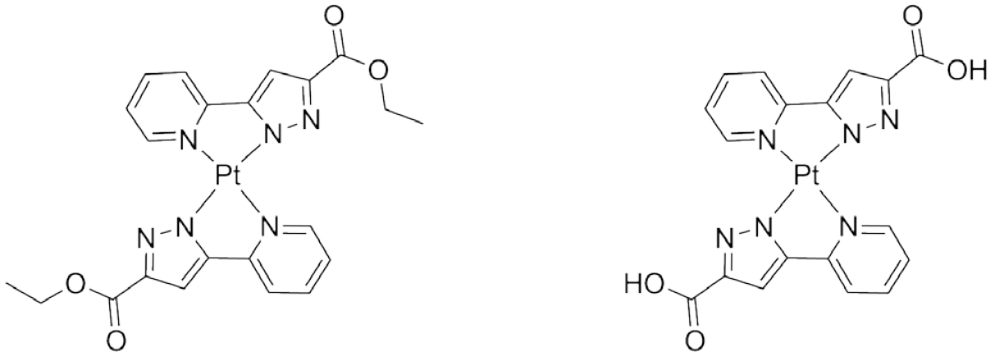


**Figure 4.4: Structures of Hcepp-based platinum complexes**

An initial crystal structure of Pt-cepp was solved with NMP solvent shown to be between the platinum complexes (Figure 4.5). Though this system was grown with solvent between the main complexes, we can still derive useful information about the parent molecule. This structural determination shows that the Pt(II) center is ligated as predicted, and the ester remains intact through the reaction. Using this crystal structure, we can also see that the molecule is planar. This material showed a light blue luminescence which may give some insights into the material's

singlet emission but does not correlate to the material that is produced in the synthesis. This is further backed up by the differences in powder patterns between the solved crystal structure and the bulk powder (Figure 4.6). The crystal has a monoclinic space group, which means there are many reflections in the PXRD due to the low symmetry.

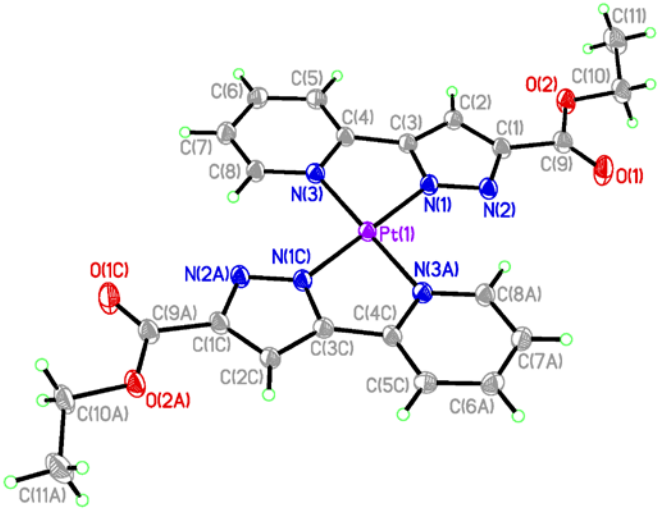


**Figure 4.5: Structure of Pt-cepp**

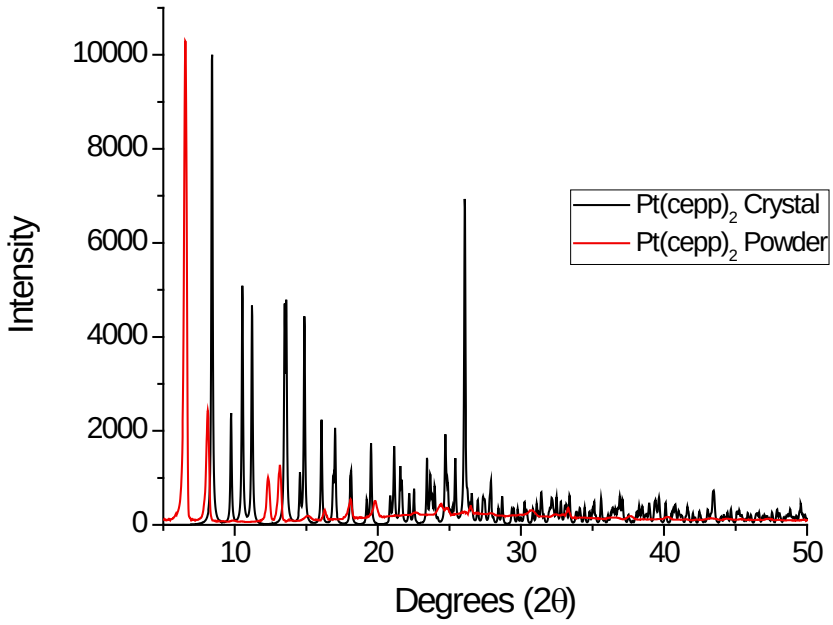


**Figure 4.6: Pt-cepp bulk material vs calculated powder pattern from the NMP/Pt-cepp crp crystal**

### 4.3.2 $Pt(cept)_2$ Family of Complexes

The triazole series of complexes proved to be significantly less soluble than the pyrazole analogs. While Pt-cepp was slightly soluble in DMSO and even slightly soluble in the solvent mixture it was synthesized in, Pt-cept proved to be insoluble. However, after hydrolysis Pt-Hcpt was soluble in basic water. Once the platinum complexes were synthesized, PXRD of the samples were analyzed to determine crystallinity. This series of complexes showed significant differences in the PXRD between the ester and carboxylic acid (Figure 4.7). The $d_{max}$ of Pt-cept is significantly higher than the hydrolyzed form, which means the Pt centers should be considerably further apart.

Once $Pt(Hcpt)_2$ was synthesized successfully, the task of forming an extended structure began. The first metal to be used was zinc since it has been a staple in MOF development for some time. Since the Pt complexes had considerable difficulties with dissolution, our conditions were limited. However, we were able to successfully combine the compound with zinc to form an extended structure. This structure, called MIF-5, was a yellow crystalline powder.

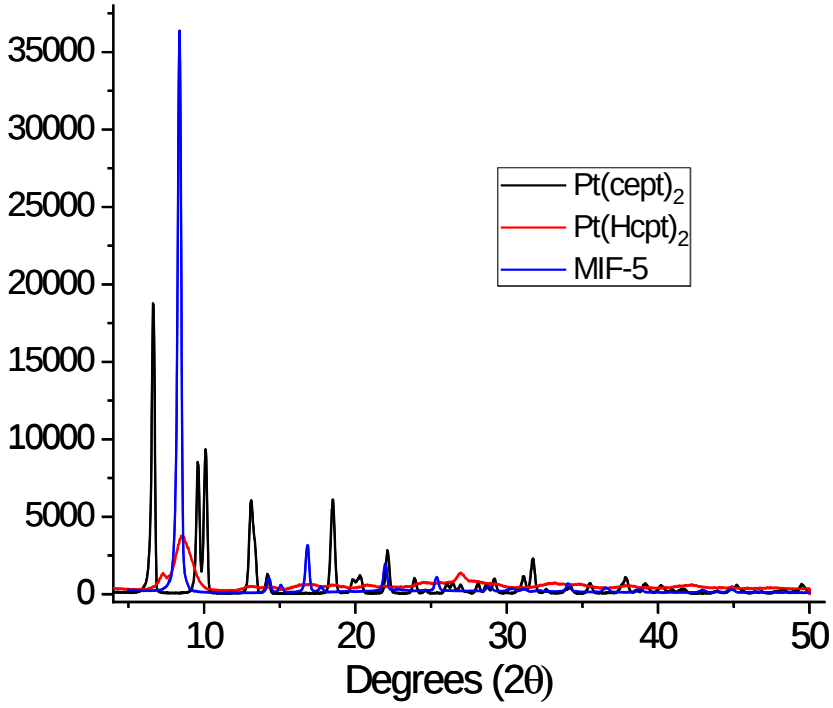


**Figure 4.7. PXRD of MIF-5 precursors and extended solid**

Above are the PXRD spectra of MIF-5 and its precursors. Qualitatively, we can see that Pt-Hcpt and MIF-5 have somewhat similar dimensions along one of its crystal faces, which will be smaller than that of $Pt(cept)_2$. Less crystalline materials will tend to have very broad peaks in their powder spectra. MIF-5 and the ethyl ester complex are both highly crystalline, and the carboxylic acid significantly less so. This could be due to the nature of the respective materials precipitating from solution; whereas $Pt(Hcpt)_2$ is recovered rather quickly by adding acid to the solution, MIF-5 and $Pt(cept)_2$ are allowed to grow slowly over a period of several hours.

A crystal structure of one of the complexes, $Pt(cept)_2$ has been solved through refinement of its powder pattern (Figure 4.8). Through the crystal structure you can see that the molecules within the complex are stacked, but the Pt-Pt distance is 4.046 Å. This is well beyond the van der Waals radius of the two platinum (II) centers, meaning there is little if any communication. This

stacking is likely caused by the ethyl group of the ester twisting outward, increasing steric bulk and interrupting the pi-stacking that we would expect to see in a material like $Pt(Hcpt)_2$.

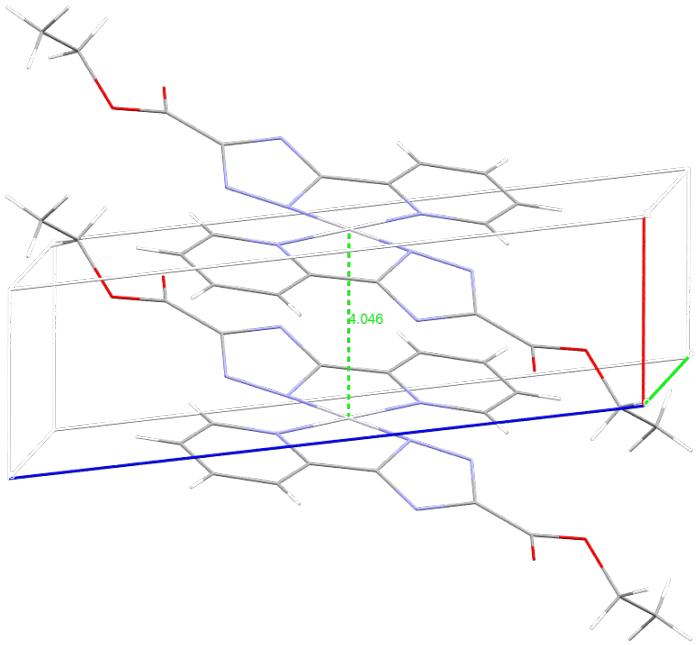


**Figure 4.8: Crystal structure of $Pt(cept)_2$ solid**

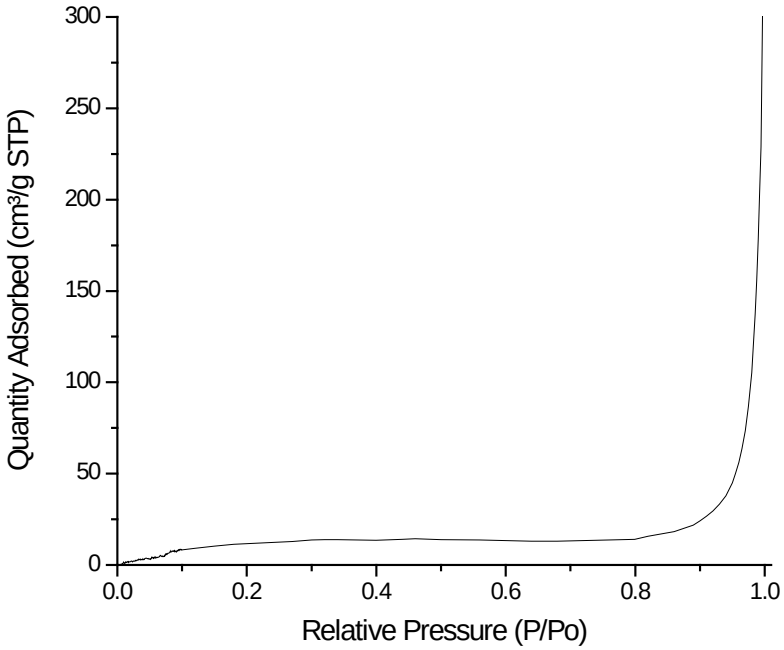


**Figure 4.9: Nitrogen isotherm of MIF-5**

Having obtained a new MIF, a nitrogen isotherm was taken to determine porosity of the solid. (Figure 4.9). The material showed a type 1 isotherm, meaning it is nonporous, and had a theoretical surface area of 44.98$m^2$/g STP at 0.3 $P/P_0$. This also makes sense from the platinum-based emissions that we will see from the MIF material in the next section, since they appear to come from platinum-platinum interactions. While these interactions could still come from a system where the ligands are stacked on one another as dimers in a larger porous stucture, such an arrangement is rare.

## 4.4 Luminescence Data of Complexes

Below are the luminescence spectra of the following complexes: Pt-cepp, Pt-cept, Pt-Hcpt, and MIF-5. Room temperature excitation, emission and quantum yield are reported in Table 4.1. Pt-cept (Figure 4.10) shows a broad emission spectrum with an adsorption max of 386 nm and emission max of 510 nm. Lifetimes for Pt-cept are all in the single microsecond range, with a small contribution of a second lifetime of around 17μs. Quantum yield increases dramatically when cooled to lower temperatures, from 12% to 81%. It is well known that cooling reduces the nonradiative decay of materials, which increases lifetimes and quantum yields accordingly; in the excitation and emission spectrum of this material at 77K, we see several peaks sharpen dramatically. Both the higher quantum yields and improved spectral resolution are well known to take place as a result of cooling to cryogenic temperatures for luminescent materials that exhibit vibronic fine structure.[114] This structured emission is consistent with the larger Pt-Pt distance within the solid, where it is more indicative of monomeric MLCT emission.

**Table 4.1: Quantum Yield of Pt-cept, Pt-Hcpt, and MIF-5**

| | Excitation | Emission | Quantum Yield | |
|---|---|---|---|---|
| | | | RT | 77K |
| Pt-cept | 365 | 510 | 12.0% | 81.3% |
| Pt-Hcpt | 560 | 660 | 39.3% | |
| MIF-5 | 450 | 565 | 7.0% | 58.9% |
| Pt-cepp | 365 | 520 | 16.4% | |

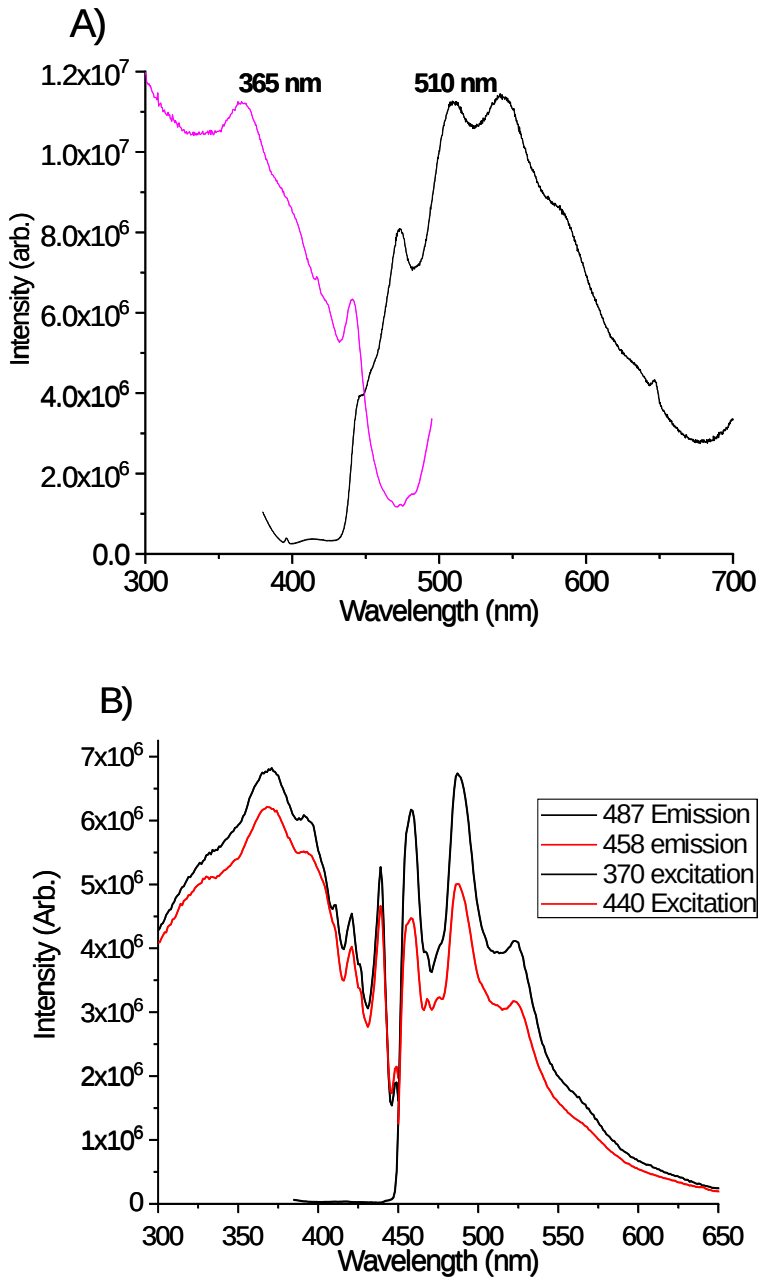


**Figure 4.10: Pt-(Hcept)$_2$ absorption and emission spectra at (A) room temperature and (B) 77K**

Pt-cepp is a bright yellow solid at room temperature, showing two emission peaks at 520 and 620 nm (Figure 4.11). This emission profile is consistent with a poorly resolved monomeric emission, as the excitation profile doesn't change between the two peaks. This is consistent with the crystal observations, as even solvated, the platinum complexes are seen unstacked. In previous examples, particularly PTA, we have seen excimeric emissions in the solid state as well as solutions as dilute as to $10^{-4}$ M.[105]

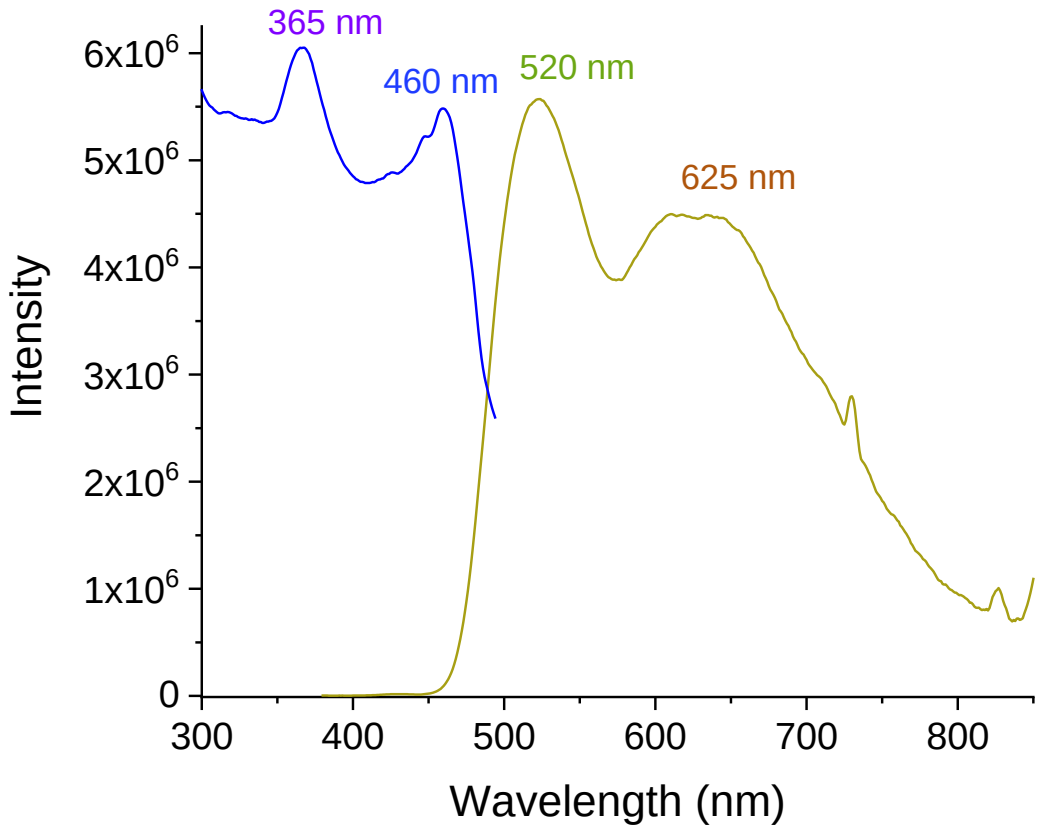


**Figure 4.11: Room temperature PL spectrum of $Pt(cepp)_2$**

Pt-Hcpt, once the ethyl groups are removed, shows a dramatically different spectrum (Figure 4.12). Its emission peak is broad and unstructured at 660 nm, owing to a metal-centered emission. Its primary excitation peak is just as broad and peaks at 570nm. Since the relatively

bulky esters are now carboxylic acids, the planar platinum complexes are able to stack closer together, leading to a strong platinum-platinum interaction. At 77K the emission hardly shifts, showing little expansion or contraction in the structure. Lifetimes are short, at room temperature sub microsecond, and at 77K only slightly higher at 1.45µs. The quantum efficiency of these materials is increased from the monomeric Pt-cept emission; at room temperature the quantum yield of Pt-Hcpt is 39.3%. This dramatic improvement is due to emission enhancement of the Pt(II) complex from the stacking. Pt-Hcpp, however, is significantly less luminescent relative to its ester analog. Since the monomeric emission of this complex is partly in the red-region of emission already, when the complex is allowed to stack and thus red-shift, the emission will shift further red toward the NIR region. As it reached the NIR region, the complex will actually begin to self-quench due to easier access to lower energy non-radiative relaxation pathways.

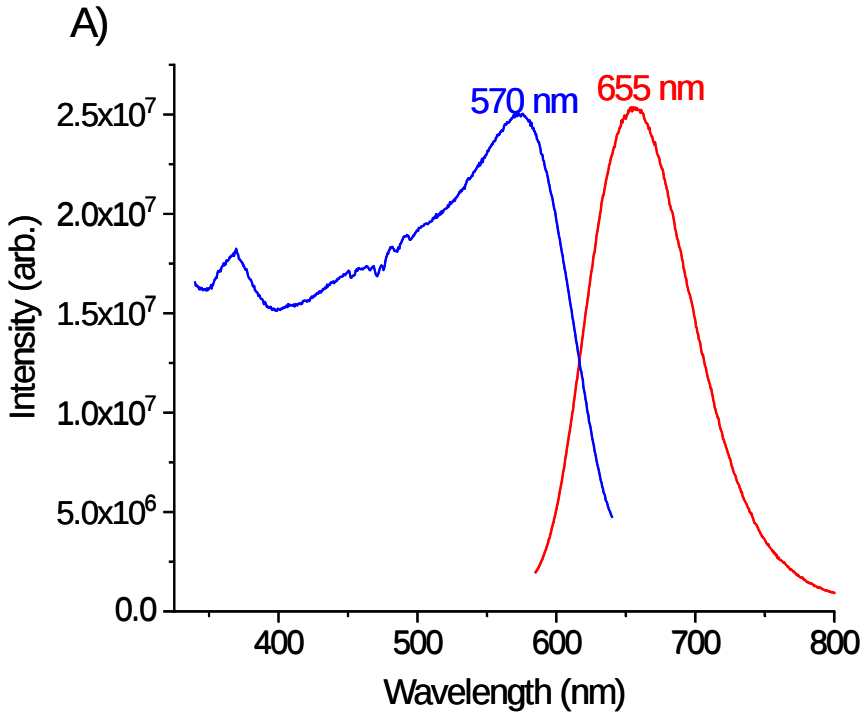

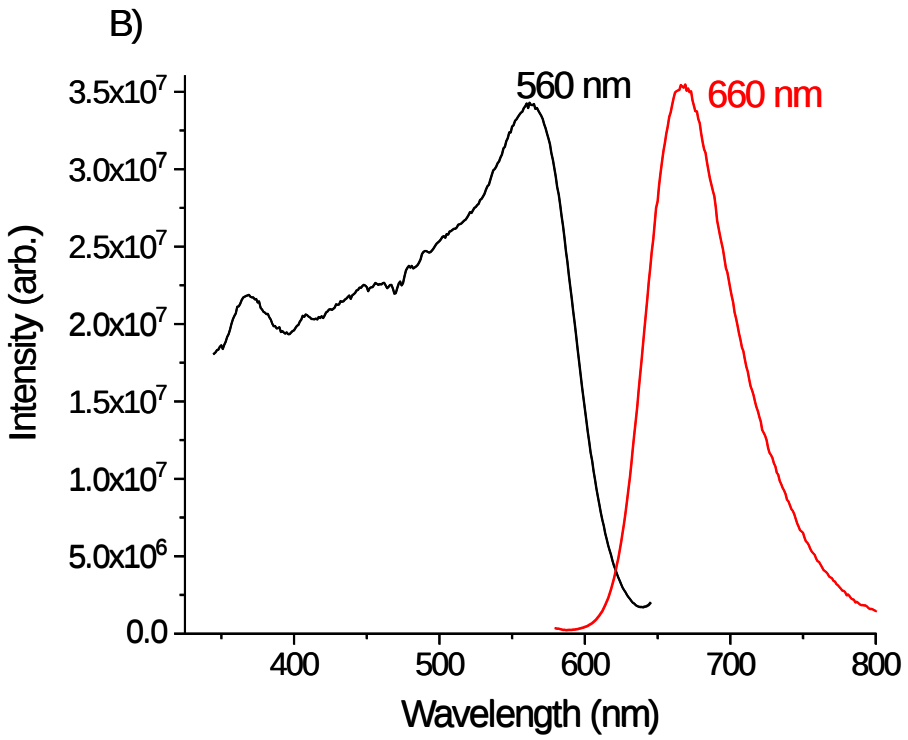


**Figure 4.12: Pt-$(Hcpt)_2$ absorption and emission spectra at (A) room temperature and (B) 77K**

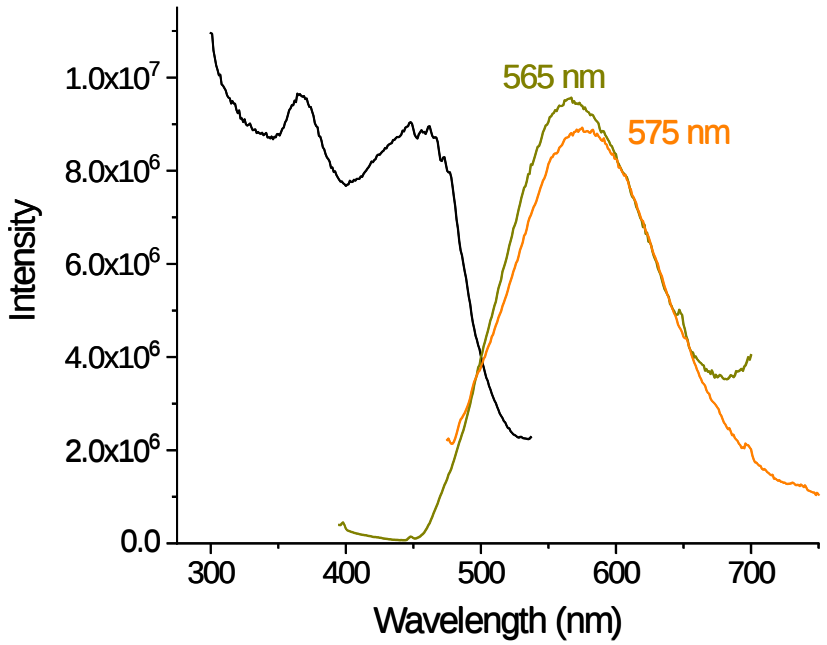


**Figure 4.13: Room temperature excitation and emission spectrum of MIF-5**

Upon complexation with zinc, the emission changes once again to an unstructured yellow emission peak. The 365 and 450nm excitation peaks are equivalent in intensity, and though the emission is broad and unstructured, it has blue-shifted to 565-575nm. A likely explanation is that the stacking of the chromophore is drastically altered versus the acid. Indeed, it is surprising to attain stacking at all in the coordination polymer regime, as tetrahedral coordination to Zn(II) is expected to distance the Pt(II) centers from one another. Nevertheless, even in absence of stacking, a certain degree of electronic communication between the Pt(II) centers through the carboxylate-zinc(II) coordination would contribute to red shifted emissions versus the monomeric species on the one hand, whereas on the other hand that remains considerably less significant than the communication due to stacking interactions in the solid form of the carboxylic acid complex. This explains the intermediate wavelength for the emission and excitation maxima in the MIF versus the acid and ester form. Like Pt-cpt, its lifetimes are sub-microsecond at room temperature. The quantum yield of MIF-5 is also diminished both at room temperature and 77K. This alludes to additional non-radiative relaxation pathways that have opened up, possibly by charge transfer into coordinated $Zn^{2+}$ centers.

## 4.5 Conclusions

A series of platinum-based luminescent complexes were synthesized as linkers for extended solids, or MIFs. Pt-cept shows strong monomeric emission as a solid, owing to its distance between platinum centers. When hydrolyzed to Pt-Hcpt the emission redshifts and narrows from the broad emission centered around 540nm, to a single unstructured peak emission at 650nm, as the platinum centers are close enough together in the second sample to

electronically communicate. This shifts the emission from a MLCT emission to one that is metal-centered. Pt-cepp shows a similar phenomenon, with a structured, if poorly resolved, emission centered around 520 nm, which turns to an unstructured, metal-centered emission upon hydrolysis. MIF-5, a new material synthesized by combining Pt-Hcpt with zinc, shows metal-centered emission at 570nm, blue shifted from that of the starting material. MIFs from these materials have yet to show porosity, but as nonporous coordination polymers they can be useful in light emitting devices.

# CHAPTER 5

# CONCLUSIONS AND FUTURE WORK

## 5.1 Conclusions and Future Direction of FMIF-1 and Derivatives

FMIF-1 has been shown to have an isosteric heat of adsorption of 15-20kJ/mol at uptakes up to 4 mol/kg. This would make it a good material for short to long term storage of $CO_2$ at these temperatures. The isosteric heat would not restrict outgassing at these temperatures, meaning storage in FMOF-1 could be used to transfer the gas to more permanent carbon sequestering solutions.

Luminescent coordination polymers have been synthesized from FMOF-1 starting materials by using secondary linkers 4,4'bipyridine and pyrazine. This shows a less typical case of room temperature luminescence from silver compounds. Several of these materials also show thermochromic shifts upon reducing temperatures to 77K. In the case of FMOF-1 being combined with a luminescent platinum complex $Pt(ptp)_2$, we see a red shift from the parent material. This extended solid also shows a thermochromic shift in its physical appearance as well as its luminescence.

### 5.1.1 FMIF-1 with Alternate Metals

Au-FMIF-1 is a first proof of concept for metal inorganic frameworks, or MIFs. By retaining FMIF-1's primary $Ag_4tz_6^{2-}$ coordination cluster and connecting them with $Au^+$ centers, we have shown that we can take metal coordination complexes and turn them into new porous materials by connecting them with new metals or metal clusters. Au-FMIF-1 shows to be isostructural to FMIF-1 and shows a similar adsorption isotherm.

In the future, FMIF-1 should be expanded to even more metal systems. Gold (I) is a good candidate to start with since the metal has well known catalytic and luminescent properties. We have found little evidence of Au-FMIF-1 showing luminescence, but its catalytic properties are still open to investigation. Other metals such as copper or earlier transition metals with a +1 oxidation state like manganese or even nickel can be incorporated into the MIF-1 framework similar to Au (I). Replacing silver (I) with these metals would allow exploration into if and how the change in metal alters pore size, and also whether the new frameworks perform catalysis.

Some work has been done previously using other metal cations to imitate the FMIF-1 synthesis, but to little success (besides Au-FMIF-1 ongoing attempts in chapter 2, which will be continued in the group). The use of zinc as a singular metal cation has led to a blue luminescent but nonporous solid, and indeed zinc has been known to react and form stable extended solids with similar compounds, i.e., triazoles, and, more notably, imidazoles in the form of ZIFs. Addition of extra bridging ligands may form interesting systems similar to those of the silver extended solids (e.g. FMOF-bpy). What is important to consider during the design of these new systems will be the geometry of the selected cation. Zinc is fond of structuring itself as a tetrahedral coordination center, so selection of ligands that would allow such a geometry to form with little distortion would likely see the most success. Of more focus however is the addition to copper to the system, particularly $Cu^{+}$. This cation is isoelectronic to the $Ag^{+}$ center we are attempting to replace in the MIF framework. In collaboration with Maspero/Galli group in Como, Italy, we have started another expansion whereby $Cu^{2+}$ was used in the FMOF and poly(tetrazolate) or poly(pyrazolate) fluorous bridging ligands to construct new FMOF materials.[28,30]

There are two primary methods for completing this. The first option is to find good synthetic conditions where the $Cu^+$ forms the bonds we desire. Doing this has the benefit of attempting a complete replacement of FMIF-1 but many side reactions could be possible, such as forming a trimer over an extended solid. However, these geometries would be difficult to produce, at least as easily as the $Ag^+$ centers are to form. The second method attempts to postsynthetically modify the FMIF-1 structure in a similar way to other MOFs. This method would involve first synthesizing FMIF-1, possibly in a crystalline form, and then submerging it in a $Cu^+$ solution for a period of time in order for the silver to be replaced slowly by copper cations. This method has been used successfully to form novel MOFs with new metal centers and could have success in making a pure copper-based isoreticular structure, or Cu-FMIF-1. Counter to what was previously shown in Au-FMIF-1, Cu(I) would prefer to replace Ag(I) in the tetrahedral-coordinated sites of FMIF-1 (Figure 5.1). According to crystal field theory, the Cu(I) centers have a smaller 10Dq, leading to a stronger preference for Td vs the trigonal planar coordination site.

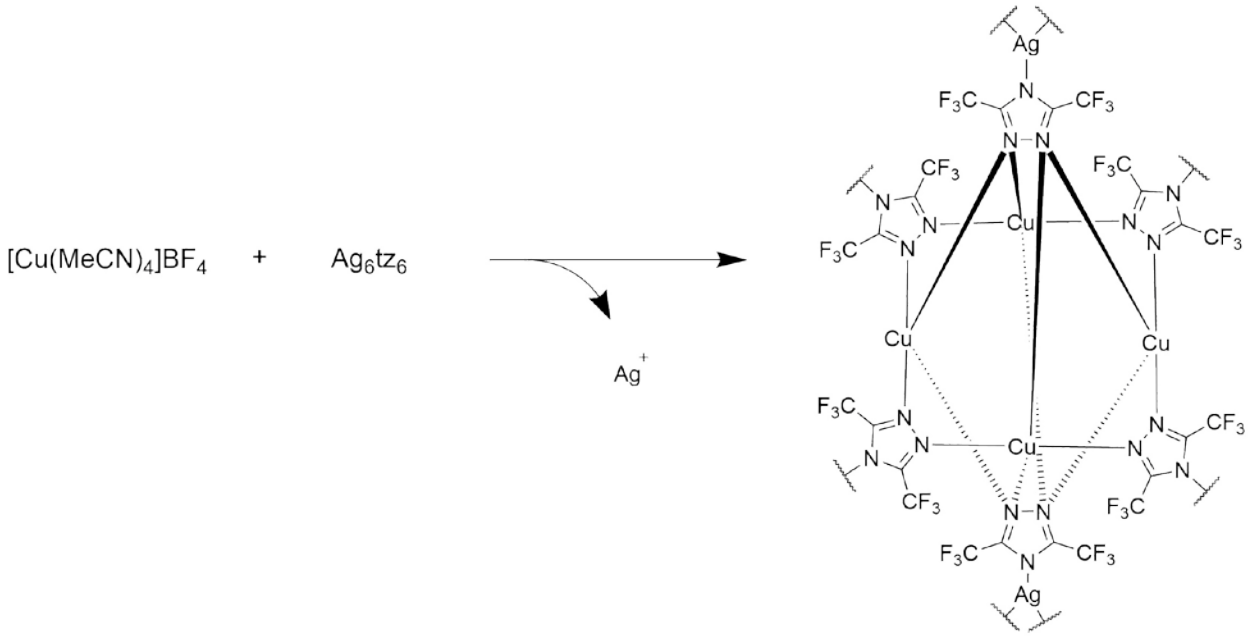


**Figure 5.1: Reaction schematic for Cu-FMOF-1 interaction**

These materials would have applications primarily in gas storage and separation. By putting more redox active metals in the framework, we may also open up applications in catalysis if small molecules can access any metal sites within the pores. The best candidate for studies to examine this behavior would likely be Au-FMIF-1, since the gold cation is both potentially catalytically active and occupies the trigonal planar coordination site in FMIF-1, which is less sterically crowded.

The uniqueness of these FMIF materials to be solubilized and regrown in their original crystalline form could have special applications in the formation of gas-permeable membranes. Previously, there has been a lot of work in using stable MOFs, particularly ZIF-8, to form thin layers or membranes for gas separation applications.[115-118] In some instances, the ZIF solids have been incorporated into polymers for enhancement of their properties. FMIF-1 and its derivatives can be used in a much similar fashion, both by growth of the base materials on a substrate through slow evaporation, or by dispersing the solid into polymers for selectivity. Using FMIF-1 in this way would also incorporate its superhydrophobic nature onto the substrate, allowing for selectivity even in humid environments, in which most MOF materials have difficulty functioning.

### 5.1.2 Investigation of Au-tz dimer

According to the mass spectrometry data of the Au-FMIF system, it appears that the Au-tz bonds are significantly stronger than the Ag-tz bond. Following this, a computational study should be performed on the gold and silver triazolate systems to provide further insight on their bonding. This should be further explored by either an Au-tz trimer or MIF synthesis, or by gradually replacing all the silver cations from the FMIF-1 material with gold. Since FMIF is

notoriously versatile in its various forms (FMOF-2, FMOF-4, FMOF-TOP, etc.), we should explore whether the Au-analog systems could be equally versatile (Figure 5.2). A full gold-based system could even prefer an FMOF-2 type structure, coordinating into a connected series of trimers. Dimeric gold systems might also have potential to form coordination polymers analogous to the bpy and pyz systems, or even the FMOF-PTA system.

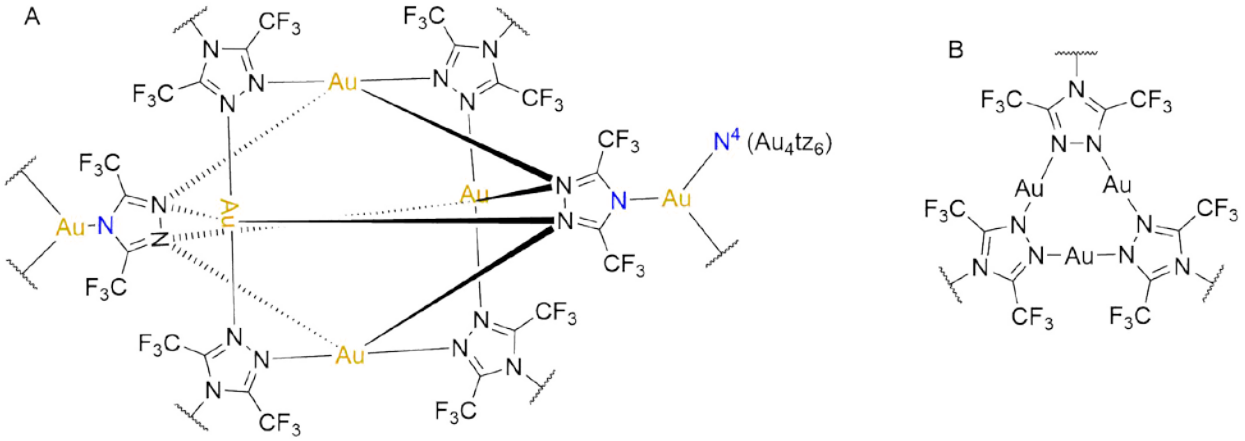


**Figure 5.2: A). Au-FMIF, with Ag(I) fully replaced with Au(I). B) $AuTz_3$ trimer, possible building block of Au-FMIF-2**

## 5.2 Pt-Pop Based Extended Solids Conclusion and Future Direction

A series of MIFs synthesized from Pt-POP were analyzed for their photophysical properties. MIF-1 and MIF-2, in which PtPOP was complexed with Zr(IV) and Zn(II) respectively, show luminescence red-shifted compared to the starting material NaPtPOP. MIF-3, complexed with Ni(II) showed a wide absorption band from diffuse reflectance, but had no detectable luminescence. MIF-4, complexed with Mn(II) likewise showed no luminescence, owing to lower energy ligand field states associated with the paramagnetic metals. All four were analyzed for porosity, and one, MIF-1, showed microporous character with a BET surface area of 266.5 $m^2/g$.

All four samples showed dramatic stability versus the parent NaPtPOP material. From previous work we have seen that PtPOP is redox active; however, by complexation into a coordination polymer, we have been able to suppress this reactive pathway, and through that, dramatically increase the solid luminescent properties of the PtPOP molecule.

The results in chapter 3 are merely qualitative, where we were primarily concerned with the relative change in PLQY upon changing the cation. Even without additional development, multiple recrystallization steps for freshly synthesized samples are expected to attain significant increases in the absolute quantum yield values. For example, simply reproducing the synthesis of MIF-2 from a freshly synthesized batch of NaPtPOP without additional recrystallization has resulted in more than tripling the quantum yield (from 12% to ~40%). From this preliminary data, it would be reasonable to expect these materials to reach quantum yields equal to that of the PtPOP solution (~50% PLQY).

### 5.2.1 Potential Luminescent MIF Linkers

Since the Omary lab has a long history of making luminescent complexes, we should leverage those already known systems into new extended solids. There have been many trimers and other luminescent gold complexes synthesized where the additional functional groups have only initially affected the luminescent properties. Using the ideas of reticular chemistry, we should be able to design syntheses that can utilize these systems to make extended solids and, potentially, porous frameworks. The rigidity that allows strong luminescent properties is also advantageous for framework linkers; targeting these rigid structures first would be most promising. Other systems Based off of Au-TPPTS (Figure 5.3), could be modified to better

facilitate crystalline MIFs, whether porous or nonporous. Replacing the sulfate group would allow for less-soluble coordination complexes to form.

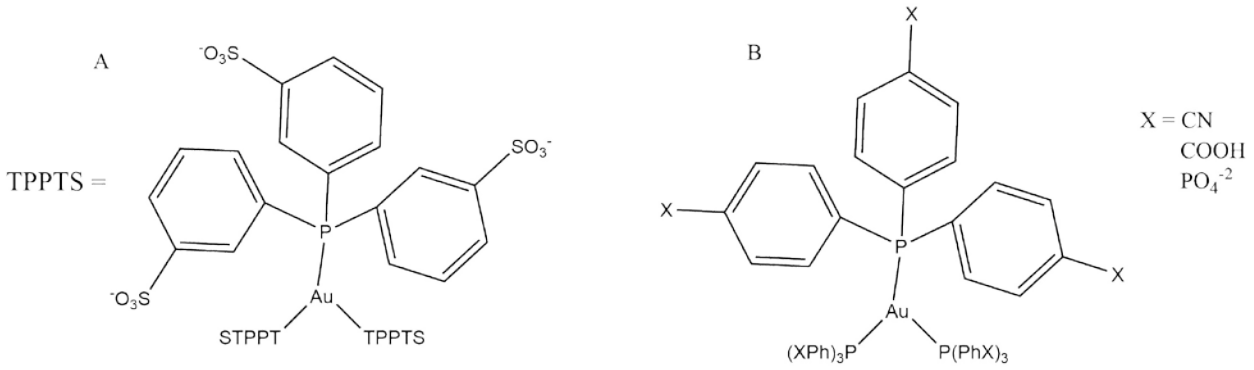


**Figure 5.3: A) Structure of Au-TPPTS. B) Proposed changes to Au-TPPTS to better-facilitate MIF formation**

### 5.2.2 Use of Trimer Systems with Carboxylate or Imide Linkers

One particular class of trimers synthesized by other members of the group are those with carboxylic acid groups on the ligands, in the 3 or 4 positions. These are prime candidates for expansion into extended solids or frameworks, similar to what was attempted with the PTA solid. These trimers would work better with metals like zirconium or aluminum, though zinc and copper could be used as well. In an effort to preserve the luminescence of these solids, we could limit the initial trials to d0 or d10 metals. Other metal cations like $Cu^{2+}$ should not be entirely excluded, as the square paddlewheel structure can lead to favorable geometries for gas adsorption.

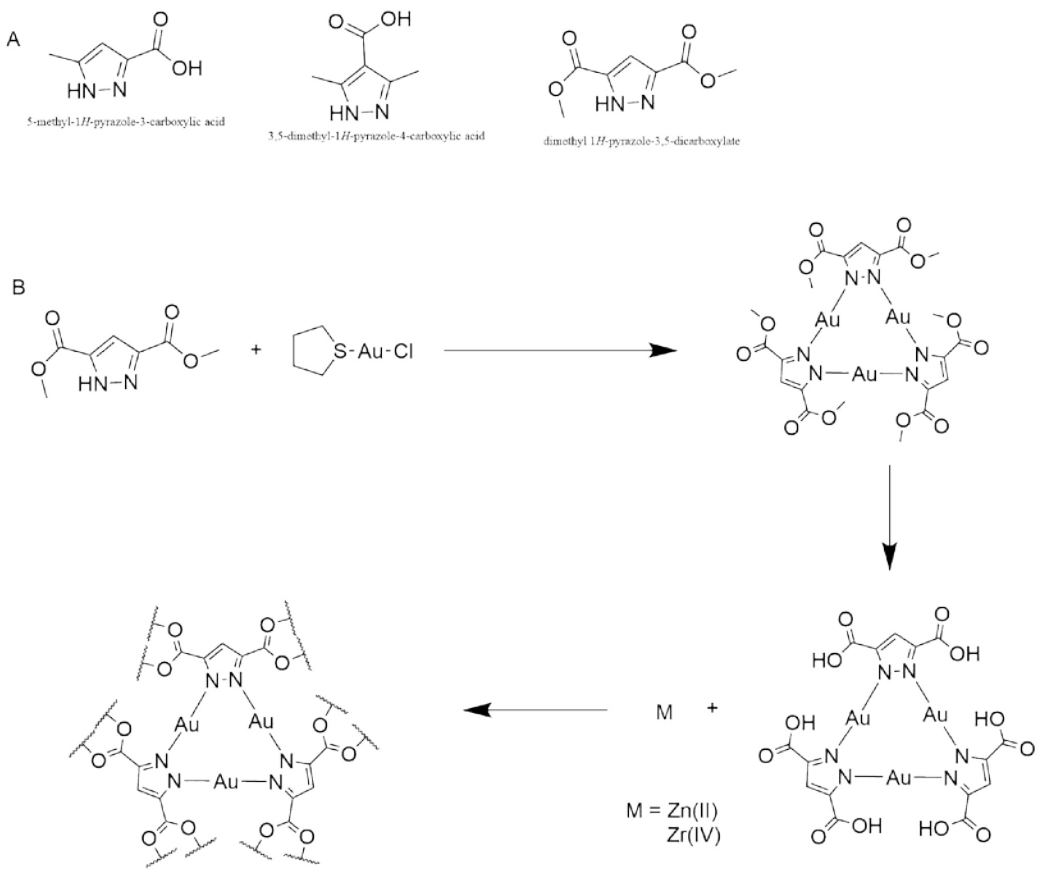


**Figure 5.4: A) Ligands previously used in trimer synthesis. B) schematic example of MIF synthesis from an Au(I) trimer**

## 5.3 Platinum Complex Based Extended Solids Conclusions and Future Work

Two platinum complexes were synthesized, $Pt(cept)_2$ and $Pt(cepp)_2$. Both show luminescent properties. $Pt(cept)_2$ was subsequently hydrolyzed and used to form a new extended solid, MIF-5. This material appeared to be crystalline via PXRD, but single crystal studies of the material are yet to be successful. $Pt(cept)_2$ showed structured MLCT emission even at room temperature, suggesting this particular material in bulk does not readily stack in a way to have strong or dominant Pt-Pt stacking between the molecules. Upon hydrolysis, the material shows strong red emission, and upon formation of MIF-5 the emission blue shifts to yellow. This can probably be attributed to the changing Pt-Pt distance in the starting $Pt(Hcpt)_2$ material versus the

MIF-5 complex. MIF-5 subsequently shows no porosity, which, pending structural refinement, likely means the material is forming in such a way that the $Pt(cpt)_2$ linker groups are stacking closely to one another. Though the MIF-5 complex is nonporous, it may have good applications in light-emitting devices due to the higher potential conductivity of the material versus the free complex and higher exciton density versus a porous analog.

### 5.3.1 Extended Solids of Already-Formed Pt-Complexes

Two new platinum complexes have already been synthesized, but there is more work to be done regarding the formation of extended solids with these materials. So far, we have only successfully formed the extended solid of $Zn[Pt(cpt)_2]$, and an amorphous form of $Zr[Pt(cpt)_2]$. These have had interesting luminescent properties but no porosity. The next objective should be extending this series to form a system with Zinc and $Pt(Hcpp)_2$ as well as zirconium, and new metal coordinating centers such as $Cu^{2+}$ and $Al^{3+}$. The aluminum complex should work similarly to the zinc system, allowing for strong luminescence since the metal would have no valence shell electrons.

### 5.3.2 Extension of Ligands to Include Extra Phenyl Rings/Additional Binding Sites

Preliminary work has already been done on extending this particular project. As reaction conditions are finalized, we can move to analogous systems with different metals; specifically, palladium. Palladium does not have the same luminescent properties of platinum, but it also could afford new systems for catalysts or be particularly good for hydrogen adsorption. Since the $Pt^{2+}$ triazolate and pyrazolate systems have been established and some success has been made

in forming extended solids, these should be expanded. One such material has already been synthesized. $Pd(cept)_2$ is a white, nonluminescent solid that shows faint orange luminescence at 77K.

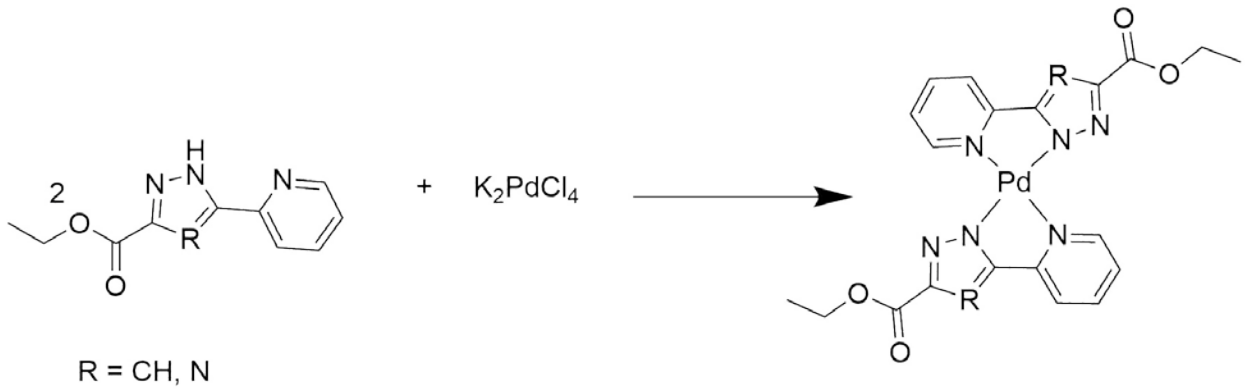


**Figure 5.5: Synthesis of $Pd(cept)_2$ and $Pd(cepp)_2$**

There are also more ligands to be explored. One concern over the reported systems is that the square planar complex is quite bulky relative to the distance from potential metal clusters of zinc and zirconium. The next step would be to synthesize additional ligands with extra phenyl rings in an attempt to allow a larger framework to form that can accommodate these bulky groups. Synthetic schematics are drawn out below, and some have been attempted already.

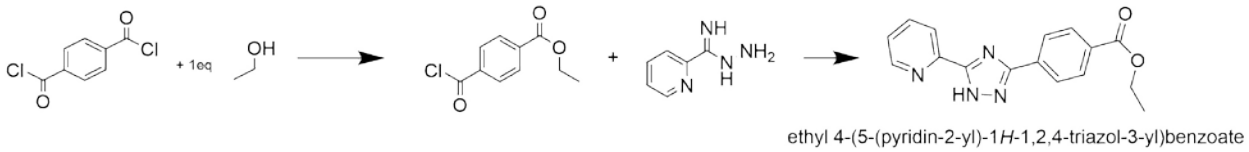


**Figure 5.6: Synthesis of ethyl 4-(5-(pyridin-2-yl) -1*H*-1,2,4-triazol-3-yl) benzoate (Hbept)**

Synthesis of this triazole has already been attempted, and the hydrolyzed ligand has been published.[119] However, upon analysis via NMR, it appears to have reacted with the ethylene glycol in the final ring-closing step, to form a different major product. This product was used to

synthesize a square-planar platinum complex. This complex has shown orange luminescence, but we have not yet generated an extended structure from this material.

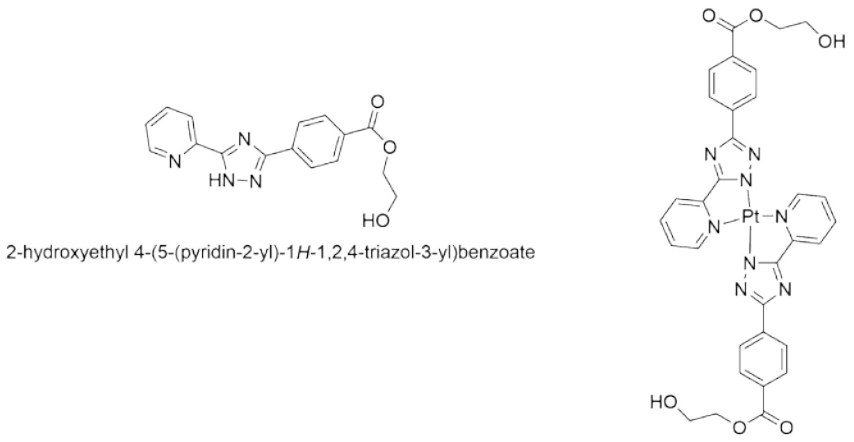


**Figure 5.7: Structure of newly synthesized ligand (Hbhept) and platinum complex ($Pt(bept)_2$)**

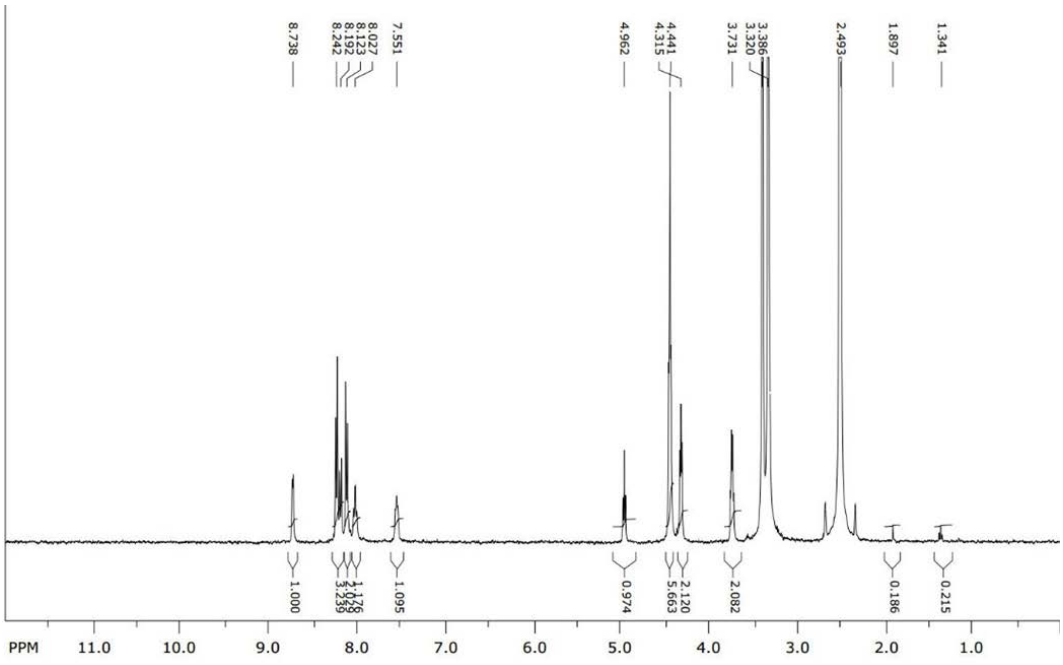


**Figure 5.8: $^1$H NMR spectrum of Hbhept**

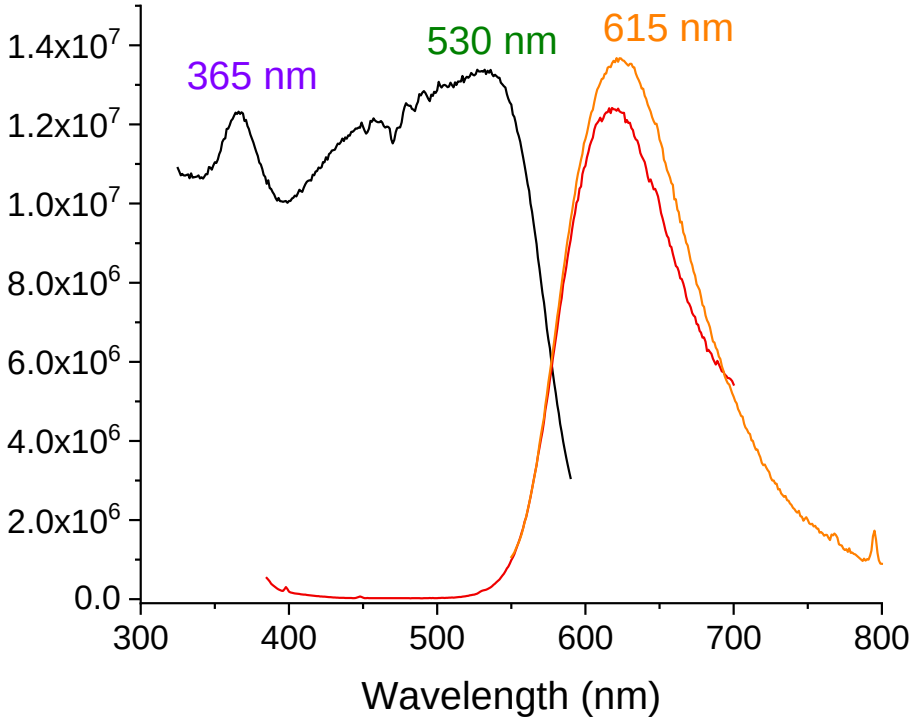


**Figure 5.9: Room Temperature luminescence spectrum of PT(bhept)$_2$**

The following pyrazolate derivative has not yet been attempted, though a proposed synthetic procedure has been provided.[120,121]

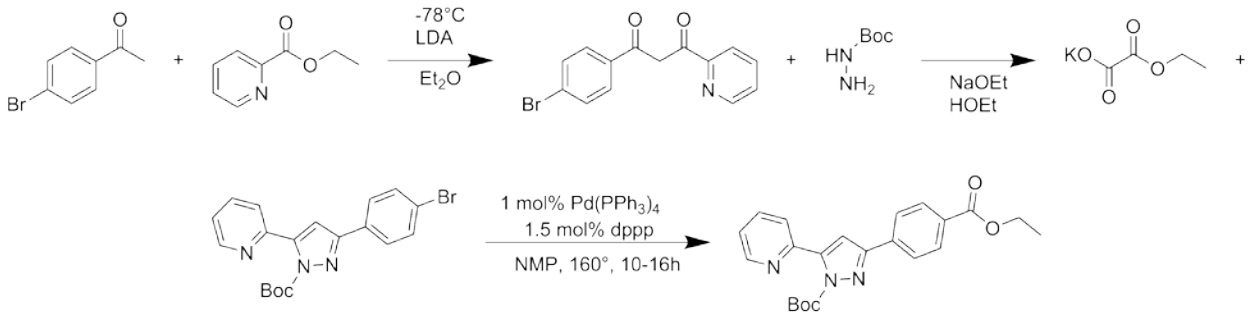


**Figure 5.10: Proposed reaction route for ethyl 4-(5-(pyridine-2-yl)-1-butoxycarbonyl-pyrazol-3-yl)benzoate (Boc-bepp)**

### 5.3.3 Zr-based Experiments

Several experiments have been attempted using zirconium instead of zinc for formation of MIF materials from the square planar platinum complexes. However, there are some compatibility problems arising from the use of zirconium with the Pt-cpt complex, namely because the latter only dissolves in basic solutions, which the former (as $ZrCl_4$) does not dissolve in at all. The work around for this was to attempt to form the Zr-carboxylate clusters first, and then add platinum afterward to form the platinum complex. This procedure results in a bright orange, crystalline solid (Figure 5.11). These signals were promising, and further attempts have been made to synthesize this material for better characterization.

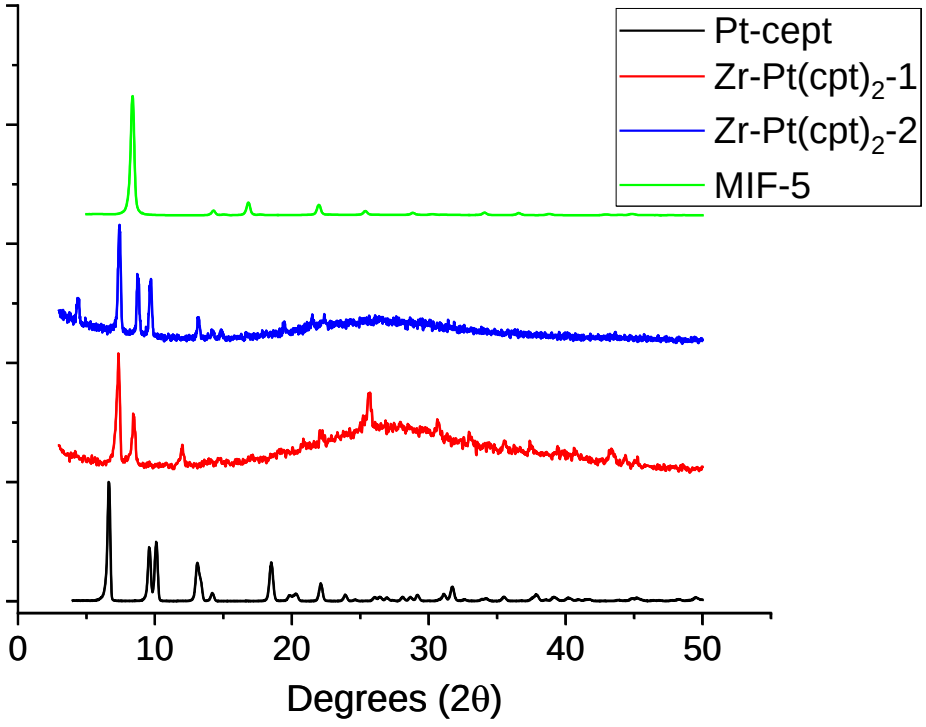


**Figure 5.11; Zr-based Pt-cpt MIF attempts vs. Pt-cept and MIF-5**

## 5.4 F-ZIFs

Following the idea of fluorinated MOFs, preliminary work has been done regarding using partially fluorinated imidazoles and benzimidazoles. Zeolitic imidazolate frameworks have been well established as robust materials, and in some instances are chemically resistant, hydrophobic, and easily synthesized. By adding fluorinated groups, new advantageous properties may be imparted on these FZIFs, such as increased hydrophobicity, which would lead to easier regeneration of the porous material, or possibly higher affinities for adsorbents. There has been work done by other groups that show some enhanced $CO_2$ and $H_2$ adsorptions upon modification of MOF ligands with fluorinated groups.[122-124] This class of FZIFs could be applied to all the same applications of ZIF-8, from thin films to gas separation. With the addition of fluorinated groups, we could impose higher mechanical hydrophobicity vis-à-vis water droplet tests, rather than the "hydrophobicity" of ZIF-8 which is only from the water isotherm.[16]

FZIF synthesis with three promising linkers both alone and combined with one another have been attempted (Figure 5.12). Each reaction was done in dimethylformamide, and all to date have formed products. Scaling the synthesis to 50-100mg for adsorption analysis will soon be performed. For the most part the products have appeared to be highly crystalline and have been submitted for single crystal XRD analysis, with results pending.

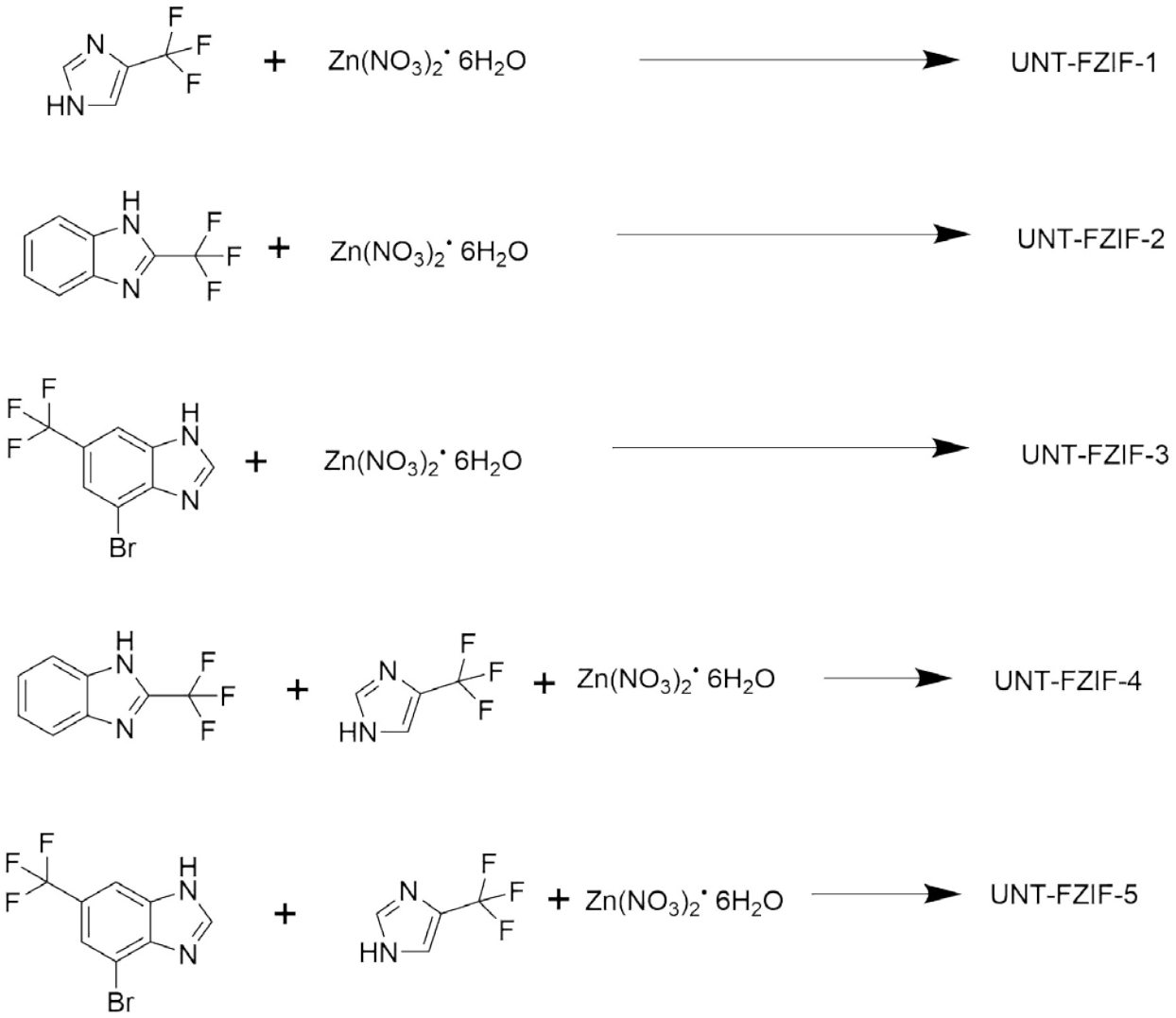


**Figure 5.12: FZIF reactions**

REFERENCES


1. Yaghi, O. M.; Li, G.; Li, H. Selective binding and removal of guests in a microporous metal-organic framework. *Nature* **1995***, 378*, 703.

2. Diercks, C. S.; Yaghi, O. M. The atom, the molecule, and the covalent organic framework. *Science* **2017***, 355*.

3. Feng, X.; Ding, X.; Jiang, D. Covalent organic frameworks. *Chem. Soc. Rev.* **2012***, 41*, 6010-6022.

4. Wong-Foy, A.; Matzger, A. J.; Yaghi, O. M. Exceptional H2 Saturation Uptake in Microporous Metal-Organic Frameworks. *J. Am. Chem. Soc.* **2006***, 128*, 3494-3495.

5. Dinca, M.; Dailly, A.; Liu, Y.; Brown, C. M.; Neumann, D. A.; Long, J. R. Hydrogen Storage in a Microporous Metal−Organic Framework with Exposed Mn2+ Coordination Sites. *J. Am. Chem. Soc.* **2006***, 128*, 16876.

6. Feng, D.; Wang, K.; Wei, Z.; Chen, Y.; Simon, C. M.; Arvapally, R. K.; Martin, R. L.; Bosch, M.; Liu, T.; Fordham, S.; Yuan, D.; Omary, M. A.; Haranczyk, M.; Smit, B.; Zhou, H. Kinetically tuned dimensional augmentation as a versatile synthetic route towards robust metal-organic frameworks. *Nature Communications* **2014***, 5*, 5723.

7. Shengwen, Y.; Desiree, W.; Alex, M.; Liu Di-Jia Porous organic polymers containing carborane for hydrogen storage. *Int. J. Energy Res.* **2013***, 37*, 732-740.

8. Nijem, N.; Canepa, P.; Kaipa, U.; Tan, K.; Roodenko, K.; Tekarli, S.; Halbert, J.; Oswald, I. W. H.; Arvapally, R. K.; Yang, C.; Thonhauser, T.; Omary, M. A.; Chabal, Y. J. Water Cluster Confinement and Methane Adsorption in the Hydrophobic Cavities of a Fluorinated Metal-Organic Framework. *J. Am. Chem. Soc.* **2013***, 135*, 12615-12626.

9. Lee, J.; Farha, O. K.; Roberts, J.; Scheidt, K. A.; Nguyen, S. T.; Hupp, J. T. Metal-organic framework materials as catalysts. *Chem. Soc. Rev.* **2009***, 38*, 1450-1459.

10. Shuai, Y.; Liang, F.; Kecheng, W.; Jiandong, P.; Matheiu, B.; Christina, L.; Yujia, S.; Junsheng, Q.; Xinyu, Y.; Peng, Z.; Qi, W.; Lanfang, Z.; Yingmu, Z.; Liangliang, Z.; Yu, F.; Jialuo, L.; Zhou Hong-Cai Stable Metal–Organic Frameworks: Design, Synthesis, and Applications. *Adv Mater* **2018***, 0*, 1704303.

11. Canivet, J.; Fateeva, A.; Guo, Y.; Coasne, B.; Farrusseng, D. Water adsorption in MOFs: fundamentals and applications. *Chem. Soc. Rev.* **2014***, 43*, 5594-5617.

12. Yang, C.; Wang, X.; Omary, M. A. Fluorous Metal-Organic Frameworks for High-Density Gas Adsorption. *J. Am. Chem. Soc.* **2007***, 129*, 15454-15455.

13. Chen, B.; Yang, Z.; Zhu, Y.; Xia, Y. Zeolitic imidazolate framework materials: recent progress in synthesis and applications. *J. Mater. Chem. A* **2014***, 2*, 16811-16831.

14. Phan, A.; Doonan, C. J.; Uribe-Romo, F.; Knobler, C. B.; O'Keeffe, M.; Yaghi, O. M. Synthesis, Structure, and Carbon Dioxide Capture Properties of Zeolitic Imidazolate Frameworks. *Acc. Chem. Res.* **2010***, 43*, 58-67.

15. Kusgens, P.; Rose, M.; Senkovska, I.; Frode, H.; Henschel, A.; Siegle, S.; Kaskel, S. Characterization of metal-organic frameworks by water adsorption. *Microporous and Mesoporous Materials* **2009***, 120*, 325-330.

16. Ortiz, A. U.; Freitas, A. P.; Boutin, A.; Fuchs, A. H.; Coudert, F. What makes zeolitic imidazolate frameworks hydrophobic or hydrophilic? The impact of geometry and functionalization on water adsorption. *Phys. Chem. Chem. Phys.* **2014***, 16*, 9940-9949.

17. Lalonde, M. B.; Mondloch, J. E.; Deria, P.; Sarjeant, A. A.; Al-Juaid, S.; Osman, O. I.; Farha, O. K.; Hupp, J. T. Selective Solvent-Assisted Linker Exchange (SALE) in a Series of Zeolitic Imidazolate Frameworks. *Inorg. Chem.* **2015***, 54*, 7142-7144.

18. Liu, C.; Huang, A. One-step synthesis of the superhydrophobic zeolitic imidazolate framework F-ZIF-90 for efficient removal of oil. *New J. Chem.* **2018***, 42*, 2372-2375.

19. Kitagawa, s.; Zhou, H. Metal-Organic Frameworks (MOFs). *Chem. Soc. Rev.* **2014***, 43*, 5415-5418.

20. Usman, M.; Lee, C.; Hung, D.; Lee, S.; Wang, C.; Luo, T.; Zhao, L.; Wu, M.; Lu, K. Intrinsic low dielectric behaviour of a highly thermally stable Sr-based metal-organic framework for interlayer dielectric materials. *J. Mater. Chem. C* **2014***, 2*, 3762-3768.

21. Eslava, S.; Zhang, L.; Esconjauregui, S.; Yang, J.; Vanstreels, K.; Baklanov, M. R.; Saiz, E. Metal-Organic Framework ZIF-8 Films As Low-k Dielectrics in Microelectronics. *Chem. Mater.* **2013***, 25*, 27-33.

22. Guo, P.; Chen, T.; Ren, X.; Ning, W.; Jin, W. A low-small kappa] dielectric metal-organic-framework compound showing novel three-step dielectric relaxations originating from orientational motion of dipolar guest molecules. *New J. Chem.* **2014***, 38*, 2254-2257.

23. Di, N. V.; Boeer, A. B.; Sandra, L.; Muryn, C. A.; Matthias, B.; Timco, G. A.; Enrico, N.; Marzio, R.; Winpenny, R. E.; Silvia, G. Functional Chromium Wheel-Based Hybrid Organic–Inorganic Materials for Dielectric Applications. *Adv. Funct. Mater.* **2009***, 19*, 3226-3236.

24. Christian, S. Superhydrophobicity in Highly Fluorinated Porous Metal–Organic Frameworks. *Angew. Chem. Int. Ed.* **2012***, 51*, 6048-6050.

25. Chen, T.; Popov, I.; Zenasni, O.; Daugulis, O.; Miljanic, O. S. Superhydrophobic perfluorinated metal-organic frameworks. *Chem. Commun.* **2013***, 49*, 6846-6848.

26. Moghadam, P. Z.; Ivy, J. F.; Arvapally, R. K.; dos Santos, A. M.; Pearson, J. C.; Zhang, L.; Tylianakis, E.; Ghosh, P.; Oswald, I. W. H.; Kaipa, U.; Wang, X.; Wilson, A. K.; Snurr, R. Q.; Omary, M. A. Adsorption and molecular siting of CO2, water, and other gases in the superhydrophobic, flexible pores of FMOF-1 from experiment and simulation. *Chem. Sci.* **2017**.

27. Wei, Z.; Gu, Z.; Arvapally, R. K.; Chen, Y.; McDougald, R. N., Jr.; Ivy, J. F.; Yakovenko, A. A.; Feng, D.; Omary, M. A.; Zhou, H. Rigidifying Fluorescent Linkers by Metal-Organic Framework Formation for Fluorescence Blue Shift and Quantum Yield Enhancement. *J. Am. Chem. Soc.* **2014***, 136*, 8269-8276.

28. Galli, S.; Cimino, A.; Ivy, J. F.; Giacobbe, C.; Arvapally, R. K.; Vismara, R.; Checchia, S.; Rawshdeh, M. A.; Cardenas, C. T.; Maspero, A.; and Omary , Mohammad A. "Fluorous Metal-Organic Frameworks and Non-Porous Coordination Polymers as Low-κ Dialectrics: A Case Study". *Submitted for Publication* **2018**.

29. Omary, M. A.; Ivy, J. F. Texas, United States Patent UNTP.P0001US.P1, 2016.

30. Omary, M. A.; Cimino, A.; Almotawa, R.; Maspero, A.; Giacobbe, C.; Palmisano, G.; Yang, C.; Ivy, J. F.; Williams, C.; Rawashdeh-Omary, M.; Galli, S. Are MOFS et al. really the next best thing since sliced bread? A case study for electronic device apps. *Prepr. - Am. Chem. Soc. , Div. Energy Fuels* **2015***, 60*, 391-392.

31. Li, H.; Eddaoudi, M.; O'Keeffe, M.; Yaghi, O. M. Design and synthesis of an exceptionally stable and highly porous metal-organic framework. *Nature* **1999***, 402*, 276-279.

32. Murray, L. J.; Dinca, M.; Long, J. R. Hydrogen storage in metal-organic frameworks. *Chem. Soc. Rev.* **2009***, 38*, 1294-1314.

33. Liu, Y.; Wang, Z. U.; Zhou, H. Recent advances in carbon dioxide capture with metal-organic frameworks. *Greenhouse Gases: Science and Technology* **2012***, 2*, 239-259.

34. Furukawa, H.; Cordova, K. E.; O'Keeffe, M.; Yaghi, O. M. The Chemistry and Applications of Metal-Organic Frameworks. *Science* **2013***, 341*.

35. Biradha, K.; Ramanan, A.; Vittal, J. J. Coordination Polymers Versus Metal-Organic Frameworks. *Crystal Growth & Design* **2009***, 9*, 2969-2970.

36. Hafizovic, J.; Bjørgen, M.; Olsbye, U.; Dietzel, P. D. C.; Bordiga, S.; Prestipino, C.; Lamberti, C.; Lillerud, K. P. The Inconsistency in Adsorption Properties and Powder XRD Data of MOF-5 Is Rationalized by Framework Interpenetration and the Presence of Organic and Inorganic Species in the Nanocavities. *J. Am. Chem. Soc.* **2007***, 129*, 3612-3620.

37. Chen, B.; Eddaoudi, M.; Hyde, S. T.; O'Keeffe, M.; Yaghi, O. M. Interwoven Metal-Organic Framework on a Periodic Minimal Surface with Extra-Large Pores. *Science* **2001***, 291*, 1021-1023.

38. Jiang, H.; Makal, T. A.; Zhou, H. Interpenetration control in metal–organic frameworks for functional applications. *Coord. Chem. Rev.* **2013***, 257*, 2232-2249.

39. Howarth, A. J.; Liu, Y.; Li, P.; Li, Z.; Wang, T. C.; Hupp, J. T.; Farha, O. K. Chemical, thermal and mechanical stabilities of metal-organic frameworks. *Nature Reviews Materials* **2016***, 1*, 15018.

40. Chen, B.; Ockwig, N. W.; Millward, A. R.; Contreras, D. S.; Yaghi, O. M. High H2 Adsorption in a Microporous Metal-Organic Framework with Open Metal Sites. *Angewandte Chemie* **2005***, 117*, 4823-4827.

41. Darensbourg, D. J.; Chung, W.; Wang, K.; Zhou, H. Sequestering CO2 for Short-Term Storage in MOFs: Copolymer Synthesis with Oxiranes. *ACS Catal.* **2014***, 4*, 1511-1515.

42. IPCC; Stocker, T. F.; Qin, D.; Plattner, G. -.; Alexander, L. V.; Zhou, T.; Et Al. Climate Change 2013: The Physical Science Basis. Contribution of Working Group I to the Fifth Assessment Report of the Intergovernmental Panel on Climate Change. **2013**.

43. Liu, J.; Thallapally, P. K.; McGrail, B. P.; Brown, D. R.; Liu, J. Progress in adsorption-based CO2 capture by metal-organic frameworks. *Chem. Soc. Rev.* **2012***, 41*, 2308-2322.

44. Wilmer, C. E.; Farha, O. K.; Bae, Y.; Hupp, J. T.; Snurr, R. Q. Structure-property relationships of porous materials for carbon dioxide separation and capture. *Energy Environ. Sci.* **2012***, 5*, 9849-9856.

45. Yazaydin, A. O.; Snurr, R. Q.; Park, T.; Koh, K.; Liu, J.; LeVan, M. D.; Benin, A. I.; Jakubczak, P.; Lanuza, M.; Galloway, D. B.; Low, J. J.; Willis, R. R. Screening of Metal-Organic Frameworks for Carbon Dioxide Capture from Flue Gas Using a Combined Experimental and Modeling Approach. *J. Am. Chem. Soc.* **2009***, 131*, 18198-18199.

46. Yang, C.; Wang, X.; Omary, M. Crystallographic Observation of Dynamic Gas Adsorption Sites and Thermal Expansion in a Breathable Fluorous Metal-Organic Framework. *Angewandte Chemie International Edition* **2009***, 48*, 2500-2505.

47. Omary, M. A.; Yang, C. Fluorinated metal-organic frameworks for gas storage. **2010**.

48. Schmitz, B.; Müller, U.; Trukhan, N.; Schubert, M.; Férey, G.; Hirscher, M. Heat of Adsorption for Hydrogen in Microporous High-Surface-Area Materials. *ChemPhysChem* **2008***, 9*, 2181-2184.

49. Simmons, J. M.; Wu, H.; Zhou, W.; Yildirim, T. Carbon capture in metal-organic frameworks-a comparative study. *Energy Environ. Sci.* **2011***, 4*, 2177-2185.

50. Wu, H.; Zhou, W.; Yildirim, T. High-Capacity Methane Storage in Metal-Organic Frameworks M2(dhtp): The Important Role of Open Metal Sites. *J. Am. Chem. Soc.* **2009***, 131*, 4995-5000.

51. Toth, J. State equations of the solid-gas interface layers. *Acta Chim Acad Sci Hungar* **1971***, 69*, 311-328.

52. Fang, M.; Zhao, B. Ln-Ag heterometallic coordination polymers. *Reviews in Inorganic Chemistry* **2015***, 35*, 81-113.

53. Wang, C.; Wang, Y.; Wang, H.; Yang, G.; Wen, G.; Zhang, M.; Shi, Q. A novel silver(I) coordination polymer based on mixed ligands bpp and 2,2'-bipyridine-4,4'-dicarboxylate. *Inorganic Chemistry Communications* **2008***, 11*, 843-846.

54. Dong, Y.; Jin, G.; Smith, M. D.; Huang, R.; Tang, B.; zur Loye, H. Ag2(C33H26N2O2)(H2O)2(SO3CF3)2]·0.5C6H6: A Luminescent Supramolecular Silver(I) Complex Based on Metal-Carbon and Metal-Heteroatom Interactions. *Inorg. Chem.* **2002***, 41*, 4909-4914.

55. Kakizoe, D.; Nishikawa, M.; Degawa, T.; Tsubomura, T. Intense blue emission and a reversible hypsochromic shift of luminescence caused by grinding based on silver(i) complexes. *Inorg. Chem. Front.* **2016***, 3*, 1381-1387.

56. Zhang, S.; Hu, T.; Li, J.; Du, J.; Bu, X. Silver(I) coordination architectures with quinoxaline-based N,S-donor ligands: structures and luminescent properties. *CrystEngComm* **2008***, 10*, 1595-1604.

57. Li, M.; Lin, M.; Chen, W.; McDougald, R.; Arvapally, R.; Omary, M.; Shepherd, N. D. High efficiency orange-red phosphorescent organic light emitting diodes based on a Pt(II)-pyridyltriazolate complex from a structure optimized for charge balance and reduced efficiency roll-off. *physica status solidi (a)* **2012***, 209*, 221-225.

58. Li, M.; Chen, W.; Lin, M.; Omary, M. A.; Shepherd, N. D. Near-white and tunable electrophosphorescence from bis[3,5-bis(2-pyridyl)-1,2,4-triazolato]platinum(II)-based organic light emitting diodes. *Organic Electronics* **2009***, 10*, 863-870.

59. Wang, Q.; Oswald, I. W. H.; Perez, M. R.; Jia, H.; Gnade, B. E.; Omary, M. A. Exciton and Polaron Quenching in Doping-Free Phosphorescent Organic Light-Emitting Diodes from a Pt(II)-Based Fast Phosphor. *Advanced Functional Materials* **2013***, 23*, 5420-5428.

60. Sperline, R. P.; Dickson, M. K.; Roundhill, D. M. New route to the directed synthesis of mixed metal chain oligomers. Identification of a platinum complex having an intense emission in the visible spectrum in aqueous solution. *J. Chem. Soc. , Chem. Commun.* **1977**, 62-63.

61. Pinto, M. A. F.; Sadler, P. J.; Neidle, S.; Sanderson, M. R.; Subbiah, A.; Kuroda, R. A novel di-platinum(II) octaphosphite complex showing metal-metal bonding and intense luminescence; a potential probe for basic proteins. X-Ray crystal and molecular structure. *J. Chem. Soc. , Chem. Commun.* **1980**, 13-15.

62. Che, C. M.; Butler, L. G.; Gray, H. B. Spectroscopic properties and redox chemistry of the phosphorescent excited state of octahydrotetrakis(phosphorus pentoxide)diplatinate(4-) ion (Pt2(P2O5)4H84-). *J. Am. Chem. Soc.* **1981***, 103*, 7796-7797.

63. Rice, S. F.; Gray, H. B. Electronic absorption and emission spectra of binuclear platinum(II) complexes. Characterization of the lowest singlet and triplet excited states of tetrakis(diphosphonato)diplatinate(4-) anion (Pt2(H2P2O5)44-). *J. Am. Chem. Soc.* **1983***, 105*, 4571-4575.

64. Markert, J. T.; Clements, D. P.; Corson, M. R.; Nagle, J. K. Phosphorescent lifetime and quantum yield measurements of K4Pt2(H2P2O5)4 from 1.6 to 300 K. *Chemical Physics Letters* **1983***, 97*, 175-179.

65. Stiegman, A. E.; Rice, S. F.; Gray, H. B.; Miskowski, V. M. Electronic spectroscopy of $d^8$-$d^8$ diplatinum complexes. $^1A_{2u}$ ($d\sigma^*$ - $p\sigma$), $^3E_u$ ($d_{xz}$,$d_{yz}$ - $p\sigma$), and $^{3,1}B_{2u}$ ($d\sigma^*$ - $d_{x2-y2}$) excited states of tetrakis(diphosphonato)diplatinate$^{(4-)}$, $Pt_2(P_2O_5H_2)_4^{4-}$. *Inorg. Chem.* **1987***, 26*, 1112-1116.

66. Roundhill, D. M.; Gray, H. B.; Che, C. M. Pyrophosphito-bridged diplatinum chemistry. *Acc. Chem. Res.* **1989***, 22*, 55-61.

67. Pan, Q.; Fu, H.; Yu, H.; Zhang, H. Theoretical Insight into Electronic Structures and Spectroscopic Properties of Pt2(pop)4]4-, Pt2(pcp)4]4-, and Related Derivatives (pop = P2O5H22- and pcp = P2O4CH42-). *Inorg. Chem.* **2006***, 45*, 8729-8735.

68. Zalis, S.; Lam, Y.; Gray, H. B.; Vlcek, A. Spin-Orbit TDDFT Electronic Structure of Diplatinum(II,II) Complexes. *Inorg. Chem.* **2015***, 54*, 3491-3500.

69. King, C.; Auerbach, R. A.; Fronczek, F. R.; Roundhill, D. M. Synthesis structure and spectroscopy of the diplatinum(II) complex Pt2(pcp)44-, a Pt2(pop)44- analog having methylenebisphosphinic acid bridges. *J. Am. Chem. Soc.* **1986***, 108*, 5626-5627.

70. Roundhill, D. M.; Shen, Z. P.; King, C.; Atherton, S. J. Triplet excited-state chemistry of diplatinum(II) complexes: comparative spectroscopy and quenching rate constants between the tetrakis(μ-pyrophosphito)diplatinate(II) and the tetrakisμ-methylenebis(phosphonito)]diplatinate(II) tetraanions. *J. Phys. Chem.* **1988***, 92*, 4088-4094.

71. Durrell, A. C.; Keller, G. E.; Lam, Y.; Sykora, J.; Vlcek, A., Jr.; Gray, H. B. Structural Control of 1A2u-to-3A2u Intersystem Crossing in Diplatinum(II,II) Complexes. *J. Am. Chem. Soc.* **2012***, 134*, 14201-14207.

72. Christensen, M.; Haldrup, K.; Kjaer, K. S.; Cammarata, M.; Wulff, M.; Bechgaard, K.; Weihe, H.; Harrit, N. H.; Nielsen, M. M. Structure of a short-lived excited state trinuclear Ag-Pt-Pt complex in aqueous solution by time resolved X-ray scattering. *Phys. Chem. Chem. Phys.* **2010***, 12*, 6921-6923.

73. Kong, Q.; Kjaer, K. S.; Haldrup, K.; Sauer, S. P. A.; van Driel, T. B.; Christensen, M.; Nielsen, M. M.; Wulff, M. Theoretical study of the triplet excited state of PtPOP and the exciplexes M-PtPOP (M = Tl, Ag) in solution and comparison with ultrafast X-ray scattering results. *Chem. Phys.* **2012***, 393*, 117-122.

74. Tan, K.; Nijem, N.; Canepa, P.; Gong, Q.; Li, J.; Thonhauser, T.; Chabal, Y. J. Stability and Hydrolyzation of Metal Organic Frameworks with Paddle-Wheel SBUs upon Hydration. *Chem. Mater.* **2012***, 24*, 3153-3167.

75. Ming, Y.; Purewal, J.; Yang, J.; Xu, C.; Soltis, R.; Warner, J.; Veenstra, M.; Gaab, M.; Müller, U.; Siegel, D. J. Kinetic Stability of MOF-5 in Humid Environments: Impact of Powder Densification, Humidity Level, and Exposure Time. *Langmuir* **2015***, 31*, 4988-4995.

76. Shuai, Y.; Liang, F.; Kecheng, W.; Jiandong, P.; Matheiu, B.; Christina, L.; Yujia, S.; Junsheng, Q.; Xinyu, Y.; Peng, Z.; Qi, W.; Lanfang, Z.; Yingmu, Z.; Liangliang, Z.; Yu, F.; Jialuo, L.; Zhou Hong-Cai Stable Metal–Organic Frameworks: Design, Synthesis, and Applications. *Adv Mater* **2018***, 0*, 1704303.

77. Satumtira, N. T. Water-soluble Phosphors for Hypoxia Detection in Chemical and Biological Media, University of North Texas, 2012.

78. Allendorf, M. D.; Bauer, C. A.; Bhakta, R. K.; Houk, R. J. T. Luminescent metal-organic frameworks. *Chem. Soc. Rev.* **2009***, 38*, 1330-1352.

79. Cui, Y.; Yue, Y.; Qian, G.; Chen, B. Luminescent Functional Metal-Organic Frameworks. *Chem. Rev. (Washington, DC, U. S. )* **2012***, 112*, 1126-1162.

80. Mueller-Buschbaum, K.; Beuerle, F.; Feldmann, C. MOF based luminescence tuning and chemical/physical sensing. *Microporous Mesoporous Mater.* **2015***, 216*, 171-199.

81. Pettinari, C.; Marchetti, F.; Mosca, N.; Tosi, G.; Drozdov, A. Application of metal - organic frameworks. *Polym. Int.* **2017***, 66*, 731-744.

82. Xie, W.; Zhang, S.; Du, D.; Qin, J.; Bao, S.; Li, J.; Su, Z.; He, W.; Fu, Q.; Lan, Y. Stable Luminescent Metal-Organic Frameworks as Dual-Functional Materials To Encapsulate Ln3+ Ions for White-Light Emission and To Detect Nitroaromatic Explosives. *Inorg. Chem.* **2015***, 54*, 3290-3296.

83. Ma, H.; Wang, L.; Chen, J.; Zhang, X.; Wang, L.; Xu, N.; Yang, G.; Cheng, P. A multi-responsive luminescent sensor for organic small-molecule pollutants and metal ions based on a 4d-4f metal-organic framework. *Dalton Trans.* **2017***, 46*, 3526-3534.

84. Gu, X.; Xue, D. Self-assembly of 3-D 4d-4f coordination frameworks based on 1-D inorganic heterometallic chains and linear organic linkers. *CrystEngComm* **2007***, 9*, 471-477.

85. Wei, Z.; Gu, Z.; Arvapally, R. K.; Chen, Y.; McDougald, R. N.; Ivy, J. F.; Yakovenko, A. A.; Feng, D.; Omary, M. A.; Zhou, H. Rigidifying Fluorescent Linkers by Metal-Organic Framework Formation for Fluorescence Blue Shift and Quantum Yield Enhancement. *J. Am. Chem. Soc.* **2014***, 136*, 8269-8276.

86. Zhan, S.; Li, M.; Ng, S. W.; Li, D. Luminescent Metal–Organic Frameworks (MOFs) as a Chemopalette: Tuning the Thermochromic Behavior of Dual-Emissive Phosphorescence by Adjusting the Supramolecular Microenvironments. *Chemistry – A European Journal* **2013***, 19*, 10217-10225.

87. Zhao, B.; Zhao, X.; Chen, Z.; Shi, W.; Cheng, P.; Yan, S.; Liao, D. Structures and near-infrared luminescence of unique 4d-4f heterometal-organic frameworks (HMOF). *CrystEngComm* **2008***, 10*, 1144-1146.

88. Zhao, X.; Zhao, B.; Wei, S.; Cheng, P. Synthesis, Structures, and Luminescent and Magnetic Properties of Ln-Ag Heterometal-Organic Frameworks. *Inorg. Chem.* **2009***, 48*, 11048-11057.

89. Afsahi, F.; Vinh-Thang, H.; Mikhailenko, S.; Kaliaguine, S. Electrocatalyst synthesized from metal organic frameworks. *J. Power Sources* **2013***, 239*, 415-423.

90. Atoini, Y.; Prasetyanto, E. A.; Chen, P.; Jonckheere, D.; De Vos, D.; De Cola, L. Tuning luminescent properties of a metal organic framework by insertion of metal complexes. *Supramolecular Chemistry* **2017**, 1-10.

91. Kobayashi, A.; Hara, H.; Yonemura, T.; Chang, H.; Kato, M. Systematic structural control of multichromic platinum(ii)-diimine complexes ranging from ionic solid to coordination polymer. *Dalton Trans.* **2012***, 41*, 1878-1888.

92. Toyao, T.; Saito, M.; Dohshi, S.; Mochizuki, K.; Iwata, M.; Higashimura, H.; Horiuchi, Y.; Matsuoka, M. Construction of Pt complex within Zr-based MOF and its application for hydrogen production under visible-light irradiation. *Research on Chemical Intermediates* **2016***, 42*, 7679-7688.

93. Kobayashi, A.; Hara, H.; Noro, S.; Kato, M. Multifunctional sensing ability of a new Pt/Zn-based luminescent coordination polymer. *Dalton Trans.* **2010***, 39*, 3400-3406.

94. Miyazaki, Y.; Kataoka, Y.; Kawamoto, T.; Mori, W. Synthesis, Crystal Structure and Gas Adsorption Properties of Four Pd–Zn Coordination Polymers Containing Potential Catalytic Active Sites. *European Journal of Inorganic Chemistry* **2012***, 2012*, 807-812.

95. Bailey, J. A.; Hill, M. G.; Marsh, R. E.; Miskowski, V. M.; Schaefer, W. P.; Gray, H. B. Electronic Spectroscopy of Chloro(terpyridine)platinum(II). *Inorg. Chem.* **1995***, 34*, 4591-4599.

96. Che, C. M.; He, L. Y.; Poon, C. K.; Mak, T. C. W. Solid-state emission of dicyanoplatinum(II) and -palladium(II) complexes of substituted 2,2'-bipyridines and 1,10-phenanthroline

and x-ray crystal structures of isomorphous M(bpy)(CN)2 (bpy = 2,2'-bipyridine; M = Pt, Pd). *Inorg. Chem.* **1989***, 28*, 3081-3083.

97. Kobayashi, A.; Kato, M. Vapochromic Platinum(II) Complexes: Crystal Engineering toward Intelligent Sensing Devices. *European Journal of Inorganic Chemistry* **2014***, 2014*, 4469-4483.

98. Kato, M.; Kosuge, C.; Morii, K.; Ahn, J. S.; Kitagawa, H.; Mitani, T.; Matsushita, M.; Kato, T.; Yano, S.; Kimura, M. Luminescence Properties and Crystal Structures of Dicyano(diimine)platinum(II) Complexes Controlled by Pt···Pt and π-π Interactions. *Inorg. Chem.* **1999***, 38*, 1638-1641.

99. Rachford, A. A.; Castellano, F. N. Thermochromic Absorption and Photoluminescence in Pt(ppy)(μ-Ph2pz)]2. *Inorg. Chem.* **2009***, 48*, 10865-10867.

100. Cui, Y.; Zhu, F.; Chen, B.; Qian, G. Metal-organic frameworks for luminescence thermometry. *Chem. Commun.* **2015***, 51*, 7420-7431.

101. Ma, B.; Li, J.; Djurovich, P. I.; Yousufuddin, M.; Bau, R.; Thompson, M. E. Synthetic Control of Pt···Pt Separation and Photophysics of Binuclear Platinum Complexes. *J. Am. Chem. Soc.* **2005***, 127*, 28-29.

102. Connick, W. B.; Henling, L. M.; Marsh, R. E.; Gray, H. B. Emission Spectroscopic Properties of the Red Form of Dichloro(2,2'-bipyridine)platinum(II). Role of Intermolecular Stacking Interactions. *Inorg. Chem.* **1996***, 35*, 6261-6265.

103. Chakraborty, A.; Yarnell, J. E.; Sommer, R. D.; Roy, S.; Castellano, F. N. Excited-State Processes of Cyclometalated Platinum(II) Charge-Transfer Dimers Bridged by Hydroxypyridines. *Inorg. Chem.* **2018***, 57*, 1298-1310.

104. Chen, W. H. Triimine Complexes of Divalent Group 10 Metals for use in Molecular Electronic Devices, University of North Texas, May 2010.

105. Oswald, I. W. H. "Design, Synthesis and Screening of Homoleptic and Heteroleptic Platinum (II) Pyridylazolate Complexes for N-Type Semiconducting and Light Emitting Devices", Master's Thesis, University of North Texas, May 2013.

106. Kim, T. K.; Lee, J. H.; Moon, D.; Moon, H. R. Luminescent Li-Based Metal-Organic Framework Tailored for the Selective Detection of Explosive Nitroaromatic Compounds: Direct Observation of Interaction Sites. *Inorg. Chem.* **2013***, 52*, 589-595.

107. Mehmetaj, B.; Haasnoot, J. G.; De Cola, L.; van Albada, G. A.; Mutikainen, I.; Turpeinen, U.; Reedijk, J. Syntheses, Characterization, X-ray Crystal Structure, Redox and Photophysical Properties of Polypyridylruthenium(II) Complexes Containing Carboxylate-Substituted Pyridyltriazoles. *European Journal of Inorganic Chemistry* **2002***, 2002*, 1765-1771.

108. Case, F. H. The Preparation of Hydrazidines and as-Triazines Related to Substituted 2-Cyanopyridines1. *J. Org. Chem.* **1965***, 30*, 931-933.

109. Dubs, C.; Yamamoto, T.; Inagaki, A.; Akita, M. Synthesis of a Library of Iridium-Containing Dinuclear Complexes with Bridging PNNN and PNNP Ligands (BL), LM(μ-BL)M'L']$BF_4$. 1. Specific Synthesis of Isomeric Heterodinuclear Complexes with Switched Metal Arrangements. *Organometallics* **2006***, 25*, 1344-1358.

110. Coelho, A. A. Indexing of powder diffraction patterns by iterative use of singular value decomposition. *J. Appl. Crystallogr.* **2003***, 36*, 86-95.

111. Coelho, A. A. TOPAS-Academic V6. *http://www.topas-academic.net.*

112. Coelho, A. A. Whole-profile structure solution from powder diffraction data using simulated annealing. *J. Appl. Crystallogr.* **2000***, 33*, 899-908.

113. Young, R. A. *The Reitveld Method;* IUCr Monograph N. 5, Oxford University Press: New York, 1981; .

114. Omary, M. A.; Patterson, H. H. Luminescence, Theory*. In *Encyclopedia of Spectroscopy and Spectrometry (Second Edition)*; Lindon, J. C., Ed.; Academic Press: Oxford, 1999; pp 1372-1391.

115. Qiu, S.; Xue, M.; Zhu, G. Metal-organic framework membranes: from synthesis to separation application. *Chem. Soc. Rev.* **2014***, 43*, 6116-6140.

116. Li, W.; Su, P.; Li, Z.; Xu, Z.; Wang, F.; Ou, H.; Zhang, J.; Zhang, G.; Zeng, E. Ultrathin metal-organic framework membrane production by gel-vapour deposition. *Nature Communications* **2017***, 8*, 406.

117. Gong, X.; Wang, Y.; Kuang, T. ZIF-8-Based Membranes for Carbon Dioxide Capture and Separation. *ACS Sustainable Chem. Eng.* **2017***, 5*, 11204-11214.

118. Wu, T.; Feng, X.; Elsaidi, S. K.; Thallapally, P. K.; Carreon, M. A. Zeolitic Imidazolate Framework-8 (ZIF-8) Membranes for Kr/Xe Separation. *Ind Eng Chem Res* **2017***, 56*, 1682-1686.

119. Orselli, E.; Kottas, G. S.; Konradsson, A. E.; Coppo, P.; Fröhlich, R.; De Cola, L.; van Dijken, A.; Büchel, M.; Börner, H. Blue-Emitting Iridium Complexes with Substituted 1,2,4-Triazole Ligands: Synthesis, Photophysics, and Devices. *Inorg. Chem.* **2007***, 46*, 11082-11093.

120. Eberhardt, H.; Reuter, A. DE2105672A, 1972.

121. Shang, R.; Fu, Y.; Li, J.; Zhang, S.; Guo, Q.; Liu, L. Synthesis of Aromatic Esters via Pd-Catalyzed Decarboxylative Coupling of Potassium Oxalate Monoesters with Aryl Bromides and Chlorides. *J. Am. Chem. Soc.* **2009***, 131*, 5738-5739.

122. Pachfule, P.; Chen, Y.; Sahoo, S. C.; Jiang, J.; Banerjee, R. Structural Isomerism and Effect of Fluorination on Gas Adsorption in Copper-Tetrazolate Based Metal Organic Frameworks. *Chem. Mater.* **2011***, 23*, 2908-2916.

123. Pradip, P.; Yifei, C.; Jianwen, J.; Rahul, B. Fluorinated Metal–Organic Frameworks: Advantageous for Higher H2 and CO2 Adsorption or Not? *Chem. Eur. J.* **2012***, 18*, 688-694.

124. Zhang, D.; Chang, Z.; Li, Y.; Jiang, Z.; Xuan, Z.; Zhang, Y.; Li, J.; Chen, Q.; Hu, T.; Bu, X. Fluorous Metal-Organic Frameworks with Enhanced Stability and High H2/CO2 Storage Capacities. *Scientific Reports* **2013***, 3*, 3312.